DOE/MC/30098 -- 5236
(DE96011327)

Development Of Fireside Performance Indices - Task 8

Topical Report
March 1996

November 1995

Work Performed Under Contract No.: DE-FC21-93MC30098

For
U.S. Department of Energy
Office of Fossil Energy
Morgantown Energy Technology Center
Morgantown, West Virginia

By
University of North Dakota
Energy & Environmental Research Center
P.O. Box 9018
Grand Forks, North Dakota 58202-9018

DISCLAIMER

DOE/MC/30098 -- 5236
(DE96011327)
Distribution Category UC-103

Development Of Fireside Performance Indices - Task 8

Topical Report
March 1996

Work Performed Under Contract No.: DE-FC21-93MC30098

For
U.S. Department of Energy
Office of Fossil Energy
Morgantown Energy Technology Center
P.O. Box 880
Morgantown, West Virginia 26507-0880

By
University of North Dakota
Energy & Environmental Research Center
P.O. Box 9018
Grand Forks, North Dakota 58202-9018

November 1996

TABLE OF CONTENTS

Continued

LIST OF FIGURES

Continued

LIST OF TABLES

Continued

DEVELOPMENT OF FIRESIDE PERFORMANCE INDICES

EXECUTIVE SUMMARY

Advanced indices have been developed by the Energy & Environmental Research Center (EERC) for predicting coal-related aspects of power plant performance, including main furnace slagging, convective pass high- and low-temperature fouling, slag tapping, sootblowing effectiveness, stack plume opacity, boiler erosion, and coal grindability. The parameters required to calculate the indices consist of coal analysis results determined by computer-controlled scanning electron microscopy (CCSEM) and chemical fractionation methods, in addition to standard American Society for Testing and Materials (ASTM) proximate, ultimate, and coal ash chemical analysis methods. Boiler specifications and operating conditions, such as the boiler type (pulverized coal or cyclone), combustion conditions (conventional or low-NO_x), maximum continuous load rating, current operating load, and furnace dimensions, are also used as input parameters. The eight indices are expressed numerically as whole numbers ranging from 1 to 100. General classifications of low, medium, and high propensity are assigned to the following specific ranges of index values: 1 to 33, 34 to 66, and 67 to 100, respectively. A greater value corresponds to an increase in severity or adverse effect for a given index. This propensity-index classification scheme applies to all the indices except the coal grindability index. The coal grindability index is directly related to the ASTM Hardgrove grindability index.

The ash deposition indices (slagging and high- and low-temperature fouling) were formulated from existing bench-, pilot-, and full-scale combustion testing data and knowledge of inorganic transformations, entrained ash formation, and ash deposition. Additional bench-scale testing in drop-tube furnaces (DTFs) was performed on eight Powder River Basin (PRB) subbituminous coals to refine and verify the ash deposition indices and to develop ash removability indices (slag tapping and sootblowing). The following combustion conditions were simulated during the testing: slagging, conventional and low-NO_x high-temperature fouling, and conventional and low-NO_x low-temperature fouling. Deposit growth rates, sticking coefficients, in situ adhesion strengths, crushing strengths, initial slagging temperatures, porosities, and chemical and phase compositions were determined. In general, the low-NO_x combustion conditions produce high-temperature fouling deposits that have less adhesion and crushing strengths relative to those produced in conventional combustion conditions. The combustion conditions, however, did not affect the relative strengths of the low-temperature fouling deposits for a given coal. Deposit porosity was found to be a poor indicator of crushing or adhesion strength.

The scattering of light by fine ash particles was the primary mechanism considered in developing the stack plume opacity index. Fine ash fractions, <2 μm in diameter, collected during bench-scale testing of eight PRB subbituminous coals, were analyzed using CCSEM. Advances in particulate sample preparation methods enabled the CCSEM analysis of individual ash particles with submicron diameters as small as 0.1 μm. The fine ash samples produced from the conventional combustion of coal consisted of discrete spherical particles, whereas particle agglomerates were characteristic of the low-NO_x ash samples. Particle-size distributions of the low-NO_x fine ash fractions were coarser because of the agglomeration. Theoretical light-scattering calculations indicate that, for a given coal, the ash produced in low-NO_x conditions generally causes less opacity as compared to conventional combustion conditions. The following phases

were abundant in the ashes: Ca aluminosilicate, Ca aluminate, aluminosilicate, silica, (Ca,Mg)O, $CaSO_4$, Na_2SO_4, and (Na,K)Cl. Primary mechanisms that produced the fine ash include the thermal metamorphism of small, <5 μm, mineral grains and the vaporization and subsequent condensation of organically bound Na, Mg, and Ca. Empirical equations for estimating the concentration of fine ash produced from burning subbituminous coals were formulated into an opacity index based on CCSEM coal mineral and fine ash analysis and on DTF testing results. The effects of combustion conditions (conventional or low-NO_x) on fine ash formation and ash electrical resistivity on electrostatic precipitator collection efficiency are also considered in the index.

A grindability index was developed by investigating the relationship of selected coal properties to the measured Hardgrove grindability index for ten subbituminous coals and a lignite coal. Grindability correlated best to the total sulfur ($r^2 = 0.845$) and ash ($r^2 = 0.694$) contents of the coals. The grindability index was derived from a multiple regression analysis of the ash and total sulfur variables. Coal rank (calorific value), moisture content, quantitative included-excluded mineralogy, and maceral compositions of the coals were not significantly correlated to the Hardgrove grindability index.

An index for comparing the relative erosiveness of coals was derived based on the quantity of quartz and pyrite grains that are excluded from coal macerals and range in diameter from 5 to 50 μm. CCSEM and digital image analysis techniques are used to obtain this information. The velocities of quartz- and pyrite-derived ash particles during transport in flue gas and relative mineral hardness are also considered in the index.

A primary goal was to develop more reliable slagging and fouling indices as well as an opacity index for comparing PRB subbituminous coals. Consequently, verification testing of these indices was conducted using eight full-scale utility boilers. Visual assessments of slagging and fouling and measurements of opacity were in general agreement with propensity index classifications (i.e., low, medium, and high).

A computer program designated as the Predictive Coal Quality Effects Screening Tool (PCQUEST) was developed for calculating and displaying the index values. Index values for multiple coals can be presented and compared in a tabular or graphical format. A coal blending option enables the blending of two to four coals in proportions specified by the user. PCQUEST is most useful for comparing the relative fireside performance of two or more coals or for determining optimum coal blending strategies. A database of 66 coal analysis files is included with the program.

DEVELOPMENT OF FIRESIDE PERFORMANCE INDICES

1.0 INTRODUCTION

The primary goal of the Fireside Performance Indices (FPI) research project at the Energy & Environmental Research Center (EERC) was to develop a series of indices to reliably predict the fireside performance of subbituminous coals in utility boilers. Individual utilities must respond quickly and effectively to changing fuel markets because of competition within the U.S. coal-fired power industry. Spot-market purchases of coal have become commonplace. The economics associated with sulfur emissions control have caused many utilities to use Powder River Basin (PRB) subbituminous coals. The PRB coals usually provide a lower-cost, medium-heating-value, low-sulfur fuel option. Although these coals possess similar overall or bulk compositional properties, their fireside performance characteristics vary considerably within a given boiler (1). Consequently, bulk compositional parameters and, hence, conventional indices such as the base-to-acid ratio, slagging factor, and fouling factor (2) are inappropriate for predicting the fireside performance of PRB coals. The development of the computer-controlled scanning electron microscopy (CCSEM) (3–5) and chemical fractionation methods (6, 7), however, has enabled a more thorough characterization of the inorganic constituents of PRB coals that contribute to the following adverse operational effects: slagging, fouling, opacity, erosion and poor grindability, slag tapping, and sootblower performance (8). Eight predictive indices, as indicated in Figure 1, have been developed based primarily on CCSEM and chemical fractionation analysis parameters to predict the propensity of a given coal or coal blend to cause operational problems. The indices were formulated using bench-, pilot-, and full-scale combustion testing data from previous research projects (9–14) combined with bench-scale data from this project to identify the primary coal inorganic properties that cause ash-related problems in utility boilers. Knowledge of inorganic transformations, entrained ash formation, and ash deposition was instrumental in formulating the indices (15, 16). General boiler information and operating conditions are also considered in the index calculations. The reliability of several of the indices has been demonstrated via utility-scale testing of PRB coals at eight different boilers.

A computer software package designated as the Predictive Coal Quality Effects Screening Tool (PCQUEST) has been developed to calculate and display the index values as whole numbers ranging from 1 to 100. General classifications of low, medium, and high propensity are assigned to the following specific ranges of index values: 1 to 33, 34 to 66, and 67 to 100, respectively. PCQUEST is most useful for comparing the relative fireside performance of two or more coals or for determining optimum coal-blending strategies. A PCQUEST Operator's Manual is provided in Appendix A.

2.0 COAL PROPERTIES

2.1 Introduction

Thirteen PRB subbituminous coals were selected for detailed testing in bench- and full-scale combustion systems. The coals were analyzed using standard American Society for Testing and Materials (ASTM) methods (proximate, ultimate, and ash elemental oxide composition) and the

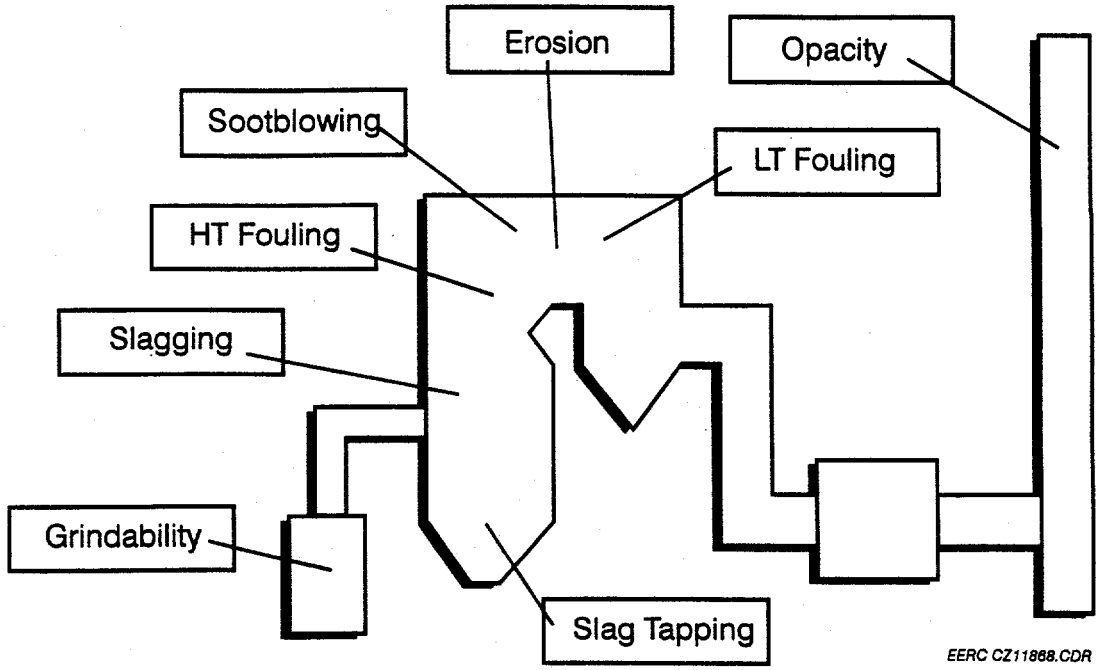

Figure 1. PCQUEST performance indices as they relate to a typical coal-fired boiler.

more recently developed CCSEM and chemical fractionation methods. The ASTM methods provide information on the bulk chemical composition and combustion characteristics of coal, whereas CCSEM and chemical fractionation methods provide quantitative information on the distribution of various elements among the maceral and mineral constituents of coal. The combination of these analysis methods provides a comprehensive characterization of the inorganic properties of coal. An additional 53 coals of varying rank and geographical origin were used throughout this project for modifying and verifying the indices. Analysis from these additional coals were acquired through other projects with the supporting sponsors.

2.2 Experimental

The thirteen PRB test coals were acquired from coal mines and utility stations as indicated in Table 1. The proximate, ultimate, and coal ash chemical analysis were conducted according to ASTM Standard Methods D3172, D3176, and D4326, respectively. Prior to CCSEM and chemical fractionation analysis, the coals were pulverized in a Micron Powder Bantam Jet Mill. Sieve analysis was performed to verify that the particle-size distributions of the test coals were consistent with standard utility boiler practice (i.e., 70%–80% of the coal particles less than 200 mesh). A representative portion of each pulverized coal was analyzed using the CCSEM method of quantitative coal mineral analysis. The CCSEM method has been described by Zygarlicke and Steadman (17) and Galbreath and others (18). Interlaboratory studies of the method by Casuccio and others (19) and Galbreath and others (20) indicate that the repeatability relative standard deviation of CCSEM results (i.e., mineral proportions) is generally less than 20%. The pulverized coals were also analyzed using chemical fractionation to deduce the distribution of elemental constituents between the mineral and maceral components of coal. Chemical fractionation is a

TABLE 1

FPI Test Coal Information

Coal	Organization*	Sampling Location	Date
Antelope	NSP	Antelope Coal Company Mine	1990
Big Sky	MNP	Clay Boswell Station	Nov. 2-4, 1993
75% Big Sky-25% Spring Creek	MNP	Clay Boswell Station	Nov. 2-4, 1993
Black Thunder	DOE	ARCO Coal Company Mine	Oct. 28, 1993
Black Thunder	KCPL	Hawthorn Station	April 5-8, 1994
Black Thunder	NSP	Sherburne County Station	June 14-15, 1994
70% Black Thunder-30% Colstrip	NSP	Sherburne County Station	June 14-15, 1994
Caballo Rojo	KCPL	Caballo Rojo, Inc., Mine	Dec. 22, 1993
Colstrip	NSP	Sherburne County Station	June 14-15, 1994
Rochelle	UE	Labadie Station	Jan. 4-7, 1993
Spring Creek	MNP	Clay Boswell Station	Nov. 2-4, 1993
Spring Creek	NSP	Spring Creek Coal Company Mine	Oct. 12, 1993
Sarpy Creek	NSP	Westmoreland Resources Mine	1990

* NSP (Northern States Power Company), MNP (Minnesota Power), DOE (Department of Energy), KCPL (Kansas City Power and Light), and UE (Union Electric).

selective leaching procedure based on the differences in solubilities of organically bound and mineral-bound inorganic constituents in stirred solutions of deionized water (H_2O), 1 M ammonium acetate (NH_4OAc), and 1 M hydrochloric acid (HCl). Elements leached by H_2O are primarily associated with water-soluble minerals (e.g., alkali halides). Exchangeable ions, principally elements associated with salts of organic acids and clay minerals, are removed by NH_4OAc. Hydrochloric acid removes elements associated with acid-soluble minerals (carbonates, oxides, and metastable sulfides) and organic coordination complexes, such as carboxylate groups on coal surfaces. Elements remaining in the final residue are presumably associated with insoluble silicate and sulfide minerals. The chemical fractionation analysis were conducted according to the procedure described by O'Keefe and Erickson (21).

2.3 Coal Analysis Results

The abbreviated coal names indicated in Table 2 are used in the subsequent sections of this report to facilitate the presentation of analysis results. The coal analysis results are summarized in Tables 3-5 and Figures 2 and 3. The analysis results for each coal have also been compiled into

TABLE 2

FPI Test Coal Nomenclature

Coal	Organization	Coal Abbreviation
Antelope	NSP	Ant
Big Sky	MNP	BS
75% Big Sky– 25% Spring Creek	MNP	BS/SC
Black Thunder	DOE	BTD
Black Thunder	KCPL	BTK
Black Thunder	NSP	BTN
70% Black Thunder– 30% Colstrip	NSP	BT/CS
Caballo Rojo	KCPL	Cab
Colstrip	NSP	CS
Rochelle	UE	Rch
Spring Creek	MNP	SCM
Spring Creek	NSP	SCN
Sarpy Creek	NSP	Sarpy

PCQUEST input files. The format and content of a PCQUEST coal analysis file is described in Appendix A.

The bulk properties (proximate, ultimate, calculated heating value, and coal ash chemical composition, Tables 3 and 4) of the coals are typical of western U.S. subbituminous coals, that is, relatively high moisture, oxygen, and calcium concentrations but low ash, sulfur, and iron concentrations.

The predominant minerals in the coals, as indicated in Table 5, are kaolinite ($Al_2Si_2O_5[OH]_4$), quartz (SiO_2), pyrite (FeS_2), illite ($K[Si,Al]_4O_{10}[(OH]_2 \cdot H_2O$), and mixed clays ($[Na,K,Ca,Mg,Fe]_x[Al,Si]_x$ [OH, H_2O]). Many of the coals also contain a relatively large proportion of a calcium aluminophosphate mineral, which has been tentatively identified as crandallite ($CaAl_3[PO_4]_2[OH]_5 \cdot H_2O$). The Antelope, Black Thunder, Caballo Rojo, and Spring Creek coals contain relatively high proportions of mineral grains classified as "others." Chemical analysis results that do not strictly conform to the compositional ranges of common coal minerals are assigned to this classification category. Compositions in this category are generally consistent with mixtures of various minerals. The abundance of mineral mixtures in these coals may be a distinct mineralogical characteristic.

TABLE 3

Proximate and Ultimate Analysis Results of the 13 FPI Test Coals, as-received wt%

	Ant	BS	BS/SC	BTD	BTK	BTN	BT/CS	Cab	CS	Rch	SCM	SCN	Sarpy
Moisture	23.5	23.6	23.3	24.3	25.6	24.8	24.0	21.0	22.3	25.3	22.3	19.3	23.6
VM[1]	36.6	31.7	32.4	35.9	34.3	34.0	33.9	36.8	32.3	31.2	34.4	36.4	32.7
Fixed C	36.2	38.3	38.6	35.3	34.9	36.6	35.5	36.9	36.8	39.2	39.5	40.8	34.5
Ash	3.79	6.33	5.68	4.49	5.21	4.56	6.63	5.23	8.53	4.26	3.71	3.51	9.17
Calorific Value, Btu/lb	8957	9439	9438	9619	9234	9498	9201	9422	9317	9444	9434	10,681	8767
H	6.29	6.24	6.25	7.04	6.78	7.09	6.51	6.05	6.26	6.74	6.28	6.51	6.24
C	52.0	54.0	54.1	52.8	51.5	52.0	51.8	54.8	52.1	52.3	54.4	59.8	49.8
N	0.75	0.75	0.74	0.70	0.69	0.71	0.70	0.97	0.77	0.74	0.69	0.66	0.61
S	0.33	0.55	0.52	0.39	0.37	0.35	0.48	0.46	0.79	0.24	0.42	0.39	0.64
O	36.9	32.1	32.7	34.5	35.5	35.3	33.8	32.5	31.5	35.7	34.5	29.2	33.6

[1] Volatile matter.

TABLE 4

Coal Ash Elemental Oxide Composition, wt%

	Ant	BS	BS/SC	BTD	BTK	BTN	BT/CS	Cab	CS	Rch	SCM	SCN	Sarpy
SiO_2	24.8	39.4	38.6	33.1	32.5	27.5	38.2	29.3	39.1	36.8	36.0	25.3	45.2
Al_2O_3	17.2	19.9	19.7	17.1	16.5	16.2	20.1	13.2	21.9	20.3	19.1	18.4	20.7
Fe_2O_3	8.65	1.83	2.41	5.77	4.07	3.90	4.67	2.16	5.59	5.56	4.15	5.15	4.57
TiO_2	2.58	0.98	1.09	1.13	1.11	2.05	0.85	1.02	0.75	0.93	1.42	1.28	1.17
CaO	33.8	12.9	13.1	22.4	22.2	26.8	18.9	20.5	17.3	21.2	13.8	18.2	21.3
MgO	8.52	6.16	5.68	4.86	6.54	7.13	6.25	4.07	7.27	5.47	4.26	4.94	3.28
Na_2O	2.71	1.00	1.75	0.94	0.99	1.56	0.99	1.09	0.41	1.74	3.99	6.87	1.76
K_2O	<0.10	0.34	0.29	0.15	0.52	0.26	0.59	0.23	0.43	0.13	0.14	0.19	0.94
SO_3	NA[1]	15.1	15.3	14.9	15.5	10.5	10.4	22.8	9.60	12.2	16.0	15.6	NA

[1] Not analyzed.

TABLE 5

Quantitative Coal Mineralogy, wt%

	Ant	BS	BS/SC	BTD	BTK	BTN	BT/CS	Cab	CS	Rch	SCM	SCN	Sarpy
Kaolinite	9.7	53.6	52.6	33.7	27.0	29.7	37.7	24.2	42.3	29.5	49.4	33.4	19.8
Quartz	34.8	23.7	23.8	24.1	22.1	26.9	23.9	33.7	17.3	40.3	24.1	17.6	24.5
Pyrite	6.0	4.9	5.7	4.7	5.9	5.5	8.3	4.5	12.3	2.6	8.0	10.2	9.6
Illite	1.5	4.1	4.0	0.7	2.7	0.5	3.1	0.9	2.8	2.2	3.6	3.4	9.4
Calcite	1.8	3.4	2.8	1.6	ND[1]	ND	2.2	0.7	11.2	0.7	1.0	ND	25.4
Hematite	2.1	0.1	0.2	4.6	0.2	0.2	0.5	0.2	ND	1.2	0.5	ND	0.1
Barite	1.2	1.1	1.4	0.6	0.8	1.6	0.7	ND	1.0	2.0	2.4	5.8	0.9
Mixed Clays	4.1	3.3	3.4	8.8	11.2	5.2	10.8	8.4	7.6	5.4	3.9	3.8	2.6
Crandallite	6.0	0.1	0.1	9.8	9.8	12.6	4.1	9.5	0.2	8.0	0.2	1.7	0.5
Others	32.8	5.7	6.0	11.4	20.3	17.8	8.7	17.9	5.3	8.1	6.9	24.1	7.2

[1] Not detected.

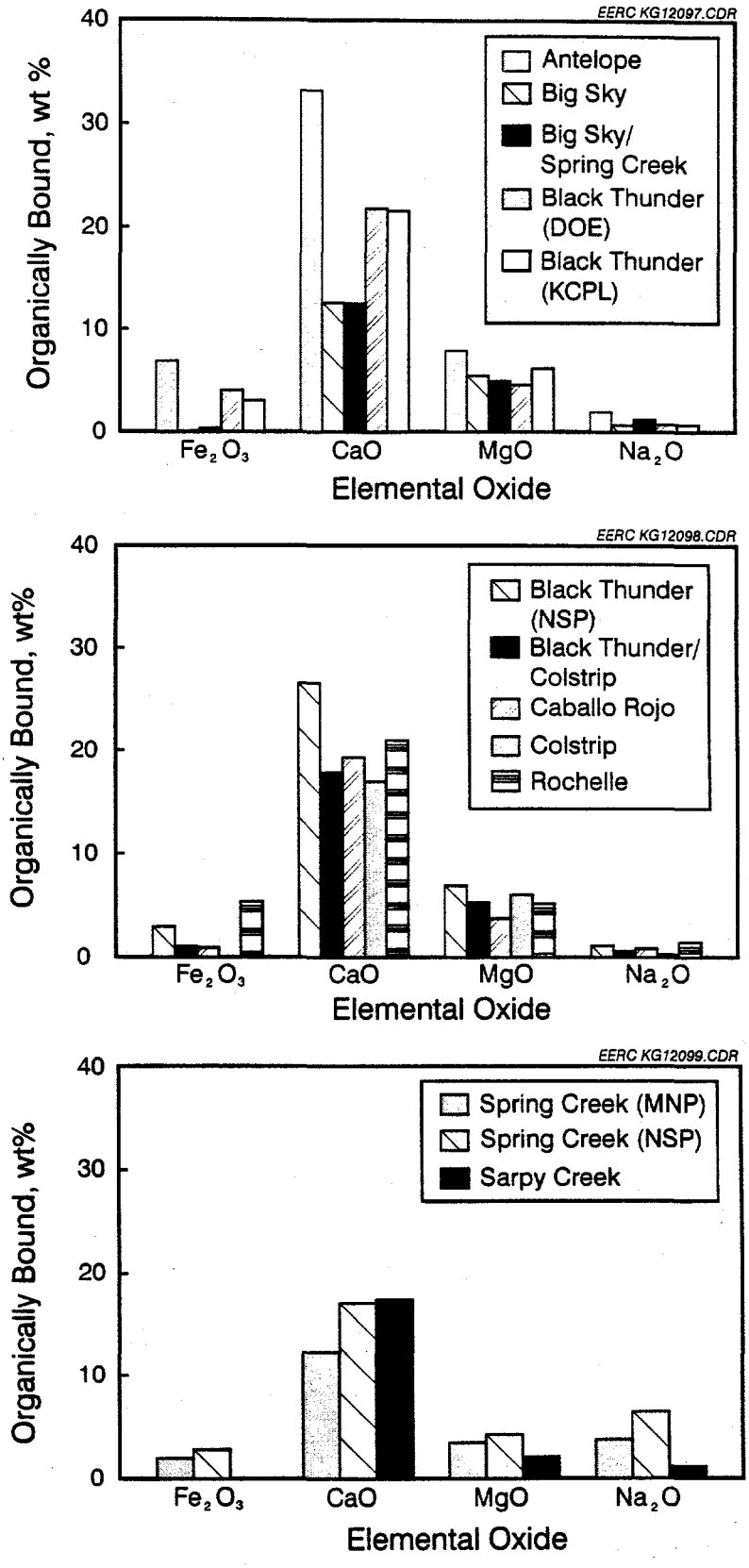

Figure 2. NH_4OAc- and HCl-soluble (organically bound) elemental oxide concentrations, wt%.

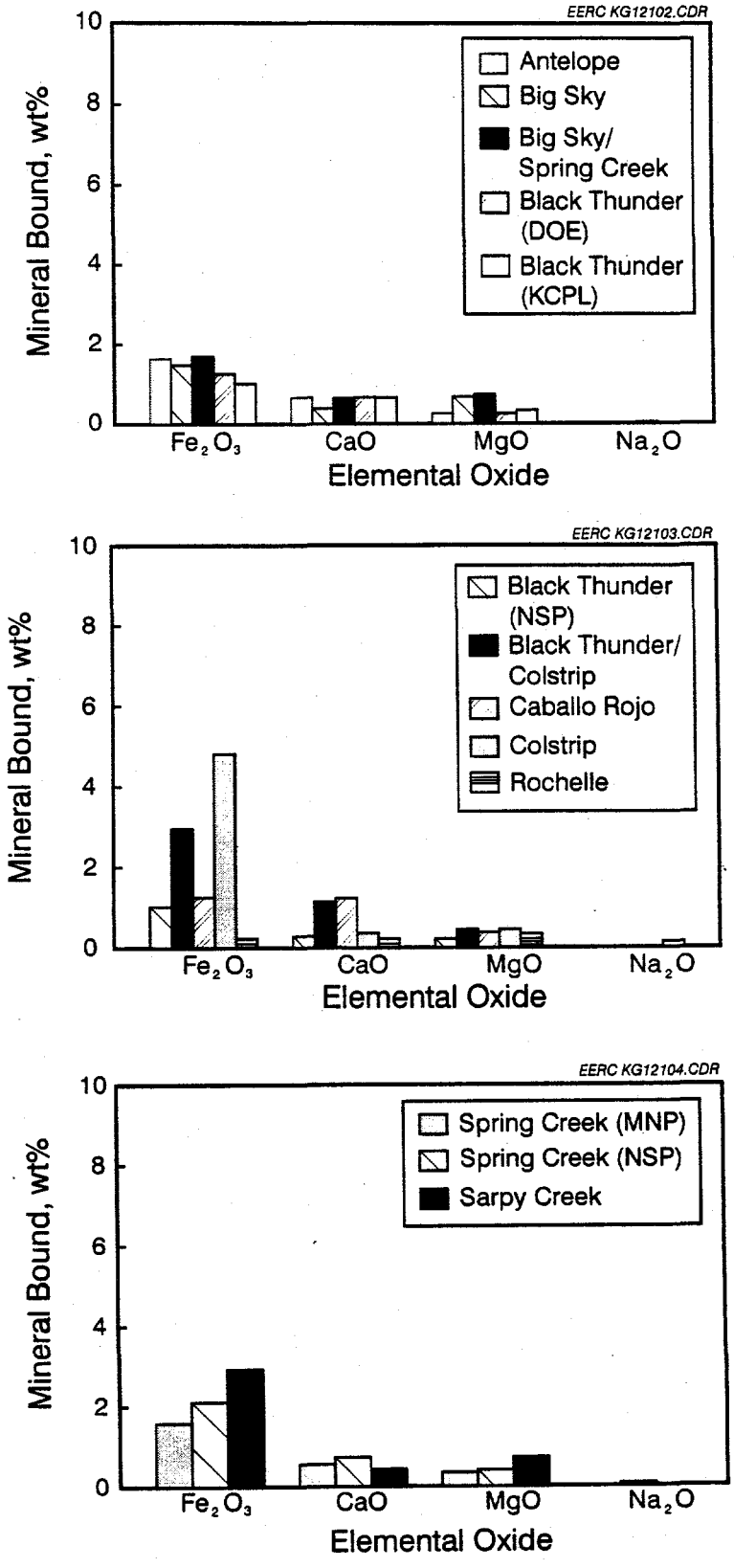

Figure 3. Insoluble (mineral-bound) elemental oxide concentrations, wt%.

The chemical fractionation analysis results are presented in Figures 2 and 3. The inorganic constituents removed by NH_4OAc and HCl, as indicated in Figure 2, are generally considered to be organically bound in the coal, whereas the inorganic constituents that remain in the residue after leaching, as indicated in Figure 3, are mineral-bound. Therefore, the chemical fractionation results indicate that Ca, Mg, and Na are associated primarily with the organic fraction of the coals, while Fe shows an intermediate affinity for the organic and mineral fractions.

3.0 DEVELOPMENT OF THE SLAGGING, HIGH- AND LOW-TEMPERATURE FOULING, SLAG-TAPPING, AND SOOTBLOWING INDICES

3.1 Introduction

Five indices pertaining to ash deposition and removability were developed: slagging, high- and low-temperature fouling, slag tapping, and sootblowing. The slagging index applies to the amorphous deposits that generally consist of aluminosilicate melts containing significant amounts of basic (fluxing) constituents. Slag deposits generally form when relatively large, sticky ash particles escape from flue gas entrainment forces and inertially impact on furnace waterwalls. In boilers designed for bituminous coals, the primary slagging coals contain relatively large amounts of pyrite and clays that can form high inertial energy and sticky entrained ash particles during combustion. Slagging severity can be greatly magnified if calcium is available to react with iron-rich phases.

The high-temperature fouling index pertains to the partially fused, silicate-based deposits that generally occur in the secondary superheater and reheater regions of a utility boiler. High-temperature fouling deposits result from the inertial impaction of relatively large particles. The particles initially impacting and adhering to the metal heat-exchange surfaces are those with sufficiently low viscosity to deform and stick rather than rebound on impact. As the deposit grows, the surface becomes insulated from the cooler heat-exchange surface, with a resulting increase in temperature and decrease in deposit viscosity. The deposit surface becomes sticky and entraps essentially all particles that impact.

The low-temperature fouling index applies to the alkali- and sulfate-bonded deposits that occur in the primary superheater and economizer regions of a boiler. Low-temperature deposits are composed of fine particles that deposit by means of thermophoretic forces and condensation. These deposits are typically rich in alkali and alkaline earth elements such as sodium and calcium. Condensation of sulfate species and reaction of the alkali and alkaline earth elements with sulfur dioxide in the gas stream results in the formation of dense, relatively hard, enamel-like layers. The speciation of calcium in coal is important for how readily it will react with sulfur to form strong calcium sulfate deposits (22). Calcium oxides and silicates react more readily than calcium that is bound as an aluminosilicate. PRB coals with an abundance of fine included quartz and organically bound calcium will usually result in abundant calcium silicates (23) that can deposit in lower-temperature regions and readily begin sulfating.

The slag-tapping index predicts how easily slag can be tapped from a cyclone boiler. Slags of relatively low viscosity are suitable for tapping. The relative effectiveness of sootblowers in removing deposits can be assessed using the sootblowing index. The removability of a deposit by

sootblowing will depend largely on the degree of strength development. Sintering is the primary mechanism by which a deposit develops strength.

The primary coal inorganic parameters that were used in developing the ash deposition and removability indices and their relation to combustion behavior can be summarized as follows:

1. Sodium content: Organically bound Na quickly enters the vapor phase as a hydroxide or sulfate and interacts with silica or aluminosilicates in deposits to accelerate deposit growth and strength development, especially in higher-temperature zones of the convective pass where silicate-based deposition occurs.

2. Calcium content: Organically bound Ca rapidly reacts with aluminosilicates and quartz, within coal particles, to form lower-melting-point eutectics that may enhance deposit formation. Depending on its association with other elements or compounds, Ca may react with S in lower-temperature zones to form $CaSO_4$-based deposits.

3. Total mineral content: Discrete minerals may have a diluting effect on deposit strength if their proportion relative to the organically bound content is greater than unity.

4. Organically bound content: Inorganics that are molecularly bound to the organic structure of the coal usually have a greater potential for reaction with minerals that are within coal particles. In addition, these dispersed inorganics are more likely to partition into the fine fly ash fraction; thus they are more readily transported to deposition areas in the convective pass of a boiler.

5. Quartz content: Fine quartz grains can react with organically bound Ca and Na within coal particles because of their large surface area-to-volume ratios. Such reactions produce relatively low melting-point phases.

6. Coal–mineral association relationships: Quartz and clay minerals are more likely to react with organically bound cations if they are included within coal particles rather than excluded from coal particles.

7. Calcite and dolomite content: Calcite and dolomite undergo decarbonation reactions very rapidly during coal combustion to produce a reactive fluxing material that readily dissolves in an aluminosilicate melt.

8. Clay content: Montmorillonite clays readily produce liquid phases during coal combustion.

9. Kaolinite content: Kaolinite can actually mitigate ash deposition by reacting with vaporized alkali and alkaline earth elements. Kaolinite decomposition products commonly react with Na and Ca to form the sodium aluminosilicate polymorphous minerals nepheline and carnegieite and calcium aluminosilicate minerals anorthite and gehlenite.

10. Pyrite content: Depending on its size, association relationship to coal particles, and association with other minerals such as carbonates and aluminosilicates, pyrite will greatly affect furnace wall slagging and high-temperature fouling deposit initiation.

The ash deposition indices were derived from bench-, pilot-, and full-scale combustion testing data (9–14). Additional bench-scale testing was performed on eight PRB subbituminous coals to verify and refine the ash deposition indices and to develop the ash removability indices (i.e., slag tapping and sootblowing). The coals were burned using the following combustion conditions: slagging, conventional and low-NO_x high-temperature fouling, and conventional and low-NO_x low-temperature fouling. The growth rates, sticking coefficients, in situ adhesion strengths, crushing strengths, initial slagging temperatures, porosities, and chemical and phase compositions of the deposits produced in the drop-tube furnaces (DTFs) were determined.

3.2 Experimental

3.2.1 Description of the Optical Drop-Tube Furnace

The optical DTF (ODTF), depicted in Figure 4, is a laboratory-scale, electrically heated, entrained-flow tube furnace for burning coal and producing ash under closely controlled conditions. The optical access section, shown in Figure 5, enables the visual and video monitoring of deposit formation and in situ deposit adhesion strength measurements. In situ temperature measurements by optical pyrometry can be made in the optical section of the furnace. The ODTF is especially designed to assess the fouling and slagging tendencies of coal ash. A cylindrical deposition probe with a controlled surface temperature can be inserted into the heated deposition zone and the initial slagging temperature, deposit adhesion strength, and deposit growth rates determined. The heated zones in the furnace reactor tube can be controlled to mimic temperature regimes in a full-scale utility boiler to a maximum temperature of 1650°C.

Growth and characterization of deposits were performed in the ODTF. The ODTF deposition probe simulates an actual boiler tube. An insulating refractory constrictor is used to accelerate the gas flow before it impinges on the deposit probe, which is located 1.0 in. below the constrictor. An expendable sample coupon is attached to the probe that can be maintained at temperatures corresponding to a boiler heat-transfer surface (350° to 540°C) by adjusting air and water-cooling flows. Coupon temperature is monitored and regulated by a Type K thermocouple.

The dimensions of deposits initially formed in the DTF systems, approximately 10 mm high with diameters of 2 to 3 mm, were inappropriate for accurately measuring crushing and adhesion strengths. The deposits were too slender because of the well-controlled laminar flow conditions in the DTF systems. A modification of the deposit probe enabled it to be translated along and rotated about the longitudinal probe axis in a controlled, repeatable pattern as the deposit formed. This resulted in the formation of uniform rectangular 4- to 5-mm-square deposits grown to a nominal height of 8 to 10 mm. To obtain valid adhesion strengths, it was necessary to ensure that the deposit was firmly adhering to the metal substrate rather than resting on a pile of loose ash particles. A miniature ceramic tube "sootblower" was fabricated and positioned close to the deposit base. Several "sootblowings" with compressed nitrogen were initiated as deposits formed to remove loose ash, thus ensuring that the remaining deposit base would adhere.

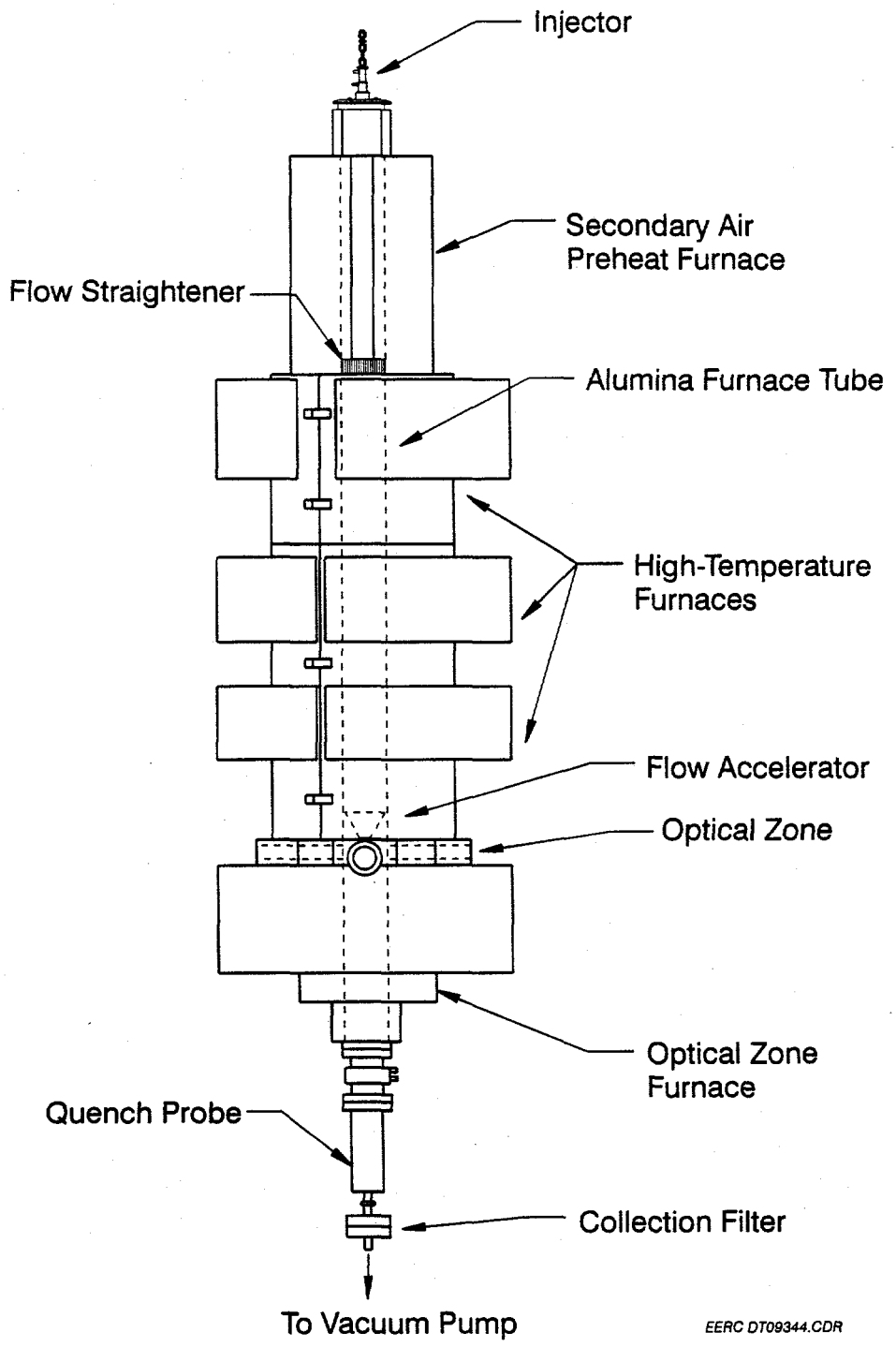

Figure 4. Schematic of the ODTF.

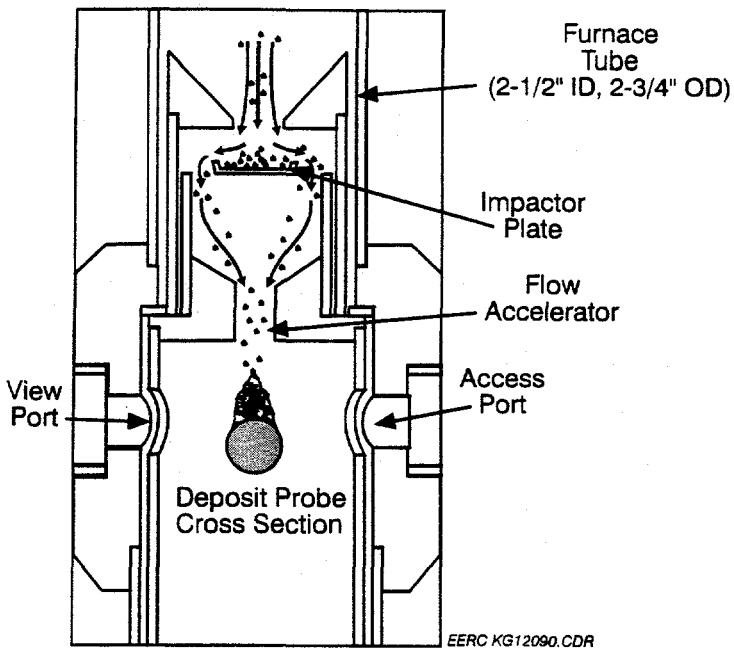

Figure 5. Schematic of the optical access section of the ODTF.

The apparatus used to determine the strength of ash deposits consisted of a miniature horizontal translator and a miniature pressure transducer. The transducer is mounted in a slot on top of an alumina block and attached to the horizontal translator. A rod inserted in the side of the block meets the sensing face of the transducer and transmits the force exerted on the deposit as the translator moves.

3.2.2 Description of the Atmospheric Drop-Tube Furnace

The atmospheric drop-tube furnace (ADTF) is similar in design to the ODTF except that it does not have an optical section. The furnace is capable of maintaining gas temperatures up to 1550°C. Combustion parameters—such as initial hot zone temperature, excess air, residence time, and gas cooling rate—can be closely controlled and monitored. Chars and ash can be collected at various residence times to examine the transformations that occur during the combustion process. Entrained ash can be collected in bulk or with size-segregating devices. Combustion gases are monitored for carbon dioxide, carbon monoxide, sulfur dioxide, and oxygen concentrations.

The ADTF was used for combustion testing involving entrained particulates. The fly ash quenching probe shown in Figure 6 is attached to the bottom of the ADTF to cool the fly ash before collection. Several collection devices can be added to the probe to collect the fly ash. The Environmental Protection Agency Southern Research Institute five-stage cyclone (EPAFSC) is used to collect size-segregated fly ash. The EPAFSC is designed to make five equally spaced

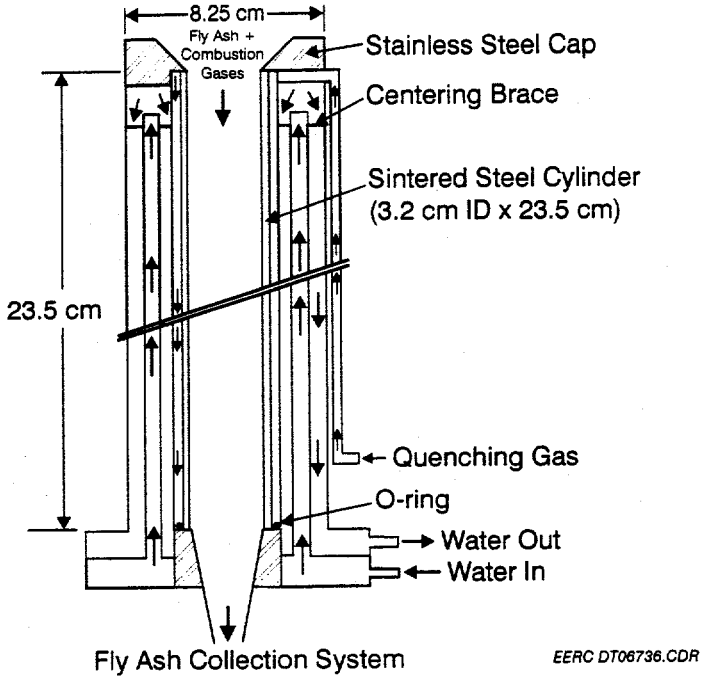

Figure 6. Schematic of the fly ash quenching probe.

particle-size cuts (D_{50}) on a logarithmic scale within the range of 0.1–10 microns. Depending on the size fractions desired, fewer cyclone stages may be used. The advantage of this system is its capability of collecting the relatively large sample amounts needed for subsequent chemical and morphological analysis. In addition to the EPAFSC, the University of Washington Mark 5 source test cascade impactor (STCI) was used during selected combustion tests. The STCI was developed as a means of measuring the size distribution of particles in stacks and ducts at air pollution emission sources. The Mark 5 impactor produces size cuts of fly ash particles by inertial separation. These data are used for comparison with the EPAFSC data to provide more detailed information concerning the effects of combustion conditions on the size distribution of the fly ashes. Finally, for collection of a bulk particulate sample, a filter assembly was attached to the exit of the quench probe.

3.2.3 Simulation of Conventional and Low-NO_x Combustion Conditions

Conventional combustion conditions were simulated in the DTF system; gas temperature at the coal injection point was maintained at 1530°C; gas temperature at the deposition point was 1230°C with a residence time of approximately 3.5 seconds, with 50% excess air injected with the coal in the primary gas stream. Low-NO_x conditions were simulated by lowering the furnace temperature profile to 1430°C and introducing 50% excess air with the secondary gas stream. Nitrogen was used to transport the coal in the primary gas stream. The lower temperature and slower mixing of fuel and air extended the burning time and significantly reduced both the thermal

and fuel NO_x, while still maintaining an acceptable level of carbon burnout and a 3.6-second residence time. Figure 7 indicates the furnace temperature profiles and gas flow configuration for conventional and low-NO_x combustion conditions.

3.2.4 Simulation of High- and Low-Temperature Fouling Conditions

Simulation of low-temperature fouling conditions in the DTF system was achieved by lowering the temperature in the deposition area, removing large ash particles from the gas stream, and introducing sulfur dioxide into the gas stream to encourage sintering. During low-temperature fouling, the temperature in the deposition zone was reduced from 1300° to 1000°C. Removal of larger particulate material was achieved by the mounting of a "cup" to act as a single-stage impactor immediately above the accelerator nozzle. Because the combustion products are highly diluted in the DTF system, sufficient SO_2 to maintain a level of 400 ppm was introduced from a separate tube coaxially surrounding the primary gas injection tube along the furnace center line.

3.2.5 Deposit Analysis

The coal deposits produced in various test conditions (conventional and low-NO_x high-temperature fouling, conventional and low-NO_x low-temperature fouling, and conventional slagging conditions) were analyzed using a scanning electron microscope point count method (SEMPC) described by Galbreath and others (18). Deposit porosity was also determined using SEM combined with digital image analysis techniques. In addition, selected crushed deposits were submitted for x-ray diffraction (XRD) analysis.

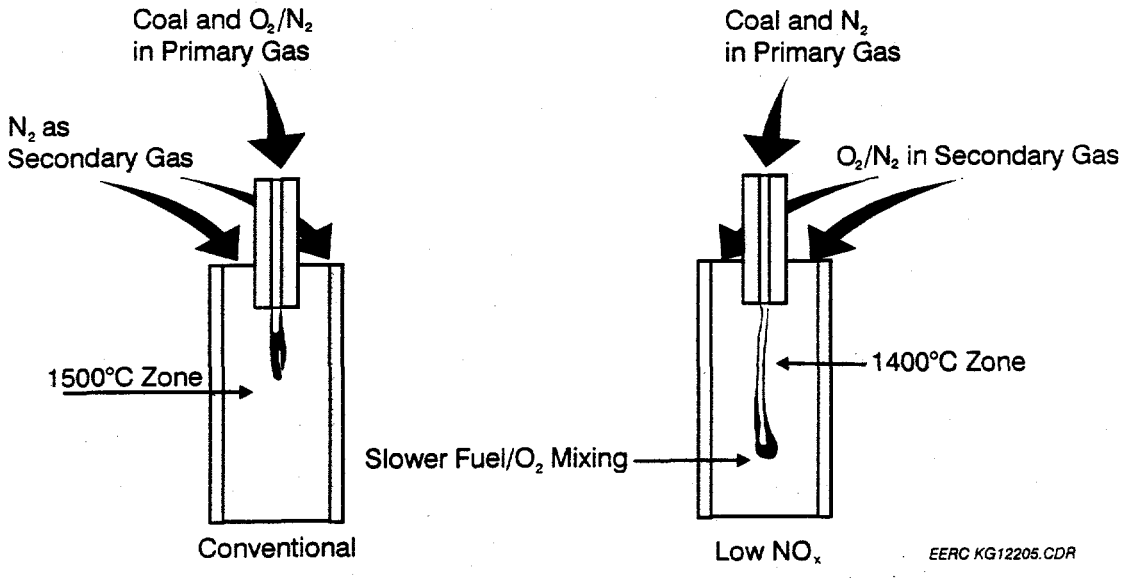

Figure 7. Comparison of temperature profiles and gas flow configurations for simulating conventional and low-NO_x combustion conditions.

3.3 Results

Deposits were produced using conventional high- and low-temperature fouling conditions as well as low-NO_x high- and low-temperature fouling conditions. Adhesion strengths, growth rates, sticking coefficients, and crushing strengths were determined for the deposits. Samples of the crushed deposits were saved for XRD analysis, and an intact deposit retained for cross-sectioning and SEM analysis. Slagging tests were performed using only conventional combustion conditions. As with the fouling deposits, deposit adhesion strength, growth rate, sticking coefficient, and crushing strength were determined. In addition, the initial slagging temperature was determined by growing a deposit and then slowly increasing the furnace temperature until the onset of deposit melting was observed.

A summary of measured deposit properties is given in Table 6. The coals produced deposits with generally similar sticking coefficients, growth rates, and initial slagging temperatures. Comparison of the deposits formed in conventional and low-NO_x combustion conditions reveals several trends. The adhesion strength of the high-temperature deposit to the substrate is generally significantly less for deposits formed in low-NO_x conditions. The exception is the Caballo Rojo deposits, which have quite low adhesion strengths in both conventional and low-NO_x conditions. Similarly, the high-temperature deposit crushing strengths, while showing a general increase from base to top of the deposit indicative of increased melting and mineral interaction, are again nearly always lower for deposits grown under low-NO_x conditions. The low-temperature fouling deposits generally do not show a significant difference between the conventional and the low-NO_x condition. This is ascribed to sulfonation of the calcium-rich deposits which is in contrast to the melting and sintering mechanism of deposit strength development that dominates in the high-temperature fouling deposits. The crushing strengths of the deposits grown under slagging conditions follow no constant trend, with the Antelope, Big Sky, Big Sky–Spring Creek Blend, and Sarpy Creek slagging deposits being weaker and the Black Thunder, Caballo Rojo, Rochelle, and Spring Creek deposits stronger than the corresponding conventional high-temperature fouling deposits. The higher temperature experienced by the deposits combined with the particular mineral composition and transformations at the elevated temperature appears to strongly influence the slagging deposit strength.

The deposits produced in the ODTF were analyzed using XRD and SEMPC methods. The deposits are largely amorphous. However, small crystals with chemical compositions consistent with the minerals clinopyroxene, melilite, plagioclase, and quartz were identified. The identity of these minerals was confirmed with XRD analysis results. In addition, several other mineral species were identified using XRD, as indicated in Table 7. A total of 250 randomly selected locations on each of the deposit samples were chemically analyzed using the SEM to estimate the relative proportions of the glass and mineral phases. The chemical compositions, in oxide weight percentages, were converted to numbers of cations per formula unit and then classified based on XRD mineral identifications and crystal chemical criteria (i.e., stoichiometry, cation-site occupancies, and charge balance) into mineral categories. Compositions that were inconsistent with the chemical formulae of minerals were classified as glass. The proportions of glass and mineral phases in the deposits are provided in Tables 8–11.

TABLE 6

Physical Properties of Deposits Produced in the ODTF

Coal Combustion Conditions	Antelope				Big Sky			75%BS-25%SC			Black Thunder (DOE)				
	HTF[1]	LNHTF[2]	LTF[3]	LNLTF[4]	HTF	LNHTF	SLAG	HTF	LNHTF	SLAG	HTF	LNHTF	SLAG	LTF	LNLTF
Adhesion Strength, psig	1.65	0.41	ND[5]	ND	0.53	0.21	NA[6]	0.92	0.27	NA	1.24	0.18	NA	ND	ND
Crushing Strength, psig															
Base	151	38	53	70	720	145	1130	1295	291	1106	125	112	1333	56	51
Middle	229	85	114	139	2207	385	978	3125	529	1348	400	114	3750	76	56
Tip	111	123	132	120	2292	259	848	1699	795	1387	700	105	2875	104	80
Average	164	82	100	110	1740	263	985	2040	538	1280	408	110	2653	79	62
Growth Factor	0.83	0.76	0.61	0.61	0.7	0.7	0.62	0.68	0.78	0.62	0.63	0.63	0.57	0.69	0.67
Sticking Fraction	0.69	0.60			0.52	0.58	0.54	0.53	0.63	0.61	0.44	0.35	0.44		
Initial Slagging Temp.,°C	NA	NA	NA	NA	NA	NA	1245	NA	NA	1240	NA	NA	1195	NA	NA

	Caballo Rojo			Rochelle			Spring Creek (NSP)					Sarpy Creek	
	HTF	LNHTF	SLAG	HTF	LNHTF	SLAG	HTF	LNHTF	SLAG	LTF	LNLTF	HTF	LNHT
Adhesion Strength, psig	0.45	0.50	NA	3.42	0.81	NA	3.40	1.13	NA	ND	ND	2.87	0.25
Crushing Strength, psig													
Base	449	132	>2500	593	45	1672	629	177	596	232	230	1235	253
Middle	684	238	>2500	1796	651	1894	1761	279	1553	519	501	984	458
Tip	571	453	>2500	2131	1113	1274	1252	923	2151	861	300	2018	319
Average	568	274	>2500	1507	603	1613	1214	460	1433	537	344	1412	343
Growth Factor	0.76	0.77	0.63	0.86	0.66	0.54	0.76	0.77	0.54	0.6	0.6	0.79	0.77
Sticking Fraction	0.53	0.55	0.5	0.69	0.5	0.47	0.55	0.52	0.4			0.57	0.56
Initial Slagging Temp.,°C	NA	NA	1180	NA	NA	1205	NA	NA	1215	NA	NA	NA	NA

[1] High-temperature fouling.
[2] Low-NO_x high-temperature fouling.
[3] Low-temperature fouling.
[4] Low-NO_x low-temperature fouling.
[5] Not determined.
[6] Not applicable.

TABLE 7

Deposit Mineral Species

Mineral	Nominal Chemical Formula
Anhydrite	$CaSO_4$
Bredigite	$Ca_{14}Mg_2(SiO_4)_8$
Brownmillerite	$Ca_2(Al,Fe)_2O_5$
Clinopyroxene	$Ca(Mg,Fe,Al)(Si,Al)_2O_6$
Hematite	Fe_2O_3
Lime	CaO
Melilite	$(Ca, Na)_2(Al,Mg,Fe)(Si,Al)_2O_7$
Merwinite	$Ca_3(Mg,Fe)Si_2O_8$
Mullite	$Al_6Si_2O_{13}$
Nepheline	$(Na,K)AlSiO_4$
Periclase	MgO
Plagioclase	$(Ca,Na,K)(Al,Si)_4O_8$
Quartz	SiO_2
Spinel	$(Mg,Fe)(Fe,Al)_2O_4$

TABLE 8

Quantitative Mineralogy of Slag Deposits Produced in the ODTF, frequency %

	BS	BS/SC	BTD	Cab	Rch	SCN
Clinopyroxene	<1	ND[1]	ND	<1.0	1	ND
Hematite	3	4	2	<1.0	ND	1
Plagioclase	<1	4	6	10	2	18
Quartz	22	18	18	19	18	10
Glass	74	74	74	69	79	71

[1] Not detected.

TABLE 9

Quantitative Mineralogy of the High-Temperature Fouling Deposits Produced in the ODTF Using Conventional Combustion Conditions, frequency %

Source Coal	Ant	BS	BS/SC	BTD	Cab	Rch	Sarpy	SCN
Brownmillerite	2	ND[1]	ND	<1	<1	ND	ND	ND
Clinopyroxene	4	2	<1	6	4	3	<1	<1
Hematite	ND	<1	<1	<1	<1	ND	<1	ND
Lime	<1	ND	ND	ND	ND	ND	ND	<1
Melilite	6	<1	4	17	20	12	17	25
Merwinite	ND	ND	ND	ND	<1	<1	<1	<1
Periclase	<1	ND	ND	<1	ND	ND	ND	ND
Plagioclase	ND	12	15	<1	ND	1	4	1
Quartz	2	8	13	6	3	7	3	4
Spinel	ND	ND	ND	ND	<1	ND	ND	ND
Glass	87	77	66	71	72	76	74	70

[1] Not detected.

TABLE 10

Quantitative Mineralogy of the High-Temperature Fouling Deposits Produced in the ODTF Using Low-NO_x Combustion Conditions

Source Coal	Ant	BS	BS/SC	BTD	Cab	Rch	Sarpy	SCN
Anhydrite	2	ND[1]	ND	<1	<1	ND	<1	ND
Brownmillerite	<1	ND	ND	ND	ND	ND	ND	ND
Clinopyroxene	1	1	<1	4	10	6	2	4
Hematite	ND	ND	1	<1	<1	<1	1	ND
Lime	<1	ND	ND	ND	ND	ND	ND	ND
Melilite	1	1	3	16	14	8	14	15
Merwinite	ND	ND	ND	<1	2	<1	<1	<1
Mullite	<1	<1	<1	ND	ND	ND	ND	ND
Periclase	<1	ND	ND	<1	ND	ND	ND	ND
Plagioclase	ND	6	14	<1	2	3	6	2
Quartz	3	14	10	4	5	10	6	3
Spinel	ND	ND	ND	<1	ND	ND	ND	ND
Glass	82	78	72	76	66	73	71	76

[1] Not detected.

TABLE 11

Quantitative Mineralogy of the Low-Temperature Fouling Deposits Produced in the ODTF Using Conventional and Low-NO_x Combustion Conditions

	Conventional Combustion			Low-NO_x Combustion		
	Ant	BTD	SCN	Ant	BTD	SCN
Anhydrite	13	8	15	21	7	18
Bredigite	<1	<1	ND[1]	<1	2	ND
Brownmillerite	2	<1	ND	<1	1	ND
$CaAl_2O_4$	<1	<1	ND	<1	<1	ND
Melilite	5	10	12	6	12	8
Nepheline	ND	ND	<1	ND	ND	<1
Periclase	<1	<1	<1	<1	<1	ND
Quartz	6	4	<1	<1	6	<1
Spinel	<1	<1	<1	<1	<1	<1
Glass	74	76	72	72	73	72

[1] Not detected.

The proportions of glass in the various types of deposits are generally similar, presumably because of the similar cooling histories that the samples experienced during collection. The mineral assemblages and proportions, however, vary significantly among the different deposit types. The slag deposits are characterized by a relatively simple mineral assemblage of quartz + plagioclase + hematite ± clinopyroxene (Table 8), which is indicative of mineral-melt equilibrium. The high- and low-temperature fouling deposits, however, are composed of complex mineral assemblages (Tables 9–11) and a compositionally heterogeneous glass phase. Quartz and melilite are ubiquitous minerals in the fouling deposits. The quartz grains are relatively large in comparison to other minerals and generally subrounded, indicating that they were relatively inert during the coal combustion and subsequent deposit formation processes. The crystal morphologies of the other silicate minerals in the deposits, however, indicate that they formed during the rapid solidification of a melt. The different combustion conditions (conventional and low-NO_x) used to produce the fouling deposits appear to have had a negligible effect on mineral and glass-phase proportions. In some deposits, however, the low-NO_x conditions apparently caused the crystallization of anhydrite and mullite.

The average bulk compositions of the deposits were calculated (on an SO_3-free basis) based on the 250 chemical microanalyses performed on each deposit. These deposit compositions were used to calculate enrichment–depletion factors (i.e., ratios of elemental oxide concentrations in the deposits to concentrations in their corresponding coal ashes). The enrichment–depletion factors are presented in Tables 12–15. Factors of greater than 1.2 or less than 0.8 are considered significant based on the dispersion introduced in the values by sampling and analytical uncertainties. The

TABLE 12

Enrichment–Depletion Factors for the Slag Deposits Produced in the ODTF

	BS	BS/SC	BTD	Cab	Rch	SCN	Average
SiO_2	1.4	1.3	1.6	1.6	1.8	2.0	1.6
Al_2O_3	0.7	0.7	0.8	0.8	0.6	0.8	0.7
Fe_2O_3	2.7	3.4	0.9	1.3	0.6	0.8	1.6
CaO	0.4	0.5	0.4	0.5	0.4	0.3	0.4
MgO	0.2	0.2	0.4	0.3	0.4	0.3	0.3
Na_2O	0.7	0.4	0.6	0.7	0.7	0.4	0.6
K_2O	1.0	1.4	1.8	1.0	2.1	1.7	1.5

TABLE 13

Enrichment–Depletion Factors for the High-Temperature Fouling Deposits Produced in the ODTF Using Conventional Combustion Conditions

	Ant	BS	BS/SC	BTD	Cab	Rch	Sarpy	SCN	Average
SiO_2	0.9	1.1	1.1	0.9	0.9	1.1	0.9	1.3	1.0
Al_2O_3	0.9	1.0	0.9	0.8	1.0	0.8	1.0	0.9	0.9
Fe_2O_3	1.0	1.2	1.0	0.8	1.6	0.8	0.8	0.6	1.0
CaO	1.3	1.1	1.0	1.3	1.2	1.1	1.3	1.0	1.2
MgO	1.0	0.7	0.7	1.2	0.8	1.0	1.1	0.9	0.9
Na_2O	0.3	1.1	0.8	0.6	0.7	0.6	0.8	0.6	0.7
K_2O	1.0	0.7	1.1	1.8	1.0	2.1	0.5	1.7	1.2

factors indicate that, on average, the slag deposits are enriched in SiO_2, Fe_2O_3, and K_2O but depleted in CaO, MgO, and Na_2O relative to their corresponding ash precursors (Table 12). A significant proportion of the SiO_2 occurs as relict quartz grains (Table 8) in the slag deposits. The Fe_2O_3 and K_2O enrichments indicate that pyrite (FeS_2) and illite ($K[Si,Al]_4O_{10}[OH]_2 \cdot H_2O$), respectively, are important indicators of slagging propensity. The high-temperature fouling deposits produced in conventional and low-NO_x combustion conditions are depleted in Na_2O relative to their corresponding ash precursors (Tables 13 and 14). The other oxide components are insignificantly enriched or depleted. Thus most of the inorganic coal constituents participate equally in the high-temperature deposit formation process. The low-temperature fouling deposits (Table 15) are generally depleted in SiO_2 and Na_2O but enriched in CaO and MgO. Apparently,

TABLE 14

Enrichment–Depletion Factors for the High-Temperature Fouling Deposits Produced in the ODTF Using Low-NO_x Combustion Conditions

	Ant	BS	BS/SC	BTD	Cab	Rch	Sarpy	SCN	Average
SiO_2	1.0	1.1	1.1	0.7	0.9	1.1	0.9	1.2	1.0
Al_2O_3	0.9	0.9	1.0	0.9	1.0	0.8	1.0	0.9	0.9
Fe_2O_3	0.9	1.8	1.4	0.9	1.9	0.9	0.8	0.7	1.2
CaO	1.3	1.0	0.9	1.4	1.1	1.1	1.3	1.1	1.1
MgO	0.9	0.6	0.6	1.5	0.9	0.9	1.0	0.9	0.9
Na_2O	0.3	0.8	0.8	0.4	0.6	0.6	0.7	0.4	0.6
K_2O	2.0	1.0	1.4	1.2	0.6	1.4	0.7	1.3	1.2

TABLE 15

Enrichment–Depletion Factors for the Low-Temperature Fouling Deposits Produced in the ODTF Using Conventional and Low-NO_x Combustion Conditions

	Conventional Combustion			Low-NO_x Combustion		
	Ant	BTD	SCN	Ant	BTD	SCN
SiO_2	1.0	0.6	0.7	0.7	0.7	0.7
Al_2O_3	0.9	0.9	1.0	1.0	0.9	1.0
Fe_2O_3	0.9	1.0	1.0	1.1	0.9	1.0
CaO	1.2	1.5	1.5	1.3	1.4	1.6
MgO	0.9	1.4	1.3	1.0	1.5	1.3
Na_2O	0.5	0.8	0.3	0.5	0.7	0.3
K_2O	2.0	1.2	0.8	1.0	1.8	0.8

the amount of organically bound Ca and Mg in a coal is an important variable to consider in predicting low-temperature fouling propensity. The low-temperature fouling deposits are also enriched in SO_3, as evidenced by the relatively high concentrations of anhydrite (Table 11).

Deposit porosities, defined here as the percentage of epoxy (voids) in the deposit structure, are given in Table 16 for the lower and upper portions of the deposits. In general, there is a significant decrease in deposit porosity (a denser deposit with fewer voids) from base to top of the deposit. This is a result of sintering processes occurring as a result of increasing temperature as the growing deposit becomes insulated from the cooled probe substrate. Comparison with the base and top deposit crushing strengths reported in Table 6 shows a general increasing trend in deposit crushing strength with height in the deposits. It is noted that the top of the deposit is usually, but not always, stronger than the middle or base. Further, it appears that deposit porosity is unrelated to deposit crushing or adhesion strength. Although the deposit porosity decreases with increased sintering and a generally higher deposit crushing strength, the crushing strength at a given porosity can vary by two orders of magnitude for different deposits. It appears that deposit mineral composition as well as the sintering transformations are the dominant causes of deposit strength, rather than the simple densification reflected by the deposit porosity. In some cases, presumably by incorporation of refractory materials at elevated temperature, the deposit crushing strength is actually less at the top than at the base or intermediate height. It can be concluded that deposit porosity is not a good indicator, per se, of deposit strength or removability.

3.4 Index Formulations

3.4.1 Slagging Index

The slagging index (SI) algorithm is of the general form:

$$SI \alpha ([A \times B] + C + D) + (E \times F) + G + (H/I).$$

The variables in the SI algorithm are defined in Table 17.

3.4.2 High-Temperature Fouling Index

The high-temperature fouling (HTF) index algorithm is of the general form:

$$HTF \alpha ([A \times B] + C + D) + (E^2 \times F^2) + (G^5 \times F) + (H/I).$$

The variables in the HTF algorithm are defined in Table 18.

3.4.3 Low-Temperature Fouling Index

The low-temperature fouling (LTF) index algorithm is of the general form:

$$LTF \alpha ([A \times B \times C \times D \times E \times F] / [G \times H \times I/J]) \times K/L \times M$$

The variables in the LTF algorithm are defined in Table 19.

TABLE 16

Deposit Porosities, % void

	Antelope		Big Sky		Big Sky/SpCreek		Black Thunder		Caballo Rojo		Rochelle		Sarpy Creek		Spring Creek	
	Base	Top	Base	Top	Base	Top	Base	Top	Base	Top	Base	Top	Base	Top	Base	Top
Slagging Conventional	84.85	58.34	81.84	61.89	79.08	53.40	84.43	19.35	83.13	30.69	ND[1]	ND	ND	ND	82.41	47.24
High-Temperature Fouling Conventional	84.37	69.65	85.60	47.37	72.61	42.90	70.54	59.04	76.79	58.23	77.14	47.92	76.76	55.20	78.66	49.47
High-Temperature Fouling Low NO_x	ND	ND	ND	ND	ND	ND	ND	ND	ND	ND	ND	ND	ND	ND	ND	ND
Low-Temperature Fouling Conventional	72.60	59.80	ND	ND	ND	ND	ND	ND	ND	ND	ND	72.70	69.70	ND	58.90	51.50
Low-Temperature Fouling Low-NO_x	60.50	49.20	ND	ND	ND	ND	ND	ND	ND	ND	ND	68.00	53.10	ND	55.90	43.60

[1] Not determined.

TABLE 17

Definitions of Slagging Index Variables

Variable	Parameter(s)	Method	Unit
A	Pyrite + clays	CCSEM	wt%, mineral basis
B	Organically bound Ca	CF[1]	% removed by NH_4OAc
C	Organically bound Mg	CF	% removed by NH_4OAc
D	Calcite + dolomite	CCSEM	wt%, mineral basis
E	$MgO + Na_2O + K_2O$	ASTM D4326	wt%, ash basis
F	Included quartz + clays	CCSEM	Frequency %
G	Included pyrite + clays	CCSEM	Frequency %
H	Quartz	CCSEM	wt%, mineral basis
I	Illite + montmorillonite + kaolinite	CCSEM	wt%, mineral basis

[1] Chemical fractionation.

TABLE 18

Definitions of High-Temperature Fouling Index Variables

Variable	Parameter(s)	Method	Unit
A	Included pyrite + clays	CCSEM	Frequency %
B	Organically bound Ca	CF[1]	% removed by NH_4OAc
C	Organically bound Mg	CF	% removed by NH_4OAc
D	Calcite + dolomite	CCSEM	wt%, mineral basis
E	Organically bound Ca + Mg + Na + K	CF	% removed by NH_4OAc
F	Included quartz + clays	CCSEM	Frequency %
G	Organically bound Na	CF	% removed by NH_4OAc
H	Organically bound Ca + Mg + Na + K + Al + Fe + Ti + P	CF	% removed by NH_4OAc
I	Ash	ASTM D3172	wt%, as-received

[1] Chemical fractionation.

TABLE 19

Definitions of Low-Temperature Fouling Index Variables

Variable	Parameter(s)	Method	Unit
A	Organically bound Na + Mg	CF[1]	% removed by NH_4OAc
B	<4.6-μm quartz	CCSEM	wt%, mineral basis
C	<4.6-μm calcite + dolomite	CCSEM	wt%, mineral basis
D	Calcium aluminophosphate	CCSEM	wt%, mineral basis
E	Organically bound Ca + Mg	CF	% removed by NH_4OAc
F	SO_3	ASTM D4326	wt%, ash basis
G	Included illite + kaolinite + montmorillonite	CCSEM	Frequency %
H	Excluded kaolinite	CCSEM	Frequency %
I	Total mineral bound inorganics	CCSEM	wt%, coal basis
J	Total organically bound inorganics	CF, ASTM D3172	wt%, coal basis
K	Quartz	CCSEM	wt%, mineral basis
L	Illite + kaolinite + montmorillonite	CCSEM	wt%, mineral basis
M	Na_2O	ASTM D4326	wt%, ash basis

[1] Chemical fractionation.

3.4.4 Slag-Tapping Index

The slag-tapping index (STI) equation is of the general form:

$$STI \alpha (A/B + C/D + 1/E + F/G + [2 \times H] - I)$$

The variables in the STI equation are defined in Table 20.

3.4.5 Sootblowing Index

The sootblowing index estimates the removability of a deposit. Adhesion and crushing strength measurements of deposits generated in the DTF were the primary factors used to derive the index. Correlations were made between the inorganic components which can cause accelerated sintering and solidifying of deposits and deposit strength as related to resistance to be removed. A higher index value indicates more difficulty for removing the deposit.

The sootblowing index (SBI) algorithm is of the general form:

$$SBI \alpha (A + B - C - D)$$

The variables in the SBI equation are defined in Table 21.

TABLE 20

Definitions of Slag-Tapping Index Variables

Variable	Parameter(s)	Method	Unit
A	Moisture	ASTM D3176	wt%, as received
B	Btu	ASTM D2015	Btu/lb, as received
C	Quartz	CCSEM	wt%, mineral basis
D	Ash	ASTM D3172	wt%, as received
E	Na_2O	ASTM D4326	wt%, ash basis
F	Kaolinite	CCSEM	wt%, mineral basis
G	Quartz	CCSEM	wt%, mineral basis
H	Pyrite + barite	CCSEM	wt%, mineral basis
I	Calcium aluminophosphate	CCSEM	wt%, mineral basis

TABLE 21

Definitions of Sootblowing Index Variables

Variable	Parameter(s)	Method	Unit
A	Organically bound Mg	CF[1]	% removed by H_2O and NH_4OAc
B	Organically bound CA	CF	% removed by H_2O and NH_4OAc
C	Organically bound Na	CF	% removed by H_2O and NH_4OAc
D	≤10-μm quartz	CCSEM	wt%, mineral basis

[1] Chemical fractionation.

3.5 Application of the Ash Deposition and Removability Indices

3.5.1 Slagging Index

Calculated slagging index values for the thirteen FPI test coals are compared in Figure 8. The values were calculated assuming conventional combustion conditions. According to the index, the Black Thunder (NSP), Caballo Rojo, and Spring Creek (NSP) coals are predicted to pose a low slagging propensity; the Antelope, Black Thunder (DOE), Black Thunder (KCPL), Rochelle, and Spring Creek (MNP) coals are expected to cause a medium slagging propensity; and the Big Sky, Big Sky–Spring Creek, Black Thunder–Colstrip, Colstrip, and Sarpy Creek coals are predicted to produce the most severe slagging problems.

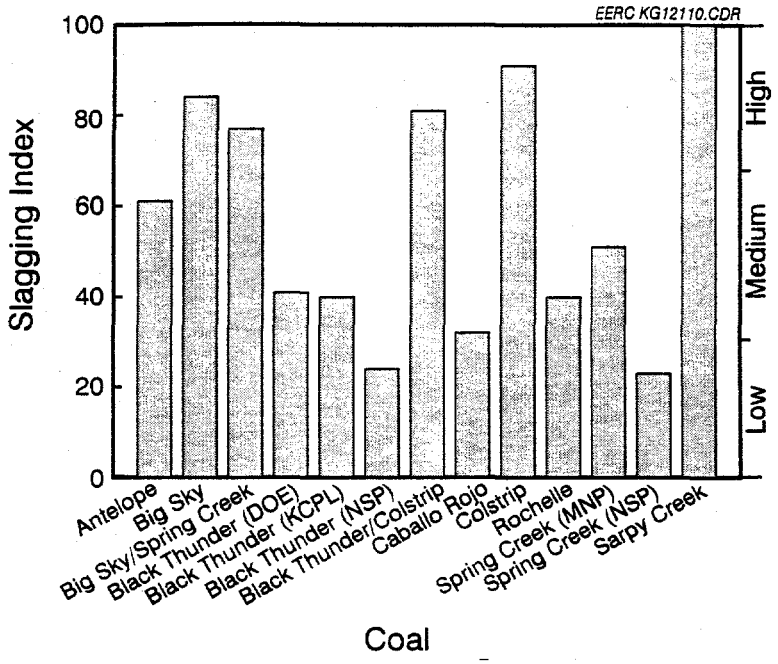

Figure 8. Comparison of slagging index values for the thirteen FPI test coals.

3.5.2 High-Temperature Fouling Index

The results of applying the high-temperature fouling index to the thirteen test coals are presented in Figure 9. Most of the coals have a medium propensity for high-temperature fouling, except the Caballo Rojo coal and the Spring Creek (NSP) coals—which are predicted to pose low and high high-temperature fouling propensities, respectively.

3.5.3 Low-Temperature Fouling Index

The application of the low-temperature fouling index to the thirteen test coals, Figure 10, indicates that the majority of coals should not cause significant fouling problems in the cooler primary superheater and economizer regions of a boiler. The Antelope coal, however, is predicted to cause significant low-temperature fouling problems.

3.5.4 Slag-Tapping Index

Slag-tapping index values for the thirteen test coals are compared in Figure 11. The values indicate that all of the coals are inappropriate for use in a cyclone boiler. The coals are predicted to produce a relatively high-viscosity slag primarily because of their high kaolinite contents (Table 5).

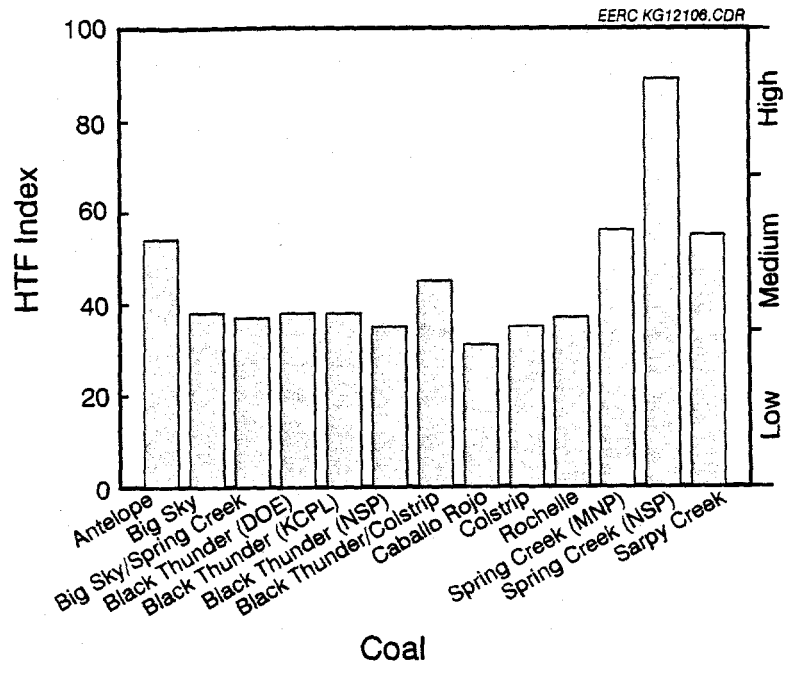

Figure 9. Comparison of high-temperature fouling (HTF) index values for the thirteen FPI test coals.

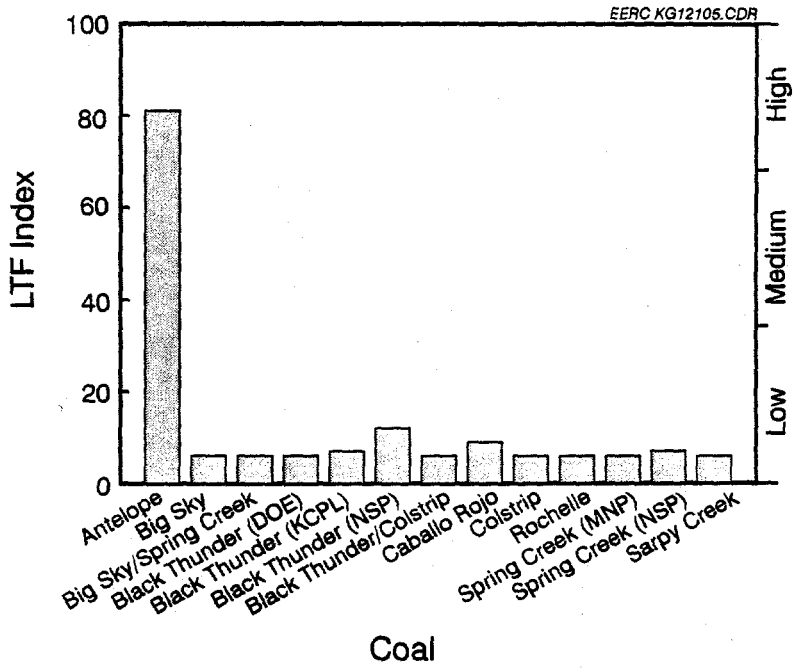

Figure 10. Comparison of low-temperature fouling (LTF) index values for the thirteen FPI test coals.

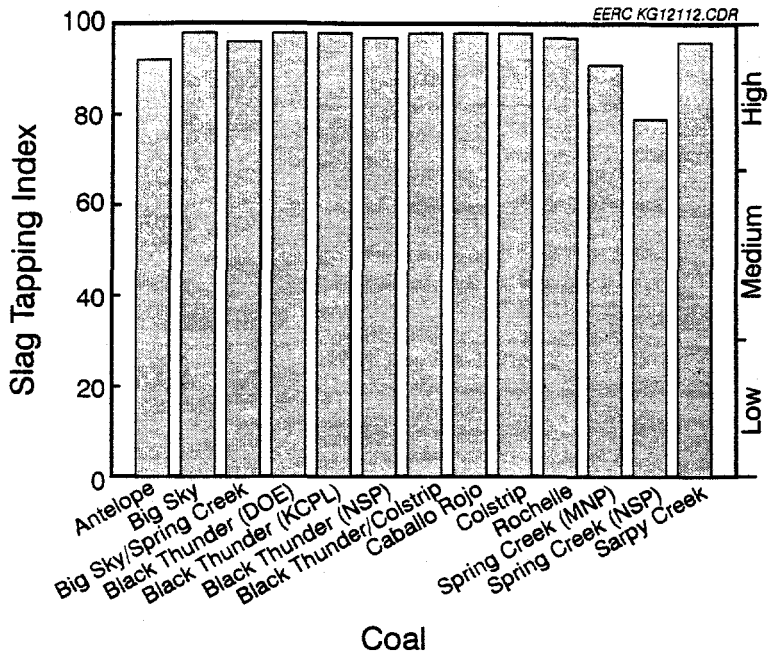

Figure 11. Comparison of slag-tapping index values for the thirteen test coals.

3.5.5 Sootblowing Index

The application of the sootblowing index indicates variability in the removability propensities of deposits produced from the thirteen test coals (Figure 12). About one-half of the coal deposits (Big Sky, Big Sky–Spring Creek, Black Thunder [DOE], Caballo Rojo, Rochelle, Spring Creek [MNP], and Spring Creek [NSP]) are expected to be easily removed by sootblowing. The other coals are expected to produce deposits more difficult to remove. Poor sootblower effectiveness is expected for the Antelope, Black Thunder (KCPL), Black Thunder (NSP), Black Thunder–Colstrip, and Colstrip coals. The effectiveness of sootblowing for removing deposits produced from the Sarpy Creek coal is predicted to be intermediate with respect to the other coals.

4.0 DEVELOPMENT OF THE STACK PLUME OPACITY INDEX

4.1 Introduction

Stack plume visibility, also known as opacity, is caused by the scattering of light by fine ash particles and by the absorption of light by fine particles and flue gas components. Ash particles in the 0.2- to 1.5-μm size range most effectively scatter light; carbon particles in the 0.15- to 0.5-μm size range most effectively absorb light; and NO_2 is the predominant flue gas species responsible for light absorption (24, 25). The concentration of fine ash particles emitted from a utility's stack

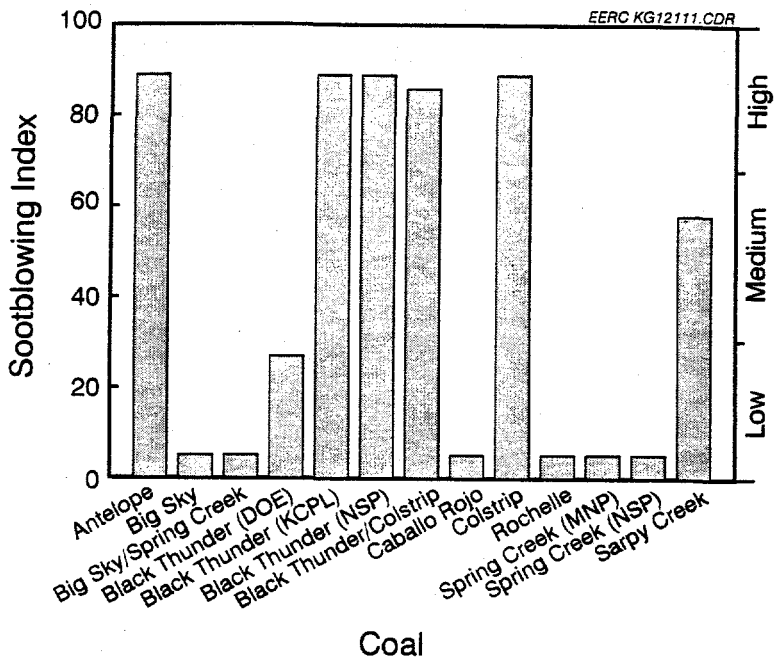

Figure 12. Comparison of sootblowing index values for the thirteen test coals.

is related primarily to coal mineral matter characteristics, whereas the emission concentrations of carbon particles and NO_2 are related primarily to boiler design and operation. In current pulverized combustion systems, carbon particle and NO_2 emissions are controlled except during periods of faulty operation. Consequently, the scattering of light by fine ash particles is the primary mechanism to consider in developing an opacity index. According to the Mie theory (26), light scattering is influenced strongly by the fine ash particle concentration.

The possible coal mineral matter sources of fine ash particles that may promote high opacity must be identified before an index can be formulated. During the combustion of pulverized coals, fine ash particles can be produced by the following mechanisms: combustion of small (< 30 μm) coal particles (27), thermal metamorphism of small (< 10 μm) extraneous mineral particles (26), char fragmentation (28, 29), mineral fragmentation (30), and mineral matter vaporization followed by condensation (31). All of these mechanisms may be operative during combustion, with the relative influence of each determined primarily by the pulverized coal and mineral particle-size distributions, the macroporosity of char, the thermal physicochemical properties of minerals, the degree of mineral–maceral association, and the amount of volatile inorganic species available to vaporize and subsequently condense.

The removal of ash from flue gas by electrostatic precipitation is influenced by ash concentration, particle-size distribution, and electrical resistivity (32, 33). The efficiency of fabric filter-based cleaning systems for removing ash is also dependent on particle size. Both systems

have reduced collection efficiencies for fine ash particles, which are the most effective in scattering light. Therefore, an opacity index must account for ash concentration, particle-size distribution, and electrical resistivity.

Bench-scale tests of ash formation were conducted on eight PRB coals using the ADTF equipped with a multicyclone ash collection device. The total fine ash mass concentration for the test coals was measured, and samples of size-fractionated ash were obtained. The fine ash fractions were analyzed using CCSEM. Improvements in particulate sample preparation methods (34) have enabled the SEM examination of a statistically significant sampling of individual ash particles with submicron diameters as small as 0.1 μm. The fine-ash mass concentrations and ash analysis results were compared to CCSEM coal mineral analysis results to deduce the mineral matter sources of fine ash production. Based on this comparison, equations for estimating the concentration of fine ash produced from burning subbituminous coals were formulated and incorporated into an index for predicting opacity propensity. The effects of combustion conditions (conventional or low-NO_x) on fine ash formation and ash electrical resistivity on electrostatic precipitator (ESP) collection efficiency were also considered in the index.

4.2 Experimental

The following coals were used in DTF ash formation tests: Antelope, Big Sky, 75% Big Sky–25% Spring Creek blend, Black Thunder (DOE), Caballo Rojo, Rochelle, Spring Creek (NSP), and Sarpy Creek. The test coals were pulverized in a Micron Powder Bantam Jet Mill. Sieve analysis were performed to verify that the particle-size distributions of the coals were consistent with standard utility boiler practice (i.e., 70%–80% of the coal particles less than 200 mesh). A representative portion of each pulverized coal was analyzed using CCSEM. DTF ash formation tests were conducted on all the coals using conventional combustion conditions and on the Black Thunder (DOE), Caballo Rojo, Rochelle, and Spring Creek (NSP) coals using low-NO_x combustion conditions. Samples of size-fractionated ash were collected from the DTF using a multicyclone. Two stages, two and five, with aerodynamic cut diameters, D_{50}, of 12.9 μm and 1.9 μm, respectively, and a filter (D_{50} nominally 0.4 μm) were used to collect ash. Portions of the Stage Five and filter ash samples were mixed proportionally by mass collected. These mixed samples, representative of the fine ash (<2 μm) mass fraction, were mounted on vitreous carbon substrates using a modified version of a freeze-drying dispersion method (33) and then analyzed using CCSEM to determine the size and chemical composition of individual microparticles. Approximately 320 particles ranging from 0.1 to 12 μm in average diameter were analyzed in each sample using CCSEM.

4.3 Results

4.3.1 CCSEM Coal Mineral Analysis

Coal mineral CCSEM analysis (Table 5) indicate that the eight PRB test coals contain similar mineral assemblages: kaolinite, quartz, pyrite, mixed clays, illite, calcite, and hematite. Kaolinite and quartz compose >50 wt% of the minerals in all the coals. Pyrite, mixed clays, and illite are present at concentrations ranging from 3 to 10 wt% and calcite and hematite at <3 wt%.

4.3.2 Multicyclone Ash Collection

The multicyclone ash collection results for the DTF tests are presented in Table 22. The total mass of sample collected on Stage Five and the filter was used as a measure of the test coal's fine ash (<2 μm) concentrations. As illustrated in Figures 13 and 14, the Rochelle coal produced the most fine ash in both the conventional and low-NO_x ash formation tests.

4.3.3 CCSEM Fine Ash Analysis Results

Particle-size distributions of the fine ash fractions produced from the conventional ash formation tests are compared in Figure 15. The Black Thunder and Sarpy Creek coals produced a much finer ash relative to the other coals. The morphology of particles in the fine ash samples was examined using an SEM. The samples produced from the conventional combustion of coal consisted of discrete spherical particles, whereas particle agglomerates were characteristic of the low-NO_x ash samples, as exemplified in Figures 16 and 17. The agglomeration is the result of sintering between individual ash particles. Apparently, the lower combustion temperature and slower mixing of fuel and air associated with the low-NO_x testing conditions enhanced the sintering propensity of individual fine ash particles. The fine ash fractions produced using the low-NO_x combustion conditions are generally coarser because of the agglomeration, as shown in Figure 18; the Caballo Rojo coal ash is an exception.

TABLE 22

Multicyclone Stage Two (D_{50} = 12.9 μm), Stage Five (D_{50} = 1.9 μm), and Filter (D_{50} nominally 0.4 μm) Ash Collection Results[1]

	Mass Gain, g			Mass %		
	Stage Two	Stage Five	Filter	Stage Two	Stage Five	Filter
Antelope	0.0835	0.0392	0.0041	65.85	30.91	3.23
Big Sky	0.0957	0.0443	0.0020	67.39	31.20	1.41
BS-SC	0.1084	0.0411	0.0015	71.79	27.22	0.99
BTD	0.0829	0.0248	0.0039	74.28	22.22	3.49
	0.4080	**0.0547**	**0.0066**	**86.94**	**11.66**	**1.41**
Caballo	0.1098	0.0228	0.0027	81.15	16.85	2.00
	0.3829	**0.0924**	**0.0073**	**79.34**	**19.15**	**1.51**
Rochelle	0.0995	0.0735	0.0113	53.99	39.88	6.13
	0.2876	**0.1805**	**0.0318**	**57.53**	**36.11**	**6.36**
SCN	0.0886	0.0496	0.0048	61.96	34.69	3.36
	0.2111	**0.0677**	**0.0067**	**73.94**	**23.71**	**2.35**
Sarpy Creek	0.1786	0.0682	0.0016	71.90	27.46	0.64

[1] Values in bold type correspond to the low-NO_x ash formation tests.

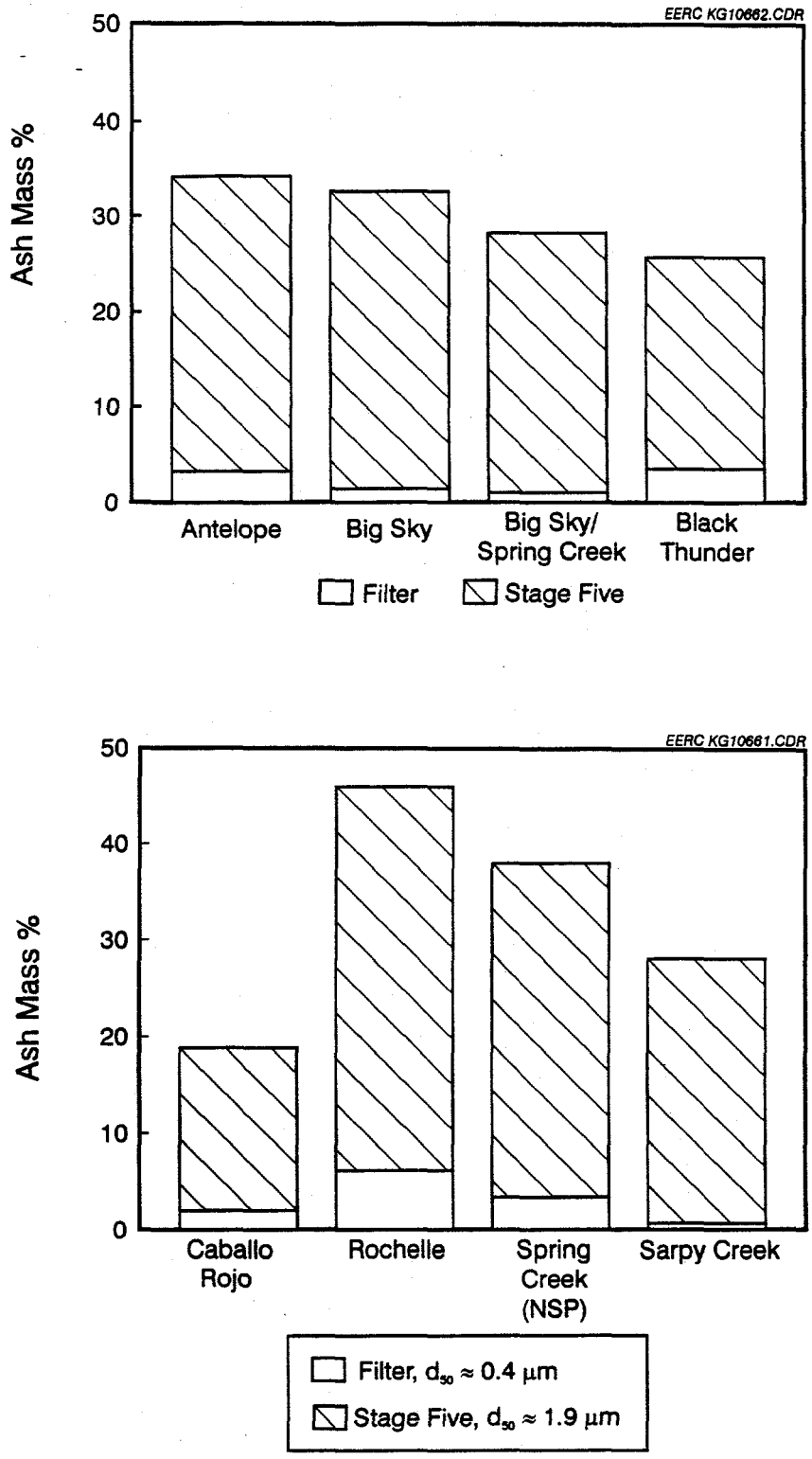

Figure 13. Multicyclone collection results, filter (D_{50} nominally 0.4 μm) and Stage Five (D_{50} = 1.9 μm) mass loadings, for conventional ash formation tests.

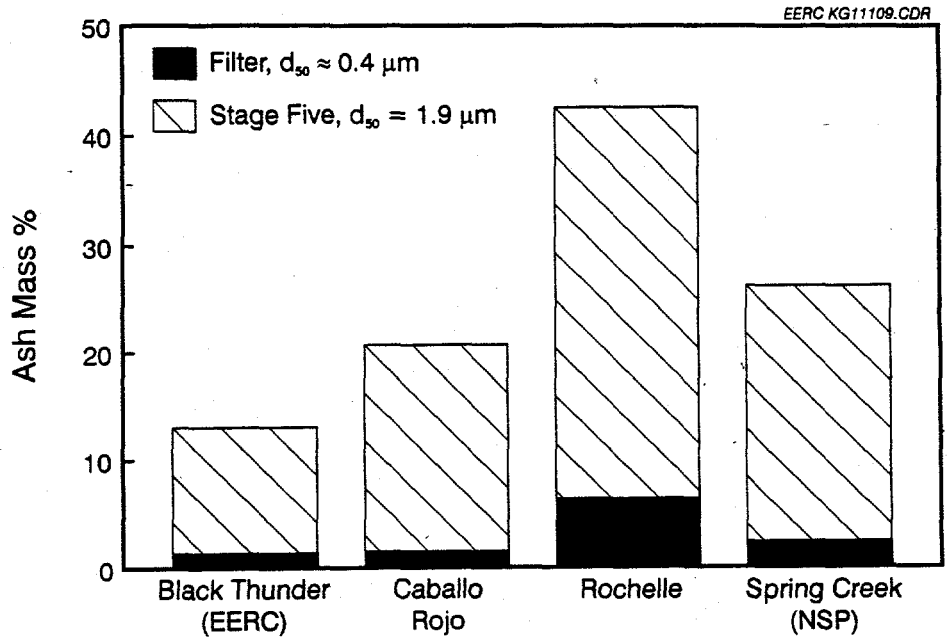

Figure 14. Multicyclone collection results, filter (D_{50} nominally 0.4 µm) and Stage Five (D_{50} = 1.9 µm) mass loadings, for low-NO_x ash formation tests.

Chemical analysis of individual ash particles indicates that the samples are composed of a very diverse particle-type assemblage consisting primarily of Ca aluminosilicate, Ca aluminate, aluminosilicate, silica, (Ca, Mg)O, $CaSO_4$, Na_2SO_4, and (Na,K)Cl (Table 23). The Caballo Rojo and Sarpy Creek fine ash fractions are distinguished by very high concentrations, about 50 frequency %, of chlorine-rich particles and a depletion in Ca aluminosilicate and aluminosilicate particles. The chlorine-rich particle source is not apparent from the corresponding coal mineral analysis results. The chlorine may be organically bound or associated with submicron minerals. The predominance of Ca aluminosilicate and Ca aluminate ash phases in all the samples is consistent with the relatively high concentrations of organically bound Ca that are available in PRB coals to react with mixed clays and kaolinite during combustion.

4.4 Opacity Index Formulation

A correlation analysis was performed to determine whether relationships exist between the proportion of fine ash produced from a coal and the corresponding coal's ash contents or elemental oxide concentrations (Tables 3 and 4). All of the calculated correlation coefficients presented in Table 24 are less than ± 0.6, indicating that the total ash contents and chemical compositions of these coals are not significantly related to the production of fine ash during combustion. The production of fine ash must, therefore, be dependent on the distribution of inorganics among the various mineral species and maceral components of coal.

The direct relationship between the abundance of fine mineral grains ($< \approx 5$ µm) in pulverized coal and the production of fine ash during combustion was documented by Holve (27). The results from this study are generally consistent with this relationship, as shown in Figure 19. A best-fit line to the particle-size trend in Figure 19 was calculated using linear regression analysis. The data points for the test coals, except for the Caballo Rojo coal, define a linear trend, with a

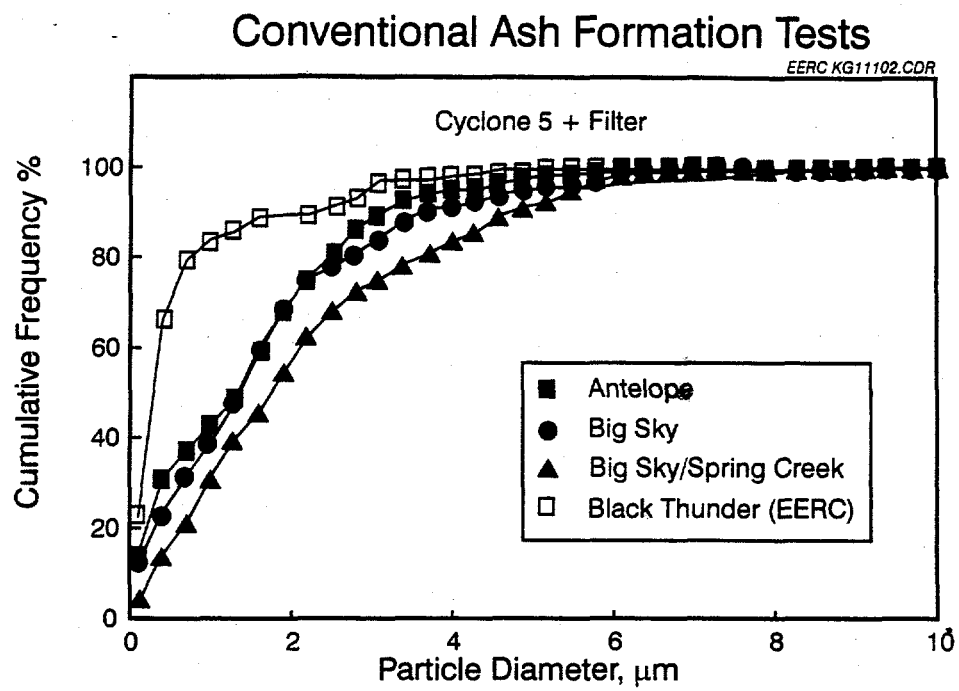

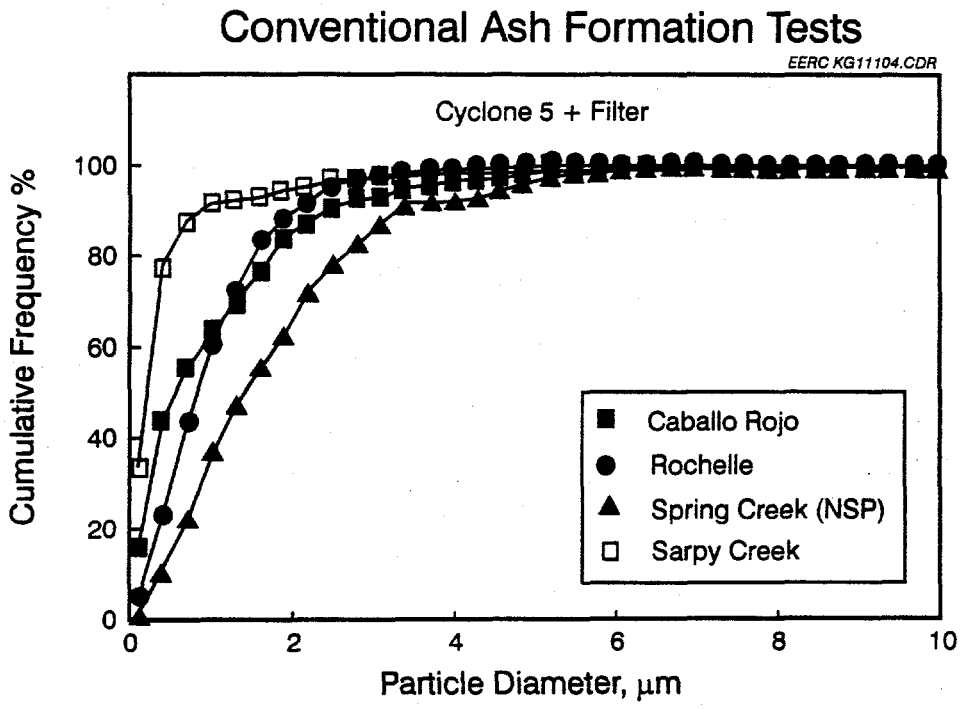

Figure 15. Comparison of particle-size distributions for the fine ash fractions produced using conventional combustion conditions.

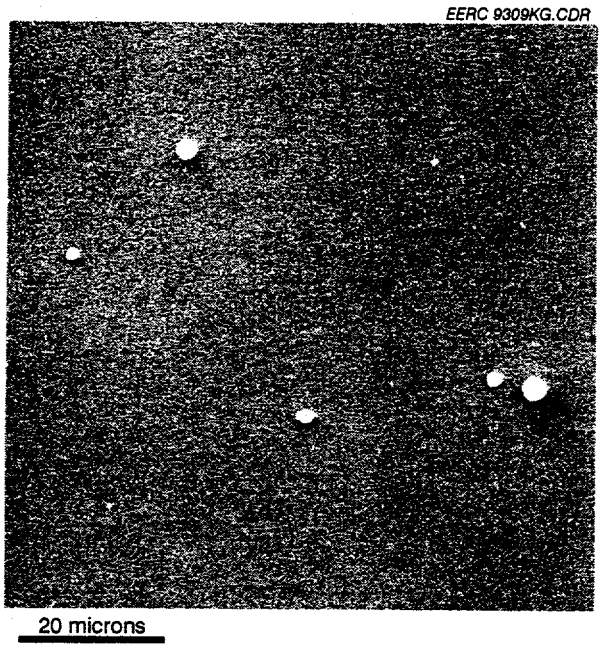

Figure 16. Secondary electron image of the Black Thunder fine ash fraction produced using conventional combustion conditions.

correlation coefficient (r^2) of 0.94. The linear regression equation in Figure 19 is useful for predicting the mass concentration of fine, approximately 2-μm, ash produced from pulverized subbituminous coal combustion.

The data in Figure 19 indicate that the 1.0- to 4.6-μm-diameter mineral size fraction is a significant source of fine ash ($\approx$2 μm) that can be directly quantified using CCSEM. Additional sources of fine ash, however, that cannot be directly analyzed with CCSEM because of spatial resolution constraints are the submicron mineral size fraction and the inorganic species that are molecularly bound to macerals. An indirect method was devised to quantify these potentially important fine ash sources. The total supermicron mineral concentration (wt% on a coal basis) can be determined using CCSEM combined with digital image analysis. The difference in mineral matter content determined by proximate analysis (ash wt% on an as-received basis) and that determined by CCSEM image analysis is an approximation of a coal's submicron mineral and organically bound inorganic contents. The following ratio, designated as the inorganic distribution coefficient (IDC), was devised to express the proportion of inorganic constituents associated with discrete supermicron minerals relative to those associated with submicron minerals and coal macerals: IDC = supermicron mineral concentration/(total ash content - supermicron mineral concentration). The calculated IDC values for the test coals are plotted against their corresponding multicyclone filter loads in Figure 20. An exponential curve fit was performed on these data yielding a r^2 of 0.85. The best-fit curve, however, intersected the ordinate at an unrealistically low filter load value. Exclusion of the Antelope coal in the curve-fitting analysis produced the best-fit curve (Figure 20), r^2 = 0.95, that more closely approximates an asymptotic relationship to the ordinate. Such a relationship is consistent with a vaporization/condensation mechanism of submicron ash formation. Submicron coal minerals may also be an inherent source of fine ash particles. The equation in Figure 20 can be used to predict the mass concentration of submicron ash particles resulting from pulverized subbituminous coal combustion.

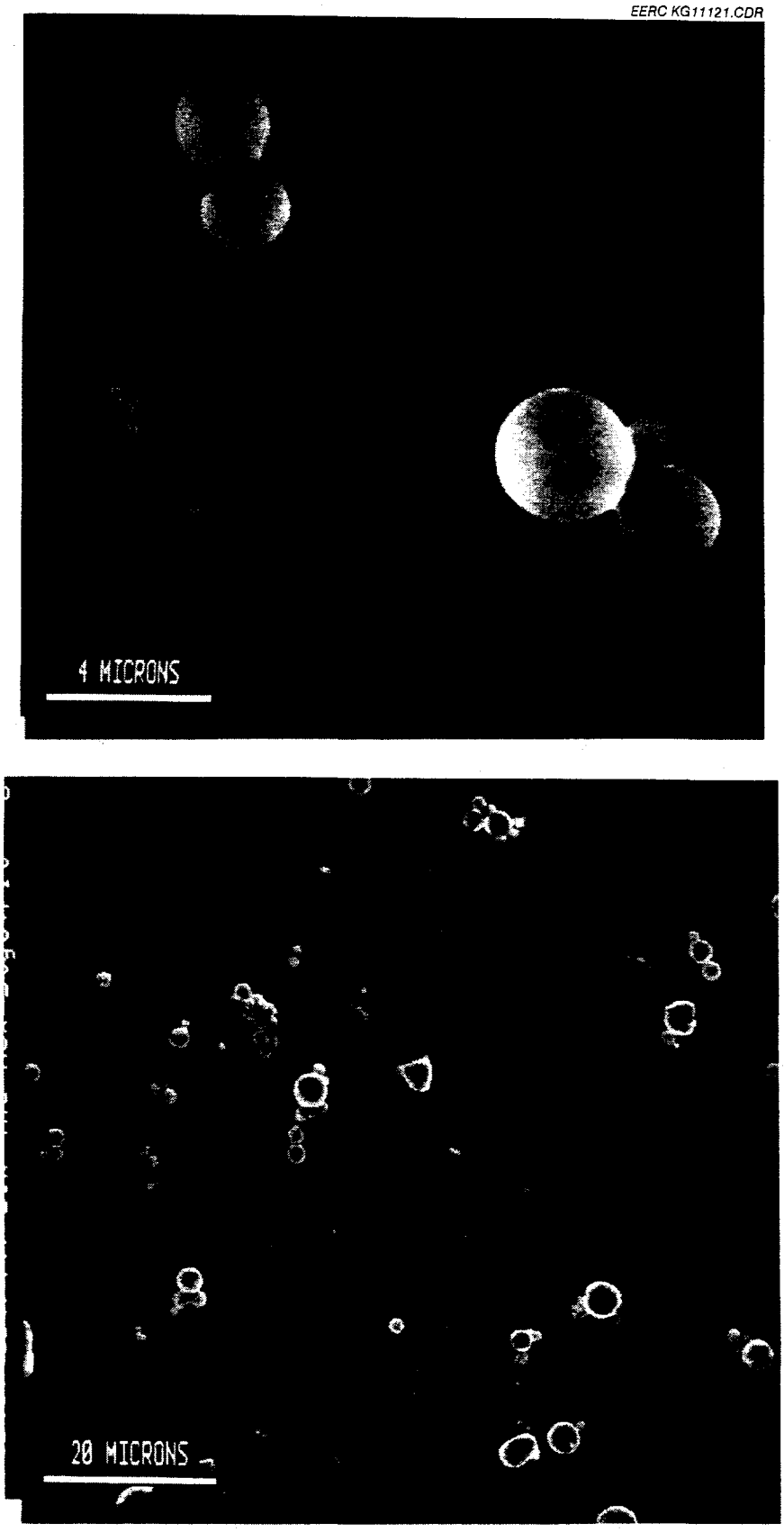

Figure 17. Secondary electron images of the Black Thunder fine ash fraction produced using low-NO_x combustion conditions.

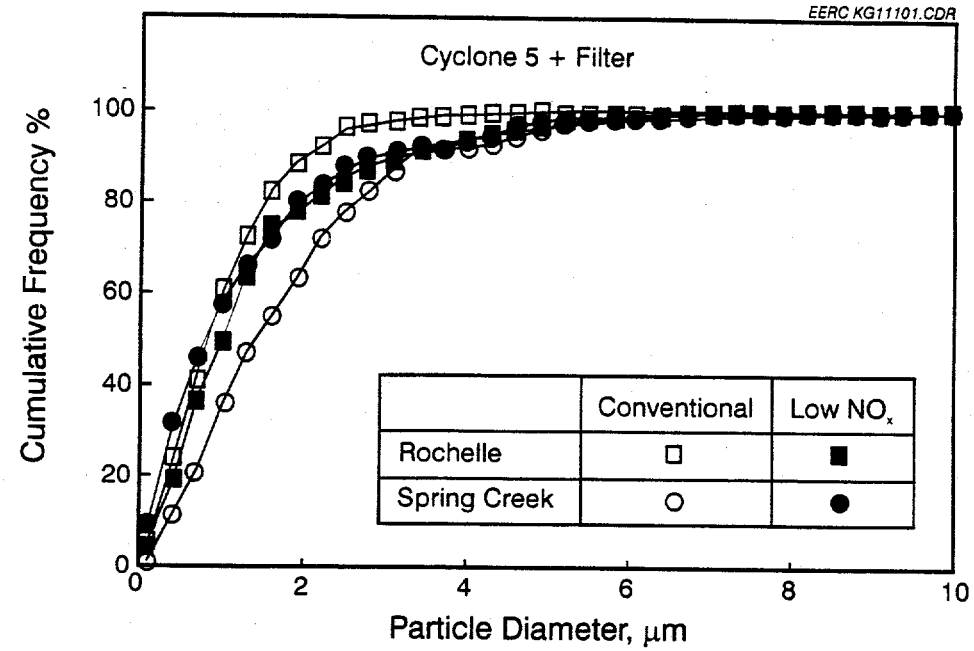

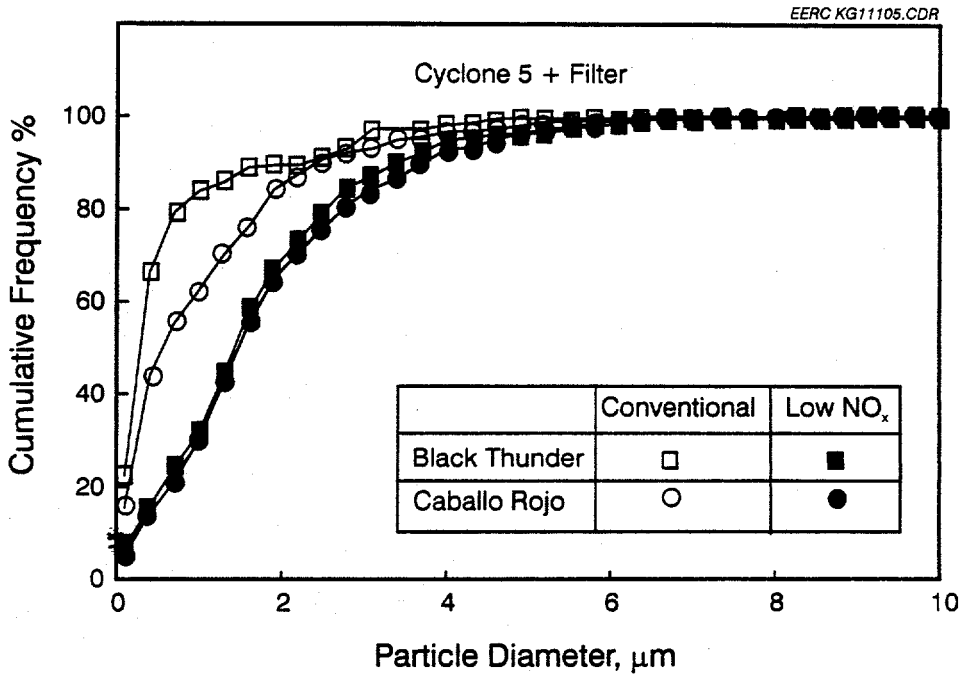

Figure 18. Comparisons of particle-size distributions for the fine ash fractions produced using conventional and low-NO_x combustion conditions.

TABLE 23

Fine Ash Phase Proportions, frequency %

	Antelope	Big Sky	BS-SC	BTD	Caballo	Rochelle	SCN	Sarpy
SiO_2	0.6	6.0	6.2	5.3 **5.1**[1]	1.2 **3.9**	2.7 **2.4**	1.7 **3.0**	ND[2]
Ca-Al-Si	3.5	20.4	18.1	19.6 **20.8**	4.5 **9.3**	28.3 **46.6**	14.0 **6.0**	1.4
(Ca,Mg)Si	4.8	ND	0.7	4.5 **8.7**	4.8 **9.0**	2.7 **2.1**	4.5 **11.3**	2.4
Al-Si	11.3	31.6	25.7	25.1 **19.9**	6.5 **23.1**	10.1 **14.2**	7.0 **16.4**	3.2
Na-Si	ND	ND	ND	ND **0.9**	ND **ND**	ND **ND**	ND **3.3**	ND
Fe-Si	1.0	ND	ND	0.8 **ND**	ND **ND**	ND **ND**	ND **ND**	2.8
Si-Rich	2.6	4.0	5.8	3.6 **6.6**	ND **8.1**	ND **7.7**	ND **21.7**	3.2
Ca-Al	7.1	2.0	6.9	16.5 **9.6**	4.5 **13.2**	26.2 **12.7**	25.6 **12.2**	ND
(Ca,Mg,Fe) CO_3, OH, or O	38.6	1.6	3.6	23.4 **16.6**	18.2 **26.7**	24.1 **8.8**	14.9 **11.0**	2.8
Al_2O_3	7.1	4.0	ND	ND **ND**	0.6 **ND**	1.3 **ND**	ND **ND**	ND
Fe_xO_x	4.5	2.4	0.4	0.6 **0.3**	3.3 **ND**	0.2 **0.3**	1.2 **3.6**	12.3
FeS_x	ND	ND	ND	ND **ND**	ND **ND**	ND **ND**	ND **ND**	3.5
Na_2SO_4	ND	1.2	ND	ND **2.1**	ND **ND**	ND **ND**	ND **1.8**	ND
$CaSO_4$	7.4	3.2	4.7	ND **3.0**	2.4 **0.9**	0.8 **0.6**	3.3 **1.2**	1.7
S-Rich	1.9	2.4	4.0	0.6 **0.6**	3.3 **2.4**	1.7 **1.2**	ND **0.9**	2.4
(Na,K)Cl	6.1	8.8	ND	ND **ND**	5.7 **ND**	0.2 **ND**	13.2 **ND**	7.7
CaCl	0.6	ND	ND	ND **ND**	3.9 **ND**	0.7 **1.8**	ND **ND**	2.8
Cl-Rich	0.6	11.6	18.1	ND **3.0**	36.6 **2.4**	0.8 **1.2**	12.8 **3.6**	48.4
(S,Cl)-Rich	ND	ND	4.7	ND **ND**	3.6 **ND**	ND **ND**	0.4 **ND**	4.2
P-Rich	0.6	ND	ND	ND **0.3**	ND **0.6**	ND **ND**	ND **0.3**	ND
Na-Rich	ND	ND	ND	ND **2.4**	ND **ND**	ND **ND**	3.6 **ND**	ND
(Ti,Ba)-Rich	1.9	0.8	1.1	ND **ND**	1.2 **0.3**	ND **0.6**	1.2 **0.3**	1.0

[1] Values in bold type correspond to the low-NO_x ash formation tests.
[2] Not detected.

TABLE 24

Correlation Analysis of Bulk Ash Chemistry and Coal Ash Content to Fine Ash Production (ash mass % on Stage Five and the filter)

Oxide	Correlation Coefficient
SiO_2	-0.058
Al_2O_3	0.596
Fe_2O_3	0.416
P_2O_5	-0.444
CaO	0.084
MgO	0.361
Na_2O	0.426
Ash	-0.364

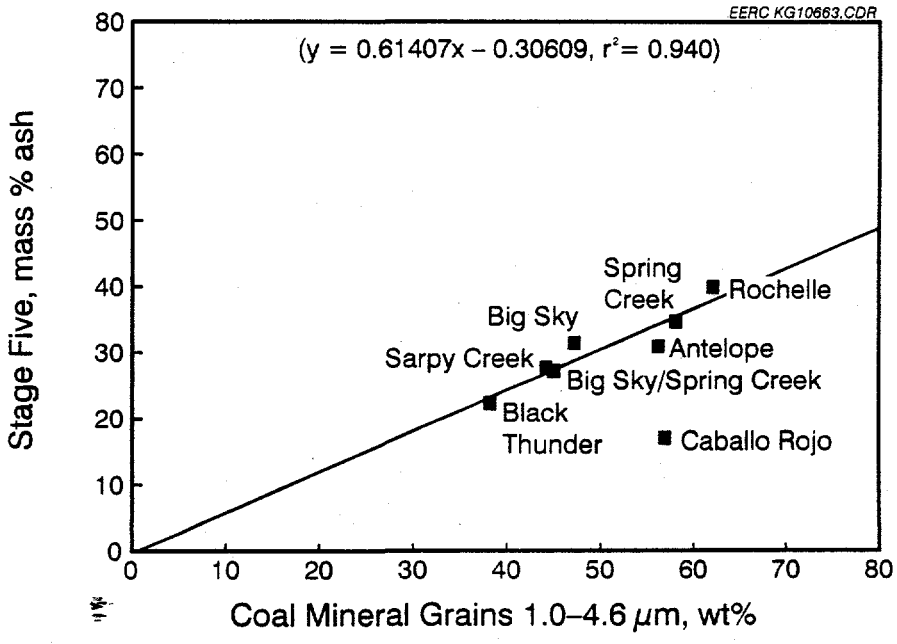

Figure 19. Multicyclone Stage Five (D_{50} = 1.9 μm) load versus concentration of the 1.0- to 4.6-μm-diameter mineral size fraction for the test coals. A best-fit line to the particle-size trend was calculated using linear regression analysis. The Caballo Rojo coal was excluded from the fit. An equation for the linear regression line is given (r^2 = correlation coefficient).

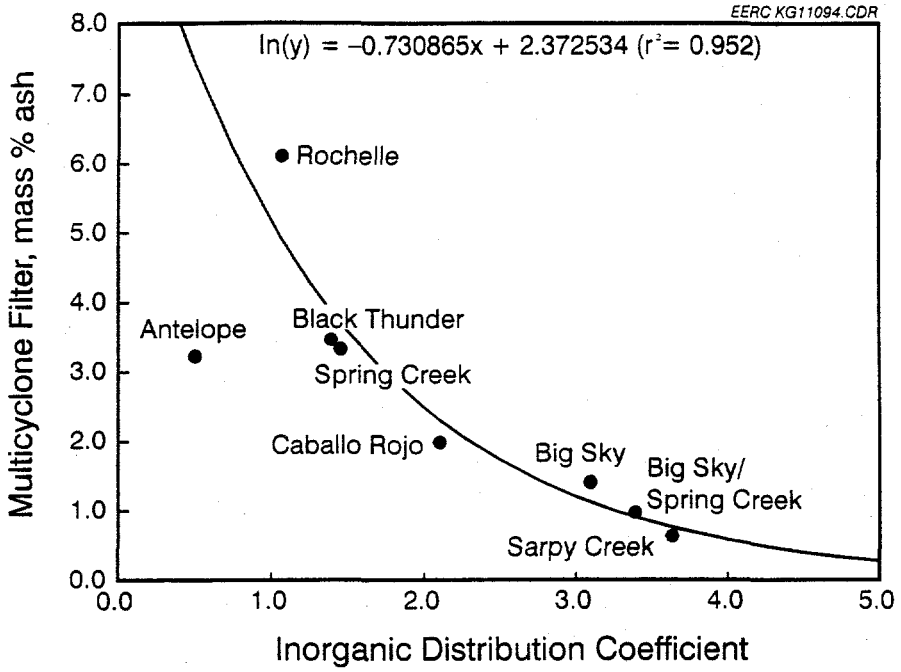

Figure 20. Multicyclone filter (D_{50} nominally 0.4 μm) load versus inorganic distribution coefficient (supermicron mineral concentration/[submicron mineral + organically associated inorganic concentration]). An equation for the best-fit curve is given (r^2 = correlation coefficient). The Antelope coal was excluded from the fit.

The removal of ash from flue gas by ESP is influenced strongly by electrical resistivity. ESPs require a specific range of ash resistivity, 10^4 to 2×10^{10} ohm-cm, to operate properly (33, 35). Coal ashes with resistivities of greater than 2×10^{10} ohm-cm retain their electrical charge after collection, causing a compacted ash layer to accumulate on the plates of an ESP. Eventually, adequate corona discharge cannot be maintained, and back ionization occurs on the ash surface causing precipitator failure. Low-resistivity ash, $< 10^4$ ohm-cm, readily dissipates its charge after collection and the uncharged ash particles are then reentrained in the flue gas. Ash resistivity is temperature-dependent: at low temperature, surface electrical conduction dominates and total resistivity increases with temperature; at high temperature, volume resistivity dominates and total resistivity decreases with temperature. The equations formulated by Bickelhaupt (36) were incorporated into the opacity index to account for the effects of ash resistivity and flue gas temperature on ESP performance. The ash resistivity calculations consider the temperature ranges appropriate for cold-side, generally 135° to 175°C, and hot-side, generally 315° to 425°C, ESP operation.

Volume resistivity, defined as the resistivity of a fly ash layer excluding the influence of flue gas components H_2O and SO_3, was estimated for each test coal using the equations of Bickelhaupt (36). The resistivity prediction is based on the atomic concentrations of Na_2O, MgO, CaO, and Fe_2O_3 in the ash, flue gas temperature, and the average ESP field intensity. The ash compositions

in Table 4 (normalized to 100 wt%), a temperature of 315° and 425°C, and an electric field intensity of 12 kV/cm were used in the calculations. The selected temperatures and field intensity value are representative of hot-side precipitator operating conditions. Predicted volume resistivities for the test coals are compared in Figures 21 and 22. At the maximum flue gas temperature of 425°C (Figure 21), all of the coals have predicted ash resistivities that are within the optimum ESP performance range of 10^4 to 2×10^{10} ohm-cm. However, at the minimum temperature, 315°C (Figure 22), the Big Sky, Black Thunder (EERC, KCPL, NSP), Black Thunder–Colstrip, Caballo Rojo, and Colstrip coal ashes have predicted resistivities that are sufficiently high (i.e., $>2 \times 10^{10}$ ohm-cm) to cause degradation of ESP performance.

The fine-particle concentration and particle-size distribution information determined from DTF tests and CCSEM analysis were used in theoretical light-scattering calculations to estimate the effect of low-NO_x combustion conditions on opacity. Opacity, the percent reduction of light intensity, is related to the optical properties of a plume according to:

$$Opacity = [1 - \exp(-b_{ext}L)]100$$

where b_{ext} is the extinction coefficient and L is the optical path length (24). The optical path length is equivalent to plume depth, and in the case of an in-stack transmission meter measurement, it is defined by the stack diameter. The extinction coefficient can be calculated from the sum of extinction efficiency factors, Q_{ext}, for discrete particle-size intervals as follows:

$$b_{ext} = \sum_{i=1}^{n} NF_i Q_{ext} A_i$$

where N is the total number of particles per unit volume of flue gas, F_i is the particle frequency concentration in size interval $_i$, A_i is the cross-sectional area of the geometric mean particle size in the size interval $_i$, and N is the number of size intervals. The Q_{ext} factors can be determined using the classic Mie formulation of light scattering by spherical particles (26). A computer program devised by Bohren and Huffman (37) was used to determine the Q_{ext} factors. The calculations were performed for an optical path length of 5 m, a refractive index of 1.5, an incident light wavelength of 550 nm, and an average particle density of 2.5 g/cm^3. The calculated opacity values for the fine ash fractions produced in conventional and low-NO_x combustion conditions are compared in Figure 23. The calculations indicate that the low-NO_x conditions generally produce a fine ash fraction that causes less opacity relative to the ash produced in conventional combustion conditions. The reduction in opacity is attributable to the generally coarser particle size of the low-NO_x fine ash fractions (Figure 18).

The regression equations in Figures 19 and 20 can be used to predict the concentration of fine ash particles, <2 μm, resulting from the conventional combustion of pulverized subbituminous coals. The opacity index is based on these equations. The equations formulated by Bickelhaupt (36) are also incorporated into the opacity index to account for the effects of ash electrical resistivity and flue gas temperature on ESP performance. Different scaling factors are applied to the index, depending on the calculated ash resistivity value for a given average ESP operating temperature and on the type of combustion (conventional or low-NO_x) employed.

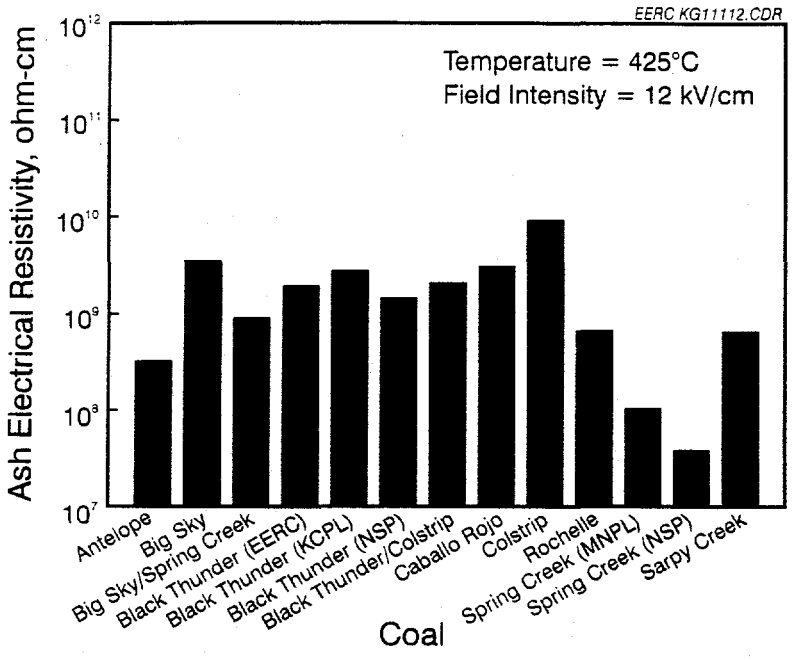

Figure 21. Predicted ash electrical resistivity at a temperature of 425°C for the thirteen test coals.

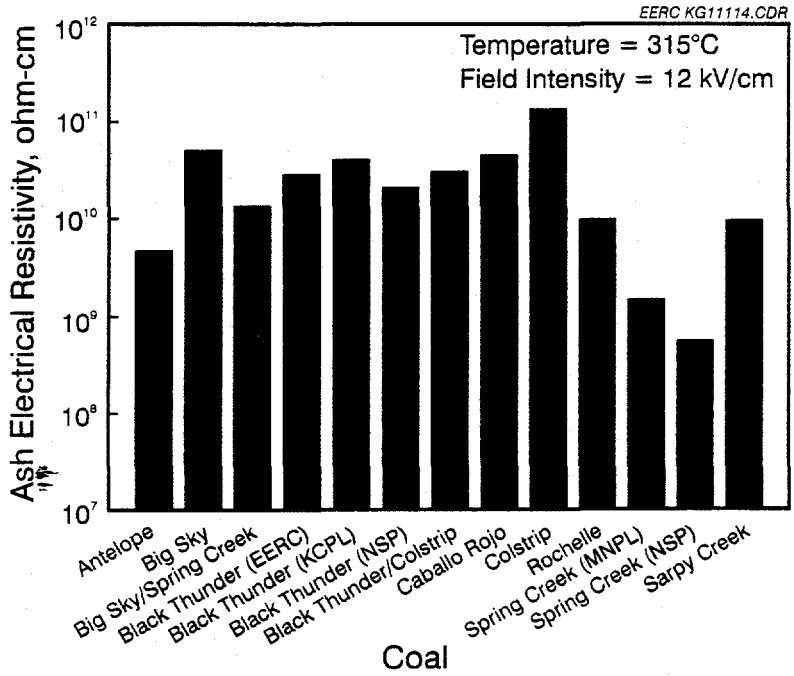

Figure 22. Predicted ash electrical resistivity at a temperature of 315°C for the thirteen test coals.

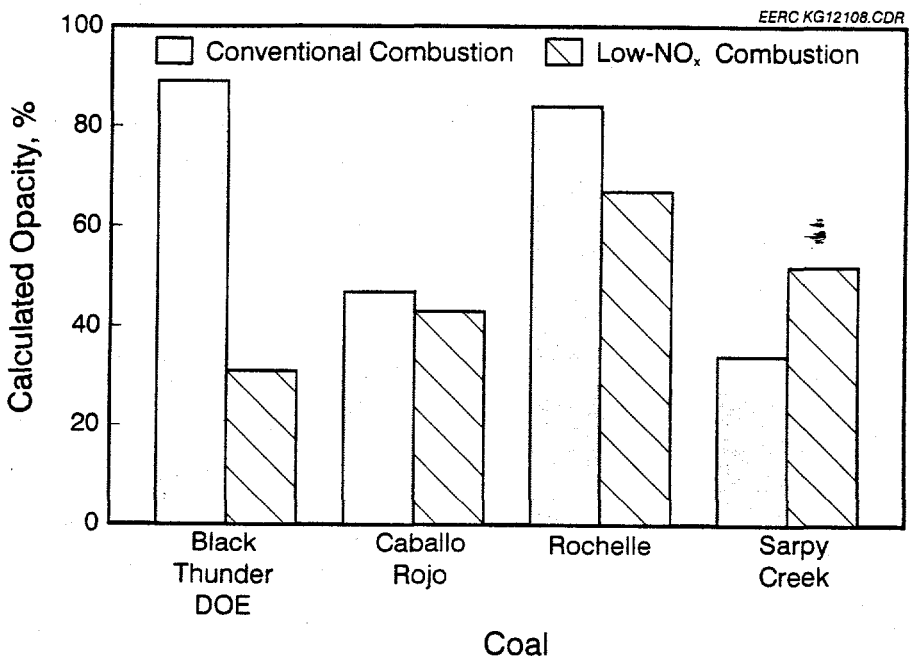

Figure 23. Comparison of calculated opacity values for the fine ash fractions produced in conventional and low-NO_x combustion conditions.

4.5 Application of the Opacity Index

Calculated opacity index values for the thirteen test coals are compared in Figure 24. The indices were calculated assuming conventional combustion conditions and a scrubber as the particulate control device. According to the index, the Antelope, Black Thunder (KCPL), Black Thunder (NSP), Caballo Rojo, Rochelle, and Spring Creek (NSP) coals are predicted to produce the highest opacity levels; the Big Sky, Big Sky–Spring Creek, Black Thunder (DOE), Black Thunder–Colstrip, Spring Creek (MNP), and Sarpy Creek coals are expected to produce similar intermediate opacity levels; and the Colstrip coal is predicted to produce the least amount of opacity.

5.0 DEVELOPMENT OF THE COAL GRINDABILITY INDEX

5.1 Introduction

The Hardgrove grindability index (HGI) is widely accepted by the power industry for expressing the relative grindability or ease of pulverization of coals (38). The HGI is useful for evaluating the yield and energy input required in a grinding or pulverization process. Pulverizers are generally rated for a specific HGI, typically 50; therefore, the difference of an HGI from the

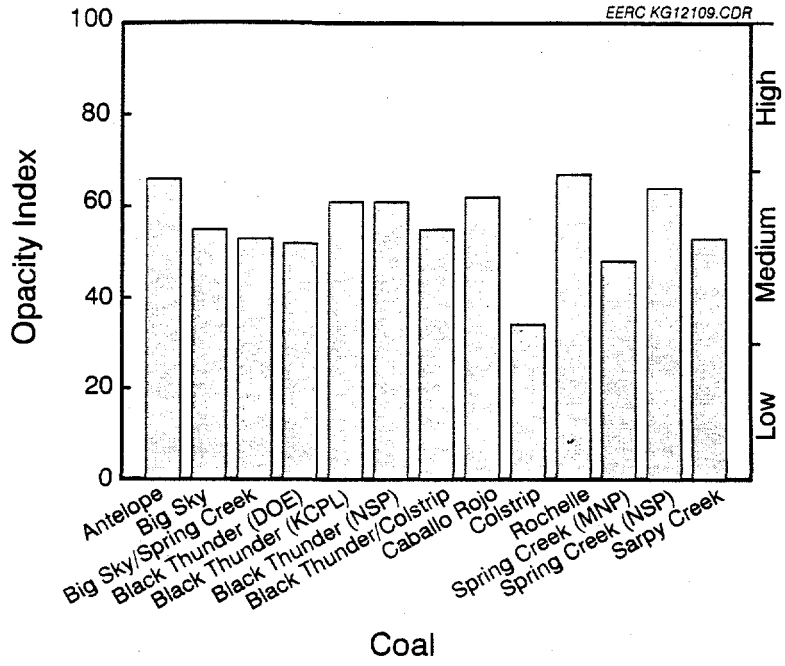

Figure 24. Comparison of opacity index values for the thirteen test coals.

design value is a coal selection criterion. Grindability is affected by the hardness, strength, tenacity, and fracture characteristics of coal constituents. Numerous studies, as reviewed by Hower and Wild (39), have successfully related coal-rank parameters (calorific value, moisture, volatile matter, and fixed carbon) and chemical, mineralogical, and maceral compositional parameters to the HGI. These studies, however, have focused on coals of bituminous rank and higher partly because of the possible adverse effect of moisture on the HGI determination. Subbituminous and lignite coals are susceptible to physical change as the natural or seam moisture is released during handling and preparation. Consequently, the HGIs determined in a laboratory may be dependent on the conditions of drying and the moisture level of the coal at the time of the test.

Ten subbituminous coals and a lignite coal with similar moisture contents were selected to investigate the relationship of coal rank (calorific value) and chemical, mineralogical, and maceral composition with HGI. It is assumed that because the coals have similar moisture contents, the HGI would be a reliable measure of the relative grindabilities of these eleven coals. This assumption was required for deriving an empirical index for ranking subbituminous coals according to grindability.

5.2 Experimental

The maceral compositions of the following coals were determined using standard petrographic techniques (40): Antelope, Big Sky, Black Thunder (EERC), Buckskin, Caballo Rojo, Jacobs Ranch, Rochelle, and Spring Creek (MNPL). The HGI values and proximate-ultimate analysis results for the Buckskin and Jacobs Ranch coals were provided by Mr. Kenneth Stuckmeyer of Union Electric. Analysis results obtained from the Penn State Coal Data Base for the Beulah, Dietz, and Wyodak coals were also included in this study. All coal grindabilities were determined using the Hardgrove machine method according to ASTM D409 (38).

5.3 Results

The HGI values and properties for the eleven coals considered in this investigation are presented in Table 25. The coal properties in Table 25 have been found useful by researchers for developing predictive models of coal grindability (39). Selected mineral abundances and the degree of mineral-maceral association, represented by the ratio of included to excluded minerals, for six of the test coals (Antelope, Big Sky, Black Thunder, Caballo Rojo, Rochelle, and Spring Creek [MNPL]) were also examined as possible predictors of grindability.

A correlation analysis was performed to identify the coal properties that are most significantly related to the HGI; correlation coefficients with absolute values of ≥ 0.7 were considered significant in this study. The calculated correlation coefficients are presented in Tables 26 and 27. The coal moisture contents show some degree of correlation to the HGI, even though the range in moisture content represented by most of the coals is limited (Figure 25). For example, the moisture contents for seven of the coals (Antelope, Big Sky, Black Thunder [EERC], Caballo Rojo, Dietz, Rochelle, and Spring Creek [MNPL]) range from only 21% to 25%, yet the HGI values range from 39 to 53, indicating that other factors are involved in the HGI variation. Grindability correlates best to the total sulfur and ash contents (Table 26) of the coals. The correlation of ash with HGI improves greatly (coefficient increases to 0.866) when the Wyodak coal is excluded from the linear regression analysis. The maceral and mineral abundances and included-excluded mineral ratio are insignificantly correlated to coal grindability.

5.4 Grindability Index Formulation

An equation for predicting the HGI of subbituminous coals was derived from a multiple regression analysis of the ash and total sulfur variables; regression coefficients are presented in Table 28. The predicted values compare favorably to the analytically determined HGI values as indicated in Figure 26. The regression equation in Table 28 is incorporated into the PCQUEST computer program to calculate a grindability index (GI). Application of the index should be restricted to comparing the grindabilities of subbituminous coals that have similar moisture contents to those used in this study, i.e., 21 to 33 wt% on an as-received basis.

TABLE 25

Coal Properties Examined for Correlations to the Hardgrove Grindability Index

		Maceral Groups, volume%, dmmf[1]			Btu/lb, AR,mmf[2]	wt%, AR basis		
	HGI[1]	Huminite	Liptinite	Inertinite	Calorific Value	Ash	Total S	Moisture
Antelope	39.0	91.85	1.50	6.64	9340	3.79	0.33	23.5
Beulah (DECS-11)[3]	56.7	73.80	6.70	19.50	7911	6.37	0.49	33.4
Big Sky	53.0	88.53	1.88	9.58	10,135	6.33	0.55	23.6
Black Thunder (DOE)	44.0	90.03	3.31	6.64	10,112	4.49	0.39	24.3
Buckskin[5]	60.5	89.20	2.50	8.30	8891	5.90	0.80	29.8
Caballo Rojo	52.0	90.50	2.13	7.37	9988	5.23	0.46	21.0
Dietz (DECS-9)[3]	40.8	87.70	5.30	7.00	9796	4.80	0.31	24.7
Jacobs Ranch[4]	54.1	90.10	3.10	6.70	9214	6.17	0.46	27.5
Rochelle	44.0	91.98	0.96	7.02	9901	4.26	0.24	25.3
Spring Creek (MNP)	44.0	93.41	1.35	5.24	9830	3.71	0.42	22.3
Wyodak (DECS-8)[4]	55.3	78.90	11.80	9.30	8951	9.90	0.52	28.4

[1] Dry mineral-matter-free basis.
[2] As-received, mineral-matter-free basis.
[3] Results obtained from the Penn State Coal Data Base.
[4] HGI values and moisture and ash contents provided by Union Electric.

TABLE 26

Correlation Analysis of Properties for Eleven Subbituminous and Lignite Coals

Parameter Correlated to HGI	Correlation Coefficient
Moisture	0.630
Ash	0.694[1]
Calorific Value	-0.558
Total S	0.845
Huminite	-0.518
Liptinite	0.352
Inertinite	0.512

[1] 0.866 excluding the Wyodak coal.

TABLE 27

Correlation Analysis of Mineral Properties for Six Subbituminous Coals to the Hardgrove Grindability Index

Parameter Correlated to HGI	Correlation Coefficient
Kaolinite	0.517
Quartz	-0.274
Pyrite	-0.234
Mixed Clays	0.133
Excluded Kaolinite	0.434
Excluded Quartz	0.552
Excluded Pyrite	0.661
Excluded Clays	0.144
Included Minerals-Excluded Minerals	-0.227

TABLE 28

Regression Coefficients for Predicting the Hardgrove Grindability Index

No. Samples	Y-Intercept	Total Sulfur[1]	Ash[1]	r^2
11	26.215	32.289	1.5515	0.822

[1] Reported on a wt% as-received basis.

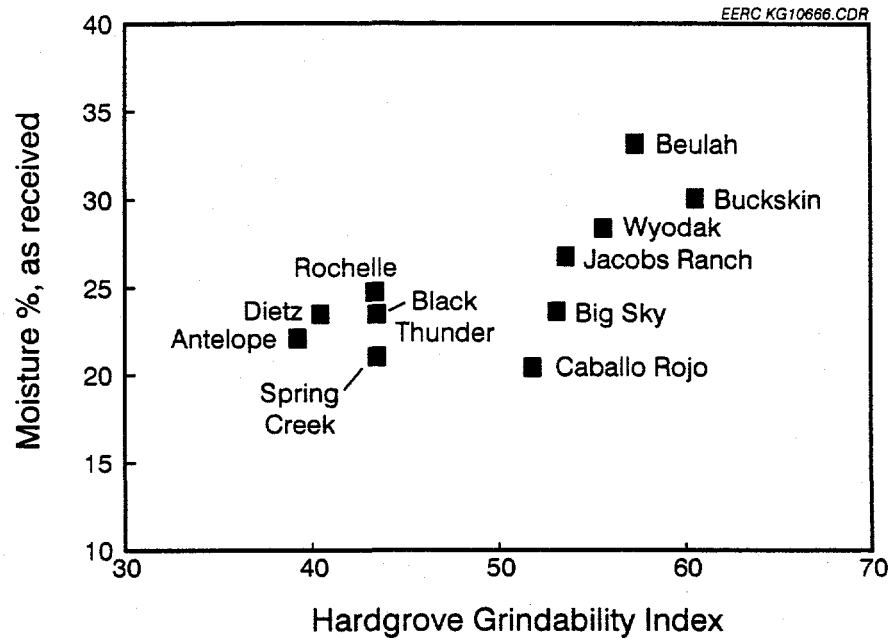

Figure 25. HGI versus moisture content for ten subbituminous coals and a lignite coal.

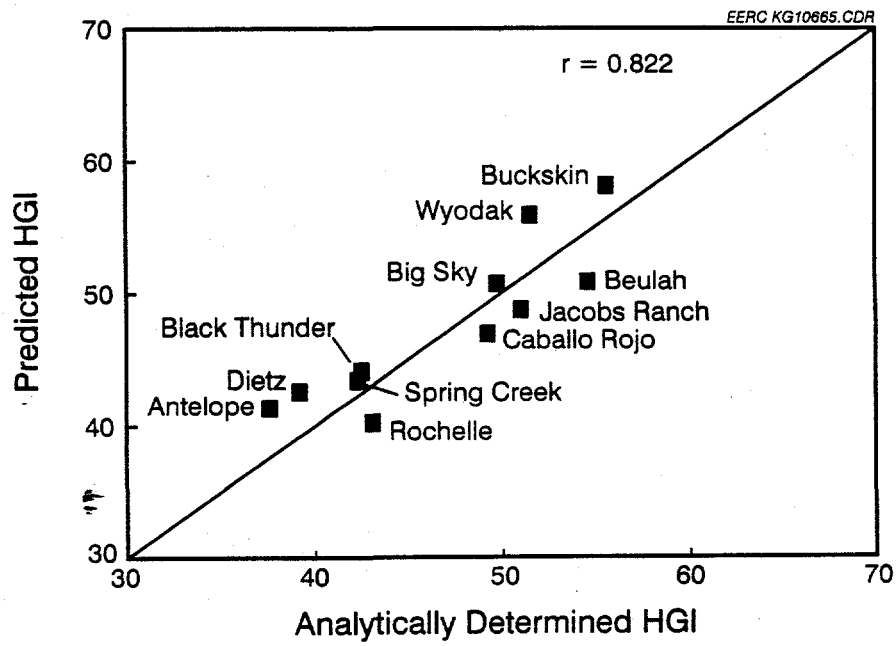

Figure 26. Predicted versus measured HGI. The plotted line corresponds to a perfect correlation (i.e., slope = 1) between the predicted and determined HGI values.

5.5 Application of the Grindability Index

Compared in Figure 27 are the grindability index values calculated by PCQUEST for all thirteen test coals. The index values range from 40 to 59. According to the index, the Colstrip and Sarpy Creek coals should pulverize more efficiently relative to the other test coals. The Antelope and Rochelle coals are predicted to be the most difficult to pulverize.

6.0 DEVELOPMENT OF THE EROSION INDEX

6.1 Introduction

Erosion of boiler components by coal minerals and fly ash is a primary cause of availability loss in power plants (41, 42). Erosion generally refers to the gradual removal of material produced by the bombardment of solid particles against stationary surfaces, such as boiler tubes. The erosion characteristics of a coal depend largely on the abundance, hardness, shape, and size of its mineral constituents. Pyrite and quartz are generally the most abundant hard minerals in coal. In addition, quartz is commonly angular in shape which enhances erosion wear. The minerals included within relatively large coal particles do not cause much erosion. Minerals excluded from coal particles, however, are available to erode pulverizer parts, coal transport pipe and fittings, and burner components. Therefore, a greater concentration of excluded quartz and pyrite grains will promote erosion. Furnace walls, secondary superheaters, and reheaters do not generally incur significant erosion damage because of the physical characteristics of quartz and pyrite-derived ash particles entrained in a high-temperature flue gas. In addition, the high gas temperatures generally

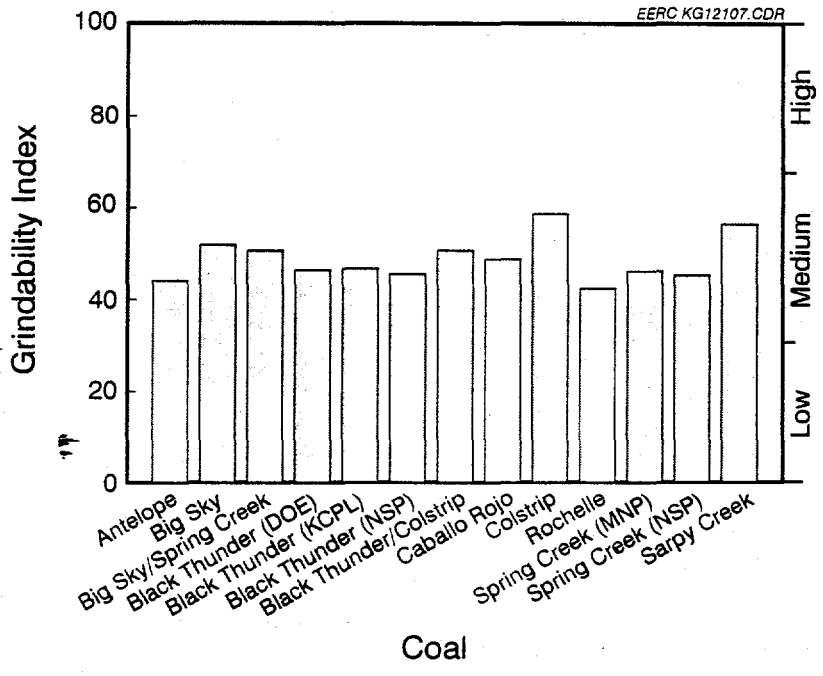

Figure 27. Comparison of PCQUEST grindability index values for the thirteen FPI test coals.

cause a layer of sintered ash to accumulate on boiler tubes; therefore, subsequent particle impactions do not erode tube material. However, in the lower-temperature regime of the primary superheater and economizer tube banks, ash particles are solidified and erosion can be a problem. Erosion rate is dependent primarily on particle-size distribution and velocity because of inertial momentum effects. Particles transported at high velocity in the size range of about 5 to 50 μm are most effective in eroding materials (43, 44). Experimental work has shown that erosion rate is an exponential function of particle velocity to between the second and fourth power (42).

6.2 Erosion Index Formulation

Prediction of the absolute rate of boiler erosion is difficult because of the large number of variables involved, e.g., temperature; particle composition, size, shape, and velocity; flue gas flow conditions; mechanical property of metal target; and angle of particle impingement. However, based on the preceding discussion, a general expression for comparing the relative erosiveness of coals can be formulated as:

$$EI \propto (C_q H_q + C_p H_p) A V^n$$

where EI is the erosion index; C_q and C_p are the weight fractions, on a total mineral basis, of excluded quartz and pyrite grains, respectively, in the size range of 5 to 50 μm; H_q and H_p are the Vickers hardness values for quartz (1350 kg/mm^2) and pyrite (1200 kg/mm^2), respectively; A is the weight percent of ash, on an as-received basis; V is particle velocity (m/sec); and n is an exponent which is generally assigned a value of 2.3 (41).

6.3 Application of Erosion Index

The CCSEM method in conjunction with digital image analysis was used to determine C_q and C_p for most of the coals considered in this project (Table 29). The Antelope and Sarpy Creek coals were analyzed prior to the incorporation of a method for acquiring image analysis data as a function of mineral particle size, thus precluding their incorporation into Table 29. Flue gas velocity can be used as an approximation for particle velocity in the erosion index equation. In a pulverized coal-fired boiler, flue gas velocities generally range from about 15 to 18 m/sec (30, 35). Erosion index values for the test coals are plotted as a function of flue gas velocity in Figure 28. Most of the index values range from 20 to 40 at typical flue gas velocities of 15 to 18 m/sec. According to the index, the Rochelle coal has the greatest erosion propensity; the Big Sky, Spring Creek (MNP), Big Sky–Spring Creek, Caballo Rojo, Black Thunder (NSP), and Black Thunder–Colstrip coals have a similar intermediate level of erosion propensity; and the Black Thunder (DOE), Black Thunder (KCPL), Colstrip, and Spring Creek (NSP) coals have the lowest levels of erosion propensity.

7.0 VERIFICATION OF PCQUEST INDICES

7.1 Introduction

The original goal of the FPI project was to develop an opacity index as well as more reliable slagging and fouling indices for comparing PRB subbituminous coals. Consequently, much more work has gone into verifying these three indices. The utility of PCQUEST's slagging and fouling

TABLE 29

Concentration (weight fraction) of Excluded Quartz and Pyrite Grains Ranging in Size from 5 to 50 μm

Coal	Organization	Quartz	Pyrite
Black Thunder	DOE	0.069	0.019
Black Thunder	KCPL	0.063	0.009
Big Sky	MNP	0.093	0.031
Caballo Rojo	KCPL	0.098	0.020
Spring Creek	MNP	0.093	0.019
Spring Creek	NSP	0.064	0.019
Rochelle	UE	0.137	0.004
75% Big Sky–25% Spring Creek[1]	MNP	0.093	0.028
Black Thunder	NSP	0.097	0.024
Colstrip	NSP	0.030	0.045
75% Black Thunder–25% Colstrip	NSP	0.072	0.041

[1]Values calculated from analysis results of the parent coals.

indices for predicting ash deposition propensity was verified by conducting slagging and fouling severity assessments at UE's Labadie Station, MNP's Clay Boswell Station, KCPL's Iatan and Hawthorn Stations, and NSP's Sherburne County Station. The opacity index was verified based on test burns and opacity measurements conducted at NSP's Sherburne County Station and TransAlta Utilities Corporation's Keephills Generating Station.

7.2 Results

7.2.1 Slagging and Fouling Indices Verification

Boiler specifications and feed coals for the four stations used to assess slagging and fouling severity are summarized in Table 30. Specific information collected during the assessments, such as the boiler operating conditions, slagging and fouling observations, in situ gas and deposit temperatures, and coal, ash, and deposit analysis results is compiled in four reports (45–48). Based on in situ observations of ash deposition, the slagging and fouling propensities of the feed coals were classified as low, medium, or high and then assigned index values of 17, 50, and 84, respectively. This empirical classification system was used to verify the PCQUEST propensity index classification scheme, in which low, medium, and high propensity are assigned to the following specific ranges of index values: 1–33, 34–66, and 67–100, respectively.

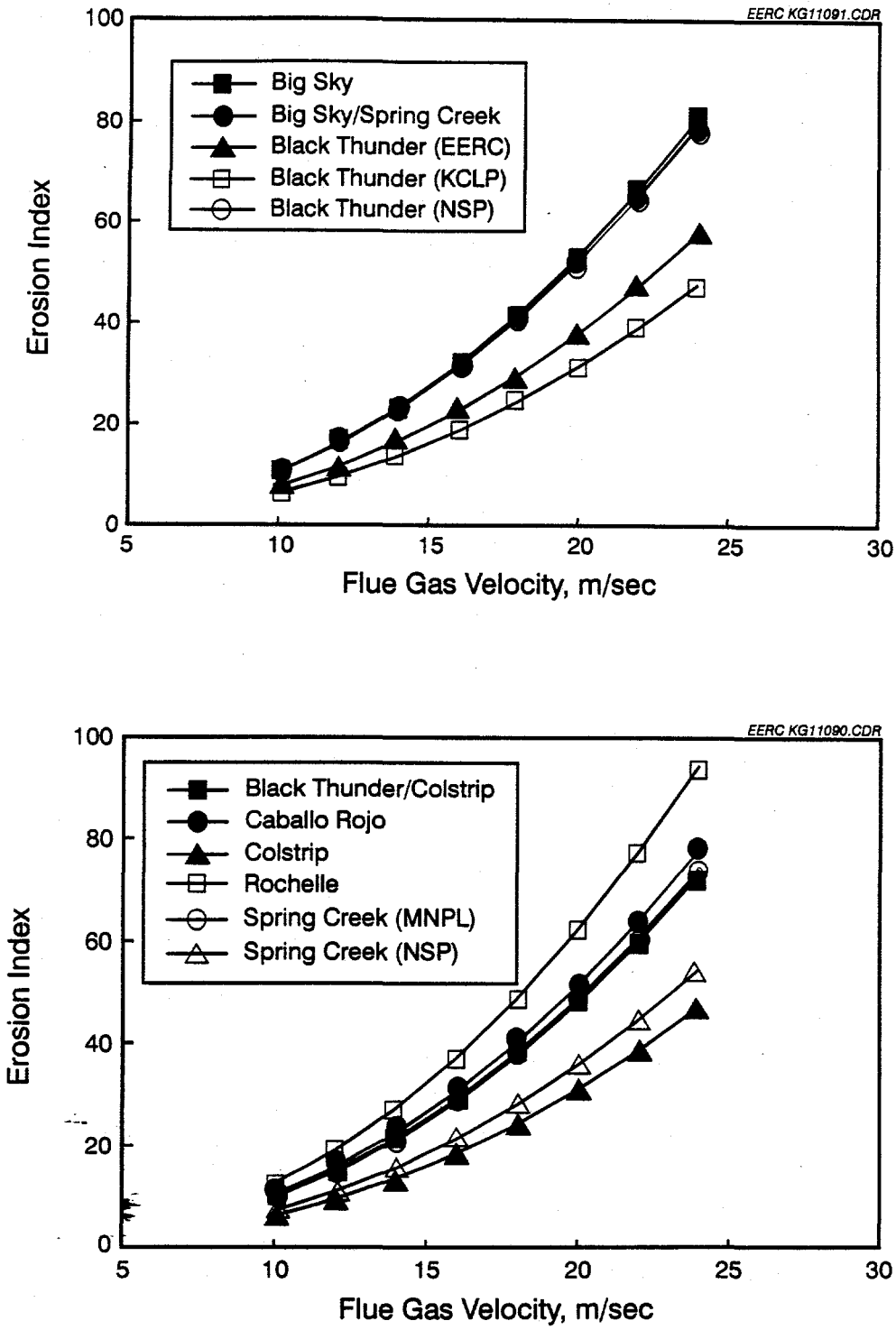

Figure 28. Erosion index values plotted as a function of flue gas velocity for eleven FPI test coals. Ranges in erosion index values corresponding to low, medium, and high levels of erosion propensity are indicated.

TABLE 30

Boiler Parameters[1]

	Labadie, UE		Clay Boswell, MNP		Iatan, KCPL	Hawthorn, KCPL	Sherburne County, NSP	
	Unit 3	Unit 4	Unit 3	Unit 4	Unit 1	Unit 5	Unit 1	Unit 2
Manufacturer	CE[2]	CE	CE	CE	B&W[3]	CE	CE	CE
Year	1972	1973	1973	1980	1980	1969	1976	1977
Rating, MW	600	600	350	535	720	520	700	700
Type	T-DB[4]	T-DB	T-DB	T-DB	O-DB[5]	T-DB	T-DB	T-DB
TSP[6] Control	ESP	ESP	Scrubber	ESP	ESP	ESP	Scrubber	Scrubber
SO_2 Control	Compl. fuel	Compl. fuel	Compl. fuel	Wet scrubber	Compl. fuel	Compl. fuel	Scrubber	Scrubber
NO_x Control	Compl. fuel	Low-No_x Burners	Compl. fuel	Staged combustion	Compl. fuel	Compl. fuel	Overfire air	Low-NO_x burners
Feed Coal	Rch.	Rch.	BS-SC	BS-SC	BTK	BTK	CS-BT	CS-BT

[1] Primary source of information: 1993 Environmental Directory of U.S. Powerplants, C.A.F. Bergesen, Editor, Edison Electric Institute.
[2] Combustion Engineering.
[3] Babcock & Wilcox.
[4] Tangential, dry bottom.
[5] Opposed, dry bottom.
[6] Total suspended particulate.

The PCQUEST slagging, high-temperature fouling, and low-temperature fouling index values are presented in Figures 29–31, respectively, for the feed coals that were used during the assessments. The calculations of the index values are primarily a function of coal properties, but also include boiler specifications and operating conditions. All the PCQUEST index values presented in Figures 29–31 were calculated for a particular boiler assuming full-load operation. The Black Thunder coal is predicted to have a much greater propensity for slagging and fouling at the Hawthorn Station relative to the Iatan Station. This large difference in the predicted ash deposition propensity of the Black Thunder coal at the two stations is related to boiler design. The Hawthorn Station boiler is a much older unit (Table 30) that was originally designed as a pressurized unit for burning bituminous coal, while the Iatan Station is equipped with a relatively new boiler designed for burning low-rank coals. The visual assessments of low, medium, or high slagging and fouling propensities are generally in agreement with the PCQUEST propensity index classifications. Consequently, the PCQUEST slagging and fouling indices appear to be reliable for predicting the ash deposition behavior of PRB subbituminous coals. Additional verification testing by Zygarlicke and others (49) indicates that the indices are also applicable to lignite and bituminous coals.

7.2.2 Opacity Index Verification

The opacity index was verified based on coal test burns and concurrent opacity measurements conducted at NSP's Sherburne County Station and TransAlta Utilities Corporation's Keephills Generating Station (50, 51). The coal used in the testing at NSP is indicated in Table 24; Keephills Station was fueled by subbituminous coal from several different seams of the Highvale mine, which is located in the central plains of Alberta, Canada. The actual measured

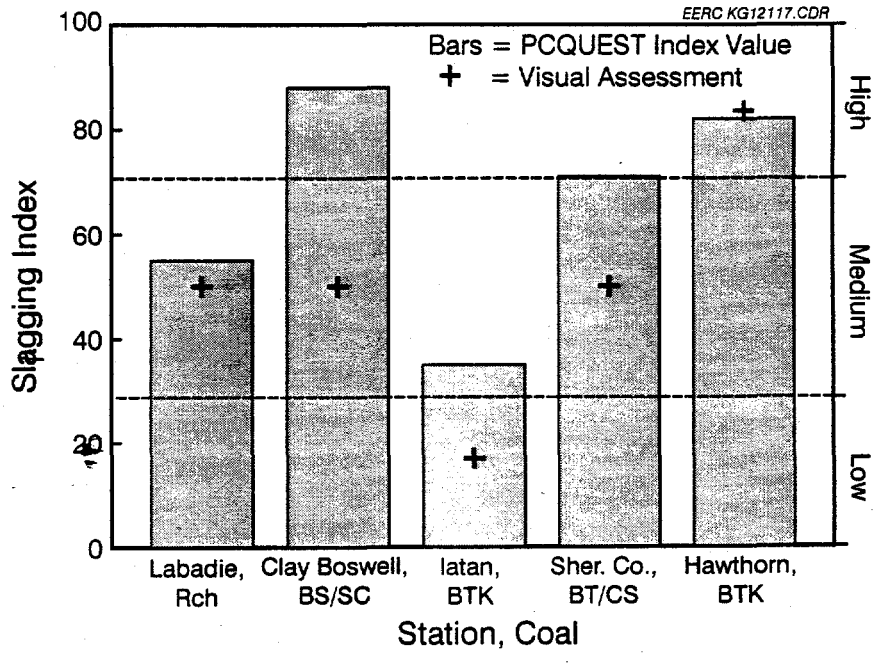

Figure 29. Full-scale verification of slagging index.

opacity values for the coals are compared to the calculated opacity index values in Figure 32. This comparison suggests that the opacity index is effective for ranking PRB subbituminous coals according to their opacity propensity.

8.0 CONCLUSIONS

A series of FPI applicable to coal-fired power plants has been developed based on theoretical considerations of inorganic transformations, entrained ash formation, and ash deposition and on experimental combustion data. The indices are calculated from CCSEM, chemical fractionation, proximate, ultimate, and ash elemental oxide analysis results. Boiler specifications and operating conditions can also be included in the index calculations to evaluate system effects on fireside performance. The index values are easily calculated and displayed using a software package designated as PCQUEST. Visual assessments of slagging and fouling and opacity measurements conducted on full-scale utility boilers are in reasonable agreement with PCQUEST propensity predictions. PCQUEST is designed to assist plant managers, fuel engineers, and researchers in screening coals and coal blends for optimum plant performance.

9.0 ACKNOWLEDGMENTS

The authors are grateful to S.E. Allen and D.N. Evenstad of the EERC for their computer programming and full-scale testing contributions, respectively. This research was supported by the United States Department of Energy Cooperative Agreement Nos. DE-FC21-86MC10637 and DE-FC21-93MC30098, Electric Power Research Institute Agreement No. RP3579-02, Kansas City Power and Light Company, Minnesota Power Company, Northern States Power Company, and

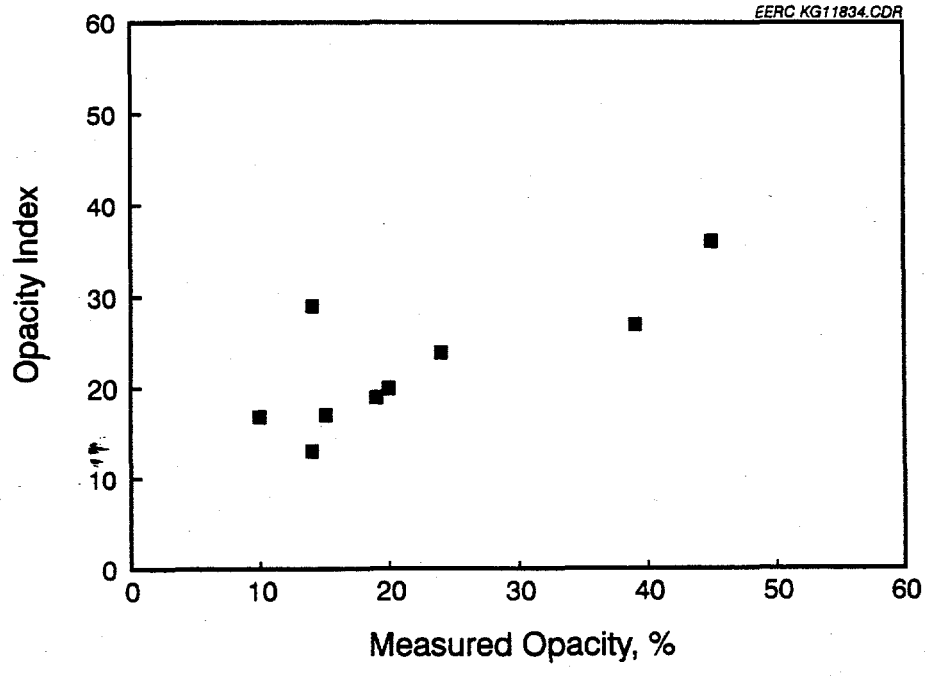

Figure 32. Comparison of calculated opacity index values to actual measured opacity values for nine subbituminous coal samples.

Union Electric Incorporated. We are grateful for the guidance provided by the following individuals: Todd Albertson, Robert Brown, Gerald Goblirsch, Philip Goldberg, Arun Mehta, George Nehls, and Kenneth Stuckmeyer. In addition, we acknowledge TransAlta Utilities Corporation for providing opacity testing information.

10.0 REFERENCES

1. Weisbecker, T.; Zygarlicke, C.J.; Jones, M.L. "Correlation of Inorganics in Powder River Basin Coals in Full-Scale Combustion," In *Inorganic Transformations and Ash Deposition During Combustion*; Benson, S.A., Ed.; ASME for the Engineering Foundation: New York, 1992; pp 699–711.

2. Winegartner, E.C. "Coal Fouling and Slagging Parameters," Prepared by the ASME Research Committee on Corrosion and Deposits from Combustion Gases, ASME, 1974, p 34.

3. Lee, R.J.; Kelly, J.F. "Overview of SEM-Based Automated Image Analysis," *Scanning Electron Microscopy* **1980**, *I*, 303–310.

4. Huggins, F.E.; Kosmack, D.A.; Huffman, G.P.; Lee, R.J. "Coal Mineralogies by SEM Automatic Image Analysis," *Scanning Electron Microscopy* **1980**, *I*, 531–540.

5. Huggins, F.E.; Huffman, G.P.; Lee, R.J. "Scanning Electron Microscope-Based Automated Image Analysis (SEM-AIA) and Mössbauer Spectroscopy: Quantitative Characterization of Coal Minerals," In *Coal and Coal Products: Analytical Characterization Techniques*; Fuller, E.L., Jr., Ed.; American Chemical Society Symposium Series 205, 1982; Chapter 12, pp 239–258.

6. Benson, S.A.; Holm, P.L. "Comparison of Inorganic Constituents in Three Low-Rank Coals," *Ind. Eng. Chem. Prod. Res. Dev.* **1985**, *24*, 145–149.

7. Miller, R.N.; Given, P.H. "A Geochemical Study of the Inorganic Constituents in Some Low-Rank Coals," United States Department of Energy Report FE-2494-TR1; 1979.

8. Karner, F.R.; Zygarlicke, C.J.; Brekke, D.W.; Steadman, E.N.; Benson, S.A. "New Analysis Techniques Help Control Boiler Fouling," *Power Engineering* **1994**, *98*, 35–38.

9. Honea, F.I. "Studies of Ash-Fouling Potential and Deposit Strength in the GFTEC Pilot Plant Test Furnace," In *Fouling and Slagging Resulting from Impurities in Combustion Gases*; Bryers, R.W.; Cole, S.S., Eds.; Proceedings of the Engineering Foundation Conference; Henniker, NH, July 12–17, 1981; pp 117–142.

10. Honea, F.I. "Survey of Ash-Related Losses at Low-Rank Coal-Fired Utility Boilers," In *Fouling and Slagging Resulting from Impurities in Combustion Gases*; Bryers, R.W.; Cole, S.S., Eds.; Proceedings of the Engineering Foundation Conference, Henniker, NH, July 12–17, 1981; pp 527–539.

11. Hurley, J.P.; Erickson, T.A.; Benson, S.A.; Brobjorg, J.N. "Ash Deposition at Low Temperatures in Boilers Firing Western U.S. Coals," Presented at the International Joint Power Generation Conference, San Diego, CA, 1991, p 8.

12. Zygarlicke, C.J.; Benson, S.A.; Borio, R.W.; Mehta, A.K. "Examination of Ash Deposition in Full-, Pilot-, and Bench-Scale Testing," *In* Proceedings of the 3rd International Conference on the Effects of Coal Quality on Power Plants; La Jolla, CA, Aug. 25-27, 1992.

13. McCollor, D.P.; Zygarlicke, C.J.; Allan, S.E.; Benson, S.A. "Ash Deposit Initiation in a Simulated Fouling Regime," *Energy & Fuels* **1993**, *7*, 761-767.

14. Zygarlicke, C.J.; Benson, S.A.; Borio, R.W. "Pilot- and Bench-Scale Combustion Testing of a Wyoming Subbituminous/Oklahoma Bituminous Coal Blend," In R.W. Bryers and N.S. Harding (Eds.), *Coal-Blending and Switching of Low-Sulfur Western Fuels*, New York, American Society of Mechanical Engineers, 1994; pp. 281-300.

15. Benson, S.A.; Hurley, J.P.; Zygarlicke, C.J.; Steadman, E.N.; Erickson, T.A. "Predicting Ash Behavior in Utility Boilers," *Energy & Fuels* **1993**, *7*, 746-754.

16. Benson, S.A.; Jones, M.L.; Harb, J.N. "Ash Formation and Deposition," In *Fundamentals of Coal Combustion for Clean and Efficient Use*; Smott, L.D., Ed.; Elsevier: New York, 1993; pp 299-374.

17. Zygarlicke, C.J.; Steadman, E.N. "Advanced SEM Techniques to Characterize Coal Minerals," *Scanning Microscopy* **1990**, *4* (3), 579-590.

18. Galbreath, K.C.; Brekke, D.W.; Folkedahl, B.C. "Automated Analytical Scanning Electron Microscopy and Image Analysis Methods for Characterizing the Inorganic Phases in Coal and Coal Combustion Products," *Prepr. Pap.—Am. Chem. Soc., Div. Fuel Chem.* **1992**, *37* (3), 1170-1176.

19. Casuccio, G.S.; Gruelich, F.A.; Hamburg, G.; Huggins, F.E.; Nissen, D.A.; Vleeskens, J.M. "Coal Mineral Analysis: A Check on Interlaboratory Agreement," *Scanning Microscopy* **1990**, *4* (2), 227-236.

20. Galbreath, K.C.; Zygarlicke, C.J.; Casuccio, G.S.; Moore, T.; Gottlieb, P.; Agron-Olshina, N.; Huffman, G.; Shah, A.; Yang, N.; Vleeskens, J.; Hamburg, G. "Collaborative Study of Quantitative Coal Mineral Analysis Using Computer-Controlled Scanning Electron Microscopy," *Fuel* (in review).

21. O'Keefe, C.A.; Erickson, T.A. "Quantitative XRF Analysis of Coal after Successive Leachings," *Advances in X-Ray Analysis* **1994**, *37*, 735-739.

22. Hurley, J.P.; Benson, S.A.; Mehta, A. "Ash Deposition at Low Temperatures in Boilers Burning High-Calcium Coals," In The *Impact of Ash Deposition on Coal-Fired Plants*; Taylor and Francis Publishing Company, 1994; pp 19-30.

23. Zygarlicke, C.J.; McCollor, D.P.; Benson, S.A.; Holm, P.L. "Ash Particle Size and Composition Evolution During Combustion of Synthetic Coal and Inorganic Mixtures," *In* Proceedings of the 24th Symposium (International) on Combustion/The Combustion Institute; 1992, pp 1171-1177.

24. Keeth, R.J.; Balfour, D.A.; Meserole, F.M.; Defries, T. "Utility Stack Opacity Troubleshooting Guidelines," Final Report GS-7180; Electric Power Research Institute, Research Project 2250-3, 1991.

25. Faxvog, F.R.; Roessler, D.M. "Carbon Aerosol Visibility vs. Particle Size Distribution," *Applied Optics* **1978**, *17*, 2612-2616.

26. Van De Hulst, H.C. *Light Scattering by Small Particles*, Wiley: New York, 1957; pp 119-130.

27. Holve, D.J. "In Situ Measurements of Fly Ash Formation from Pulverized Coal," *Combustion Science and Technology* **1986**, *44*, 269-288.

28. Graham, K.A.; Helble, J.; Kang, S.-G.; Sarofim, A.F.; Beér, J.M. "Mechanisms of the Transformation of Mineral Matter to Ash in Coal and Model Chars," In *Mineral Matter and Ash Deposition from Coal*; Bryers, R.W.; Vorres, K.S., Eds.; Engineering Foundation Conference, Santa Barbara, CA, Feb. 22-26, 1988; pp 165-185.

29. Helble, J.J.; Sarofim, A.F. "Influence of Char Fragmentation on Ash Particle Size Distributions," *Combustion and Flame* **1989**, *76*, 183-196.

30. Raask, E. "Mineral Impurities in Coal Combustion," Hemisphere Publishing Corporation, 1985, Chapter 18.

31. Flagen, R.C.; Friedlander, S.K. "Particle Formation in Pulverized Coal Combustion—A Review," In *Recent Developments in Aerosol Science*; Shaw, D. T.; Ed.; Wiley: New York, 1978, Chapter 2.

32. Oglesby, S.; Nichols, G.B. *Electrostatic Precipitation*; Marcel Dekker, Inc.: New York, 1978; Pollution Engineering and Technology Series, No. 8, p 368.

33. Hesketh, H.E. *Air Pollution Control: Traditional and Hazardous Pollutants*, Techonmic Publishing Company, Inc., 1991; p 475.

34. Katrinak, K.A.; Brekke, D.W.; Hurley, J.P. "Freeze-Dried Dispersions for Automated Scanning Electron Microscope Analysis of Individual Submicron Airborne Particulates," *In* Proceedings of the 50th Electron Microscopy Society of America Annual Meeting; Bailey, G.W.; Bentley, J.; Small, J.A., Eds.; San Francisco Press: San Francisco, CA, 1992.

35. Singer, J.G. *Combustion Fossil Power Systems*; Combustion Engineering, Inc.: Windsor, 1981, Chapter 17.

36. Bickelhaupt, R.E. "A Study to Improve a Technique for Predicting Fly Ash Resistivity with Emphasis on the Effect of Sulfur Trioxide," U.S. Environmental Protection Agency Report SoRI-EAS-85-841; 1985.

37. Bohren, C.F.; Huffman, D.R. "Absorption and Scattering of Light by Small Particles," Wiley: New York, 1983; p 530.

38. American Society of Testing and Materials. "Standard Test Method for Grindability of Coal by the Hardgrove-Machine Method," In *Annual Book of ASTM Standards*; 1991; 05.05, pp 206–211.

39. Hower, J.C.; Wild, G.D. "Relationship Between Hardgrove Grindability Index and Petrographic Composition for High-Volatile Bituminous Coals from Kentucky," *J. Coal Quality* **1988** *7*, 122–126.

40. American Society of Testing and Materials. "Standard Method for Microscopical Determination of Volume Percent of Physical Components of Coal," In *Annual Book of ASTM Standards*, 1991; 05.05, pp 315–316.

41. Nayak, R.V.; Bauer, F.W.; Tonden, T.P. "Mineral Matter in Coal—Origin, Identification, High-Temperature Transformation, and Boiler Erosion," *J. of Coal Quality* **1987**, 37–43.

42. Dooley, B. "Fly Ash Erosion of Boiler Tubes," *EPRI Journal* **1989**, *Jan./Feb.*, 54–56.

43. Kotwal, R.; Tabakoff, W. "A New Approach for Erosion Prediction Due to Fly Ash," *J. Eng. for Power, Trans. of ASME* **1981**, *103*, 265–270.

44. Raask, E.; Goetz, L. "Characterization of Captured Ash, Chimney Stack Solids and Trace Elements," *J. Inst. Energy* **1981**, *54*, 163.

45. Zygarlicke, C.J.; McCollor, D.P.; Toman, D.L.; Katrinak, K.A. "Fireside Performance Indices Report on the Site Visit to Union Electric Labadie Station," draft report submitted to the Fireside Performance Indices Participants; May 1993, 27 p.

46. McCollor, D.P.; Galbreath, K.C.; Evenstad, D.N.; Zygarlicke, C.J. "Fireside Performance Indices Report on the Site Visit to Minnesota Power & Light Company Clay Boswell Station," EERC Topical Report 94-EERC-04-9; April 1994, p 30.

47. Galbreath, K.C.; McCollor, D.P.; Zygarlicke, C.J. "Fireside Performance Indices Report on the Site Visits to Kansas City Power & Light Company's Iatan and Hawthorn Stations," EERC topical report; Aug. 1994, p 26.

48. Zygarlicke, C.J.; McCollor, D.P.; Evenstad, D.N.; Galbreath, K.C. "Fireside Performance Indices Report on the Site Visit to Northern States Power Company, Sherburne County Station, Becker, Minnesota," EERC Topical Report 94-EERC-09-08; Oct. 1994, p 24.

49. Zygarlicke, C.J.; Galbreath, K.C.; McCollor, D.P.; Toman, D.L. "Development of Fireside Performance Indices for Coal-Fired Utility Boilers," Presented at Engineering Foundation Conference: Application of Advanced Technology to Ash-Related Problems in Boilers, Waterville Valley, NH, July 16–22, 1995.

50. Galbreath, K.C.; Katrinak, K.A. "Coal Mineral Matter and Stack Emission Opacity Relationship: Keephills Power Station, Alberta, Canada," EERC final report; Nov. 1993, p 10.

51. Galbreath, K.C. "Source of Plume Opacity at Keephills Power Station, Alberta, Canada," EERC Final Report. 95-EERC-03-11; March 1995, p 12.

APPENDIX A

PCQUEST OPERATION MANUAL

Energy & Environmental Research Center

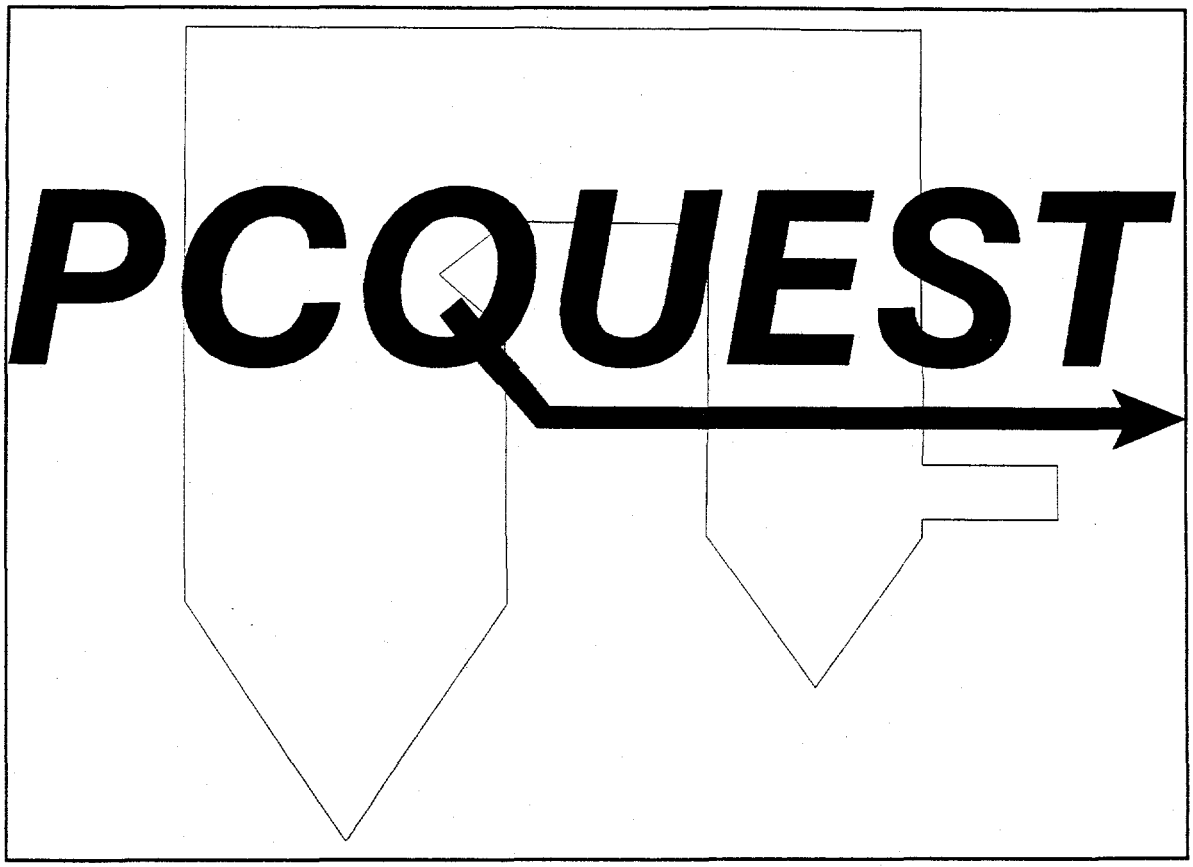

Operation Manual

Version 1.1

Printed on Recycled Paper

University of North Dakota

DISCLAIMER OF WARRANTIES AND LIMITATION OF LIABILITIES

This computer program manual was prepared by the University of North Dakota Energy & Environmental Research Center (EERC) as an account of work sponsored by the U.S. Department of Energy, Electric Power Research Institute, Kansas City Power and Light Company, Minnesota Power Company, Northern States Power Company, and Union Electric Company. Because of the research nature of the work performed, neither the EERC, any sponsor, nor any person acting on behalf of any of them makes any warranty, express or implied, or assumes any legal liability or responsibility for the accuracy, completeness, or usefulness of any information, apparatus, product, or process disclosed, or represents that its use would not infringe privately owned rights. Reference herein to any specific commercial product, process, or service by trade name, trademark, manufacturer, or otherwise does not necessarily constitute or imply its endorsement or recommendation by the EERC or any sponsor.

PCQUEST

Predictive Coal Quality Effects Screening Tool

 Energy & Environmental Research Center
University of North Dakota
PO Box 9018
Grand Forks, North Dakota 58202-9018
Telephone: (701) 777-5000
Fax: (701) 777-5181
Telex: 7-332537
World-Wide Web Address: http://www.eerc.und.nodak.edu

TABLE OF CONTENTS

1.0 BRIEF INTRODUCTION TO PCQUEST AND THE ENERGY & ENVIRONMENTAL RESEARCH CENTER

The Predictive Coal Quality Effects Screening Tool (PCQUEST) is a user-friendly fireside coal combustion performance software package. PCQUEST uses information derived from advanced coal analysis methods combined with general boiler information to predict the combustion performance of a pulverized coal. Eight empirical indices are computed by PCQUEST, including low-temperature fouling, high-temperature fouling, slagging, slag tapping, stack-plume opacity, boiler erosion, coal grindability, and sootblowing effectiveness. The indices were recently developed as part of a Fireside Performance Indices research project (1). Bench- and full-scale testing of Powder River Basin subbituminous coals were involved in formulating and verifying the indices. PCQUEST is designed to assist plant managers, fuel engineers, and consultants in making the best possible coal combustion performance decisions.

PCQUEST has been developed by the Energy & Environmental Research Center (EERC), a research, consulting, and development organization affiliated with the University of North Dakota in Grand Forks, North Dakota. The Center is recognized as an international leader in low-rank coal research providing energy and environmental research and consulting services for public and private clients in the United States and abroad. Additional information about the EERC is available by calling (701) 777-5000 or by accessing the World-Wide Web at http://www.eerc.und.nodak.edu.

1.1 Data Input

Input to PCQUEST consists of coal analysis results determined by computer-controlled scanning electron microscopy (CCSEM)[1] and chemical fractionation[2] methods, in addition to standard American Society for Testing and Materials (ASTM) proximate, ultimate, and coal ash chemical analysis methods. The CCSEM and chemical fractionation methods provide quantitative information on the distribution of various elements (Na, Mg, Al, Si, P, S, Cl, K, Ca, Ti, Fe, and Ba) among the maceral and mineral constituents of coal, whereas ASTM methods provide information on the bulk chemical composition and combustion characteristics of coal. The combination of these analysis data provides a more comprehensive basis for predicting the combustion performance characteristics of a pulverized coal. Boiler specifications and operating conditions, such as the combustion system (conventional or low-NO_x), design fuel specifications, current operating load, and furnace dimensions are also used as input into PCQUEST.

---

[1]The CCSEM method of coal mineral analysis was originally developed in the late 1970s and early 1980s by Lee et al.(2) and Huggins et al.(3,4). The method and its applications in coal mineral research were reviewed recently by Skorupska and Carpenter (5).

[2]A selective leaching procedure based on the differences in solubilities of organically bound and mineral bound inorganic constituents in stirred solutions of deionized water (H_2O), 1 M ammonium acetate (NH_4OAc), and 1 M hydrochloric acid (HCl).

1.2 Data Output and Manipulation

The eight indices are expressed numerically as whole numbers ranging from 0 to 100. General classifications of low, medium, and high propensity are assigned to the following specific ranges of index values: 1–33, 34–66, and 67–100, respectively. A greater value corresponds to an increase in severity or adverse effect for a given index. This propensity-index classification scheme applies to all the indices except the coal grindability index. The coal grindability index is directly related to the ASTM Hardgrove grindability index. A value of 0 for any of the indices indicates that the proper input data required to calculate the index were not provided.

Index values for multiple coals can be presented and compared in a tabular or graphical format. A coal blending option enables the blending of two to four coals in proportions specified by the user. PCQUEST is most useful for comparing the relative fireside performance of two or more coals or for determining optimum coal-blending ratios.

2.0 SYSTEM AND SOFTWARE REQUIREMENTS

PCQUEST will run on a 386 or higher personnel computer equipped with a VGA or EGA video adapter and DOS version 3.1 or higher. It requires a minimum of 2 MB of RAM to operate properly. A 3.5-in. high-density (1.44 MB) disk drive and at least 1 MB of free memory on a hard drive is required to install the PCQUEST package. The package consists of 1) the PCQUEST program that calculates index values and displays them; 2) a RESIST program, originally developed by Bickelhaupt (6), used by PCQUEST in the stack-plume opacity index for predicting fly ash resistivity as a function of temperature; 3) coal analysis and boiler parameter files; 4) two Lotus 1-2-3 spreadsheet files, COAL.WK3 and BOILER.WK3, for creating coal analysis and boiler parameter input files, respectively; and 5) an INSTALL program for installing PCQUEST.

3.0 INSTALLATION

PCQUEST is designed to be installed on a hard drive designated as the "C:" drive. A directory designated as C:\PCQUEST, along with subdirectories, C:\PCQUEST\ANALYSIS and C:\PCQUEST\INDICES, are created during installation. To install PCQUEST, use the following step-by-step procedure:

1. Insert the PCQUEST installation disk into a 3.5-in. disk drive.

2. Specify the 3.5-in. drive as the current drive by typing *a:* or *b:* and pressing ENTER.

3. Type *install* and press ENTER.

4. Directory creation and installation will proceed.

4.0 INPUT DATA FILES

The coal analysis parameters indicated in Table 1 and the boiler specifications and operating conditions indicated in Table 2 must be organized into ASCII files with *.ana* and *.boi* extensions, respectively, and then saved in the Analysis subdirectory before PCQUEST can be executed. Most database, spreadsheet, and word processing programs can produce ASCII files. Provided with the PCQUEST installation disk are several coal analysis files and boiler parameter files.

TABLE 1
PCQUEST Coal Analysis Input Parameters

Method	Parameter(s)	Unit(s)
CCSEM	Total mineral content	wt%, coal basis
CCSEM	Quantitative mineralogy as a function of particle diameter	wt%, mineral basis
CCSEM	Excluded mineralogy as a function of particle diameter	Frequency %
Chemical Fractionation	Leachable Si, Al, Fe, Ti, P, Ca, Mg, Na, and K by H_2O, NH_4OAc, and HCl	% Removed and % remaining
Proximate	Moisture, volatile matter, fixed C, and ash	wt%, as-received
Ultimate	H, total C, N, S, O, and ash	wt%, as-received
Heating Value	Calorific	Btu/lb, as-received
Chemical Composition	SiO_2, Al_2O_3, Fe_2O_3, TiO_2, P_2O_5, CaO, MgO, Na_2O, K_2O, and SO_3	wt%, ash basis

TABLE 2
PCQUEST Boiler Input Parameters

Parameter	Unit or Available Options
Flue Gas Velocity	m/sec
Type of Particulate Emission Control Device	Baghouse, cold- or hot-side ESP[1], scrubber
Average ESP Temperature	°C
Furnace Box Cross-Sectional (Plan) Area	ft^2
Design Maximum Continuous Rating, firing rate	lb/hr
Design Coal Heating Value	Btu/lb
Design Coal Ash	wt%, as-received
Combustion System	Conventional or low-NO_x
Type of Boiler	Pulverized coal-fired or cyclone

[1] Electrostatic precipitator.

4.1 Coal Analysis File Format

The required format of a coal analysis (*.ana*) file is shown in Figure 1. A coal analysis file consists of six sections: 1) header, 2) CCSEM mineral analysis results, 3) CCSEM-excluded mineral analysis results, 4) chemical fractionation analysis results, 5) proximate and ultimate analysis results, and 6) ash chemical composition. The content and format of these six sections are described below.

4.1.1 Header

The header section, as exemplified below, includes the following input parameters: coal identification number, date, coal analysis file name, and sample description. The number of characters and spaces that can be entered after the colon of each input parameter is limited as indicated below.

Identification number:	47106280	*[10 character and space limit]*
Date:	10/24/94	*[25 character and space limit]*
File name:	COAL B.ana	*[12 character and space limit]*
Sample description:	Coal B for Boiler C	*[80 character and space limit]*
PCQUEST input version:	1.1	

Identification number: 47106280
Date: 10/24/94
File name: CoalB.ana
Sample description: Coal B for Boiler C
PCQUEST input version: 1.1

CCSEM Analysis:

MINERAL FRACTION	3.543							
Size bins	1.0-2.2	2.2-4.6	4.6-10	10-22	22-46	46-100	Total	%Excluded:
QUARTZ	6.4	9.2	8.9	6.1	2.5	0.7	33.7	59
IRON OXIDE	0.1	0.2	0.0	0.0	0.0	0.0	0.2	100
PERICLASE	0.0	0.0	0.0	0.0	0.0	0.0	0.0	0
RUTILE	0.4	0.3	0.1	0.0	0.0	0.0	0.9	9
ALUMINA	0.1	0.0	0.0	0.0	0.0	0.0	0.1	45
CALCITE	0.1	0.4	0.1	0.0	0.0	0.0	0.6	5
DOLOMITE	0.0	0.1	0.0	0.0	0.0	0.0	0.1	0
ANKERITE	0.0	0.0	0.0	0.0	0.0	0.0	0.0	0
KAOLINITE	5.1	6.5	5.1	3.6	1.2	1.3	22.9	50
MONTMORILLONITE	0.7	1.8	1.5	1.8	0.8	0.0	6.1	66
K AL-SILICATE	0.3	0.3	0.3	0.0	0.1	0.0	0.9	77
FE AL-SILICATE	0.1	0.0	0.0	0.0	0.0	0.0	0.1	24
CA AL-SILICATE	0.9	0.4	0.2	0.1	0.0	0.0	1.6	30
NA AL-SILICATE	0.0	0.0	0.0	0.0	0.0	0.0	0.0	0
ALUMINOSILICATE	0.1	0.4	0.6	0.3	0.1	0.0	1.3	39
MIXED AL-SILICA	0.4	0.1	0.2	0.0	0.0	0.0	0.6	19
FE SILICATE	0.0	0.0	0.0	0.0	0.0	0.0	0.0	0
CA SILICATE	0.0	0.1	0.0	0.0	0.0	0.0	0.1	0
CA ALUMINATE	0.0	0.0	0.0	0.0	0.0	0.0	0.0	0
PYRITE	1.4	0.6	0.6	1.4	0.6	0.0	4.5	77
PYRRHOTITE	0.0	0.0	0.0	0.0	0.0	0.0	0.0	0
OXIDIZED PYRRHOTITE	0.0	0.0	0.0	0.0	0.0	0.0	0.0	0
GYPSUM	0.0	0.0	0.0	0.0	0.0	0.0	0.0	0
BARITE	0.0	0.0	0.0	0.0	0.0	0.0	0.0	0
APATITE	0.0	0.0	0.0	0.0	0.0	0.0	0.1	34
CA AL-PHOSPHATE	1.9	5.8	1.5	0.1	0.1	0.0	9.5	21
KCL	0.0	0.0	0.0	0.0	0.0	0.0	0.0	0
GYPSUM/BARITE	0.1	0.0	0.0	0.0	0.0	0.0	0.1	0
GYPSUM/AL-SILICATE	0.3	0.4	0.0	0.2	0.1	0.0	1.0	8
SI-RICH	0.4	0.1	0.4	0.8	0.1	0.4	1.9	45
CA-RICH	0.0	0.0	0.0	0.0	0.0	0.0	0.0	52
CA-SI RICH	0.0	0.0	0.0	0.0	0.0	0.0	0.0	0
UNKNOWN	5.9	6.1	0.9	0.4	0.2	0.0	13.6	23
TOTALS	24.6	32.4	20.5	14.4	5.7	2.4	100.0	

CCSEM %Excluded Analysis:

QUARTZ	45.1	69.5	54.4	52.1	71.0	100.0
IRON OXIDE	100.0	100.0	0.0	0.0	0.0	0.0
PERICLASE	0.0	0.0	0.0	0.0	0.0	0.0
RUTILE	17.4	0.0	0.0	0.0	0.0	0.0
ALUMINA	44.9	0.0	0.0	0.0	0.0	0.0
CALCITE	52.1	0.0	0.0	0.0	0.0	0.0
DOLOMITE	0.0	0.0	0.0	0.0	0.0	0.0
ANKERITE	0.0	0.0	0.0	0.0	0.0	0.0
KAOLINITE	56.1	36.6	46.1	51.2	55.7	100.0
MONTMORILLONITE	52.8	83.6	51.3	54.0	100.0	0.0
K AL-SILICATE	87.4	100.0	43.5	0.0	100.0	0.0
FE AL-SILICATE	24.3	0.0	0.0	0.0	0.0	0.0
CA AL-SILICATE	17.1	34.0	26.8	100.0	0.0	0.0
NA AL-SILICATE	0.0	0.0	0.0	0.0	0.0	0.0
ALUMINOSILICATE	0.0	0.0	33.9	100.0	100.0	0.0
MIXED AL-SILICA	20.7	0.0	23.1	0.0	0.0	0.0
FE SILICATE	0.0	0.0	0.0	0.0	0.0	0.0
CA SILICATE	0.0	0.0	0.0	0.0	0.0	0.0
CA ALUMINATE	0.0	0.0	0.0	0.0	0.0	0.0
PYRITE	67.7	100.0	84.3	71.0	79.1	0.0
PYRRHOTITE	0.0	0.0	0.0	0.0	0.0	0.0
OXIDIZED PYRRHOTITE	0.0	0.0	0.0	0.0	0.0	0.0
GYPSUM	0.0	0.0	0.0	0.0	0.0	0.0
BARITE	0.0	0.0	0.0	0.0	0.0	0.0
APATITE	100.0	0.0	0.0	0.0	0.0	0.0
CA AL-PHOSPHATE	27.2	15.4	26.8	0.0	100.0	0.0
KCL	0.0	0.0	0.0	0.0	0.0	0.0
GYPSUM/BARITE	0.0	0.0	0.0	0.0	0.0	0.0
GYPSUM/AL-SILICATE	4.9	0.0	0.0	0.0	100.0	0.0
SI-RICH	0.0	100.0	36.9	77.5	100.0	0.0
CA-RICH	52.1	0.0	0.0	0.0	0.0	0.0
CA-SI RICH	0.0	0.0	0.0	0.0	0.0	0.0
UNKNOWN	14.7	20.3	70.4	40.1	100.0	0.0

Chemfraction Analysis:

Silicon	0	0	0	100
Aluminum	0	0	0	100
Iron	3	0	42	55
Titanium	6	0	0	94
Phosphorus	4	0	88	8
Calcium	3	0	94	3
Magnesium	2	0	91	7
Sodium	23	0	75	2
Potassium	0	0	6	94

ProxUlt Analyses:

Moisture	21.00
Volative Matter	36.83
Fixed Carbon	36.94
Ash	5.23
Hydrogen	6.05
Carbon	54.78
Nitrogen	0.97
Sulfur	0.46
Oxygen	32.50
Ash	5.23
BTU	9422

XRF Analysis:

SIO2	30.55
AL2O3	13.73
FE2O3	2.25
TIO2	1.06
P2O5	1.63
CAO	21.38
MGO	4.24
NA2O	1.14
K2O	0.24
SO3	23.79

Figure 1. Example of a PCQUEST coal analysis (*.ana*) file.

4.1.2 CCSEM Mineral Analysis Results

The CCSEM mineral analysis section consists of 9 columns and 37 rows as shown below. The first row header, "CCSEM Analysis:," is a title line that demarcates the beginning of the CCSEM mineral analysis section. The total mineral content, measured by CCSEM on a wt% coal basis, is entered after the second row header "MINERAL FRACTION." The third row consists of column headings for the remaining 34 rows of mineral analysis data. The CCSEM data reduction program, PARTCHAR©, employed at the EERC, classifies coal minerals into 33 mineral and chemical categories as indicated below. The last row in the CCSEM mineral analysis section contains the total wt% of all minerals in each size interval. The eighth column indicates the total wt% for a given mineral or chemical category. The last column indicates the proportion, frequency %, of the corresponding mineral–chemical type that is excluded from coal particles.

CCSEM Analysis:								
MINERAL FRACTION	3.543							
Size Bins	1.0-2.2	2.2-4.6	4.6-10	10-22	22-46	46-100	Total	%Excluded:
QUARTZ	6.4	9.2	8.9	6.1	2.5	0.7	33.7	59.0
IRON OXIDE	0.1	0.2	0.0	0.0	0.0	0.0	0.2	100.0
PERICLASE	0.0	0.0	0.0	0.0	0.0	0.0	0.0	0.0
RUTILE	0.4	0.3	0.1	0.0	0.0	0.0	0.9	9.0
ALUMINA	0.1	0.0	0.0	0.0	0.0	0.0	0.1	45.0
CALCITE	0.1	0.4	0.1	0.0	0.0	0.0	0.6	5.0
DOLOMITE	0.0	0.1	0.0	0.0	0.0	0.0	0.1	0.0
ANKERITE	0.0	0.0	0.0	0.0	0.0	0.0	0.0	0.0
KAOLINITE	5.1	6.5	5.1	3.6	1.2	1.3	22.9	50.0
MONTMORILLONITE	0.7	1.6	1.5	1.6	0.6	0.0	6.1	66.0
K AL-SILICATE	0.3	0.3	0.3	0.0	0.1	0.0	0.9	77.0
FE AL-SILICATE	0.1	0.0	0.0	0.0	0.0	0.0	0.1	24.0
CA AL-SILICATE	0.9	0.4	0.2	0.1	0.0	0.0	1.6	30.0
NA AL-SILICATE	0.0	0.0	0.0	0.0	0.0	0.0	0.0	0.0
ALUMINOSILICATE	0.1	0.4	0.6	0.3	0.1	0.0	1.3	39.0
MIXED AL-SILICATE	0.4	0.1	0.2	0.0	0.0	0.0	0.6	19.0
FE SILICATE	0.0	0.0	0.0	0.0	0.0	0.0	0.0	0.0
CA SILICATE	0.0	0.1	0.0	0.0	0.0	0.0	0.1	0.0
CA ALUMINATE	0.0	0.0	0.0	0.0	0.0	0.0	0.0	0.0
PYRITE	1.4	0.6	0.6	1.4	0.6	0.0	4.5	77.0
PYRRHOTITE	0.0	0.0	0.0	0.0	0.0	0.0	0.0	0.0
OXIDIZED PYRRHOTITE	0.0	0.0	0.0	0.0	0.0	0.0	0.0	0.0
GYPSUM	0.0	0.0	0.0	0.0	0.0	0.0	0.0	0.0
BARITE	0.0	0.0	0.0	0.0	0.0	0.0	0.0	0.0
APATITE	0.0	0.0	0.0	0.0	0.0	0.0	0.1	34.0
CA AL-PHOSPHATE	1.9	5.8	1.5	0.1	0.1	0.0	9.5	21.0
KCL	0.0	0.0	0.0	0.0	0.0	0.0	0.0	0.0
GYPSUM/BARITE	0.1	0.0	0.0	0.0	0.0	0.0	0.1	0.0
GYPSUM/AL-SILICATE	0.3	0.4	0.0	0.2	0.1	0.0	1.0	8.0
SI-RICH	0.4	0.1	0.4	0.6	0.1	0.4	1.9	45.0
CA-RICH	0.0	0.0	0.0	0.0	0.0	0.0	0.0	52.0
CA-SI RICH	0.0	0.0	0.0	0.0	0.0	0.0	0.0	0.0
UNKNOWN	5.9	6.1	0.9	0.4	0.2	0.0	13.6	23.0
TOTALS	24.6	32.4	20.5	14.4	5.7	2.4	100.0	

4.1.3 CCSEM-Excluded Mineral Analysis Results

The format for the CCSEM-excluded mineral analysis section is similar to that of the CCSEM mineral analysis section. The size-interval headings in row three of the CCSEM mineral analysis section also apply to the six columns of data in the CCSEM-excluded mineral analysis section. The six columns contain the proportion, in frequency %, of the corresponding mineral-chemical type that is excluded from coal particles for a given mineral size interval.

CCSEM % Excluded Analysis:						
QUARTZ	45.1	69.5	54.4	52.1	71.0	100.0
IRON OXIDE	100.0	100.0	0.0	0.0	0.0	0.0
PERICLASE	0.0	0.0	0.0	0.0	0.0	0.0
RUTILE	17.4	0.0	0.0	0.0	0.0	0.0
ALUMINA	44.9	0.0	0.0	0.0	0.0	0.0
CALCITE	52.1	0.0	0.0	0.0	0.0	0.0
DOLOMITE	0.0	0.0	0.0	0.0	0.0	0.0
ANKERITE	0.0	0.0	0.0	0.0	0.0	0.0
KAOLINITE	56.1	36.6	46.1	51.2	55.7	100.0
MONTMORILLONITE	52.8	83.6	51.3	54.0	100.0	0.0
K AL-SILICATE	87.4	100.0	43.5	0.0	100.0	0.0
FE AL-SILICATE	24.3	0.0	0.0	0.0	0.0	0.0
CA AL-SILICATE	17.1	34.0	26.8	100.0	0.0	0.0
NA AL-SILICATE	0.0	0.0	0.0	0.0	0.0	0.0
ALUMINOSILICATE	0.0	0.0	33.9	100.0	100.0	0.0
MIXED AL-SILICA	20.7	0.0	23.1	0.0	0.0	0.0
FE SILICATE	0.0	0.0	0.0	0.0	0.0	0.0
CA SILICATE	0.00	0.0	0.0	0.0	0.0	0.0
CA ALUMINATE	0.0	0.0	0.0	0.0	0.0	0.0
PYRITE	67.7	100.0	84.3	71.0	79.1	0.0
PYRRHOTITE	0.0	0.0	0.0	0.0	0.0	0.0
OXIDIZED PYRRHOTITE	0.0	0.0	0.0	0.0	0.0	0.0
GYPSUM	0.0	0.0	0.0	0.0	0.0	0.0
BARITE	0.0	0.0	0.0	0.0	0.0	0.0
APATITE	100.0	0.0	0.0	0.0	0.0	0.0
CA AL-PHOSPHATE	27.2	15.4	26.8	0.0	100.0	0.0
KCL	0.0	0.0	0.0	0.0	0.0	0.0
GYPSUM/BARITE	0.0	0.0	0.0	0.0	0.0	0.0
GYPSUM/AL-SILICATE	4.9	0.0	0.0	0.0	100.0	0.0
SI-RICH	0.0	100.0	36.9	77.5	100.0	0.0
CA-RICH	52.1	0.0	0.0	0.0	0.0	0.0
CA-SI RICH	0.0	0.0	0.0	0.0	0.0	0.0
UNKNOWN	14.7	20.3	70.4	40.1	100.0	0.0

4.1.4 Chemical Fractionation Analysis Results

The chemical fractionation analysis results are organized into four columns. The elemental losses, in percents relative to the unfractionated coal, resulting from the H_2O, 1 M NH_4OAc, and 1 M HCl extractions are reported in the first three columns. The last column indicates the percent of each element that was insoluble and thus remained in the final coal residue after the leaching treatments.

Chemfraction Analysis:				
Silicon	0	0	0	100
Aluminum	0	0	0	100
Iron	3	0	42	55
Titanium	6	0	0	94
Phosphorus	4	0	88	8
Calcium	3	0	94	3
Magnesium	2	0	91	7
Sodium	23	0	75	2
Potassium	0	0	6	94

4.1.5 Proximate and Ultimate Analysis Results

The standard ASTM proximate and ultimate analysis results are reported, on an as-received basis, in a single column as indicated below.

Prox/Ult Analysis:	
Moisture	21.00
Volatile Matter	36.83
Fixed Carbon	36.94
Ash	5.23
Hydrogen	6.05
Carbon	54.78
Nitrogen	0.97
Sulfur	0.46
Oxygen	32.50
Ash	5.23
Btu Calorific	9422

4.1.6 Ash Chemical Analysis

The chemical composition of coal ash (in wt%) is also tabulated in a single column as indicated below.

XRF Analysis:	
SiO_2	30.55
Al_2O_3	13.73
Fe_2O_3	2.25
TiO_2	1.06
P_2O_5	1.63
CaO	21.38
MgO	4.24
Na_2O	1.14
K_2O	0.24
SO_3	23.79

4.1.7 Creation of a Coal Analysis (.ana) File

A Lotus 1-2-3 spreadsheet containing a generic coal analysis file is provided on the PCQUEST installation disk as COAL.WK3. A user can create a coal analysis file by simply replacing the zeros in COAL.WK3 with data, and then saving the spreadsheet as a text file in the PCQUEST analysis subdirectory (C:\PCQUEST\ANALYSIS\filename.ana). The coal analysis data can be entered manually from the keyboard, or if available, transferred directly from the appropriate coal analysis result files. PCQUEST will run on incomplete coal analysis files, provided that zeros are inserted at the corresponding location(s) of the missing data. The indices, however, that require the missing data will assume a value of zero.

4.2 Boiler Parameter File

The required format of a boiler (*.boi*) file is shown below. The first three rows compose the header section of the file. The remaining eleven rows consist of boiler specification and operating input parameters. The flue gas velocity variable is used to calculate the boiler erosion index. In a pulverized coal-fired boiler, flue gas velocities generally range from about 15 to 18 m/sec. The average hot- or cold-side ESP temperature is used in the calculation of the opacity index if an ESP is selected as the particulate control device. Typical average hot- and cold-side ESP temperatures are 370° and 150°C, respectively. The effects of the remaining boiler parameters on the index calculations can be invoked or negated by entering the desired response to the prompt, "Use Boiler Parameters 1=yes 0=no."

Boiler name:	Example
Date:	1/1/95
PCQUEST input version:	1.0
Flue gas velocity (m/sec):	16.0
Baghouse 1, Cold-side ESP 2, Hot-side ESP 3, Scrubber 4:	2
Average hot-side ESP Temp (°C):	0
Average cold-side ESP Temp (°C):	150
Use Boiler Parameters 1=yes 0=no:	1
Furnace box cross-sectional area (ft^2):	2500
Design maximum continuous rating, firing rate (lb/hr):	4.00e05
Design coal heating value (Btu/lb):	11000
Design coal % ash:	10.0
1=Conventional, 2=Low NO_x:	1
1=pc-fired, 2=Cyclone:	1

A Lotus 1-2-3 spreadsheet containing a boiler parameter file is provided on the PCQUEST installation disk as BOILER.WK3. A user can create a boiler parameter file by simply replacing the zeros in BOILER.WK3 with data, and then saving the spreadsheet as a text file in the PCQUEST analysis subdirectory (C:\PCQUEST\ANALYSIS\filename.boi).

5.0 PCQUEST OPERATION

Access the PCQUEST directory by typing the command, *cd C:\PCQUEST*, and pressing ENTER. Execute the PCQUEST program by typing *PCQUEST* and pressing ENTER. An opening logo will appear when PCQUEST begins. PCQUEST is a menu-driven program. Press any key to proceed to the initial PCQUEST main menu, shown below. Four options are available in the PCQUEST Main Menu. An option is executed by entering its corresponding highlighted first letter. Both lowercase and uppercase letters are accepted by the program.

Note: The main menu can be redisplayed at any time during the execution of PCQUEST by pressing ESC.

PCQUEST
Version 1.0

About PCQUEST
Run
View Results
Exit

ENTER A HIGHLIGHTED LETTER

5.1 About PCQUEST Option

The About PCQUEST option provides a general description of PCQUEST.

5.2 Run Option

The Run option initiates the data input and indices calculation processes. After selecting the Run option, the user is prompted with "Do you want to use the coal blending option?" If the coal blending option is rejected by typing *N*, a listing of coal analysis files in the PCQUEST\ANALYSIS subdirectory with the file extension *.ana* will be displayed as exemplified below. A maximum of nine coal analysis files can be listed simultaneously on the screen. Additional analysis files can be listed by entering *M*. The files can be relisted by entering *R*. A maximum of five coals can be selected for calculating indices by entering the highlighted letters next to the desired coals.

RUN PCQUEST
CHOOSE 1 TO 5 COALS TO ANALYZE:

A COAL1.ANA
B COAL2.ANA
C COAL3.ANA
D COAL4.ANA
E COAL5.ANA
F COAL6.ANA
G COAL7.ANA
H COAL8.ANA
I COAL9.ANA

Press Enter to continue More Files

ENTER A HIGHLIGHTED LETTER.

If the blending option was selected by typing *Y*, the coal selection menu shown below will be displayed. Two to four coals can be selected for blending by entering the highlighted letters next to the desired coal analysis files.

RUN PCQUEST
CHOOSE 2 TO 4 COALS TO BLEND:

A COAL1.ANA
B COAL2.ANA
C COAL3.ANA
D COAL4.ANA
E COAL5.ANA
F COAL6.ANA
G COAL7.ANA
H COAL8.ANA
I COAL9.ANA

Press Enter to continue More Files

ENTER A HIGHLIGHTED LETTER.

Press ENTER after completing the appropriate coal selection process. If the blending option was selected, then the user will be prompted to enter the blending percentages as integer values for each selected coal as exemplified below. The sum of the entered blending percentages must equal 100, or the blending percentage menu will be redisplayed.

RUN PCQUEST

PLEASE ENTER IN THE BLEND PERCENTAGE FOR
THE HIGHLIGHTED NAME. DO NOT USE A DECIMAL.
COAL1.ANA
COAL2.ANA
COAL3.ANA
COAL4.ANA

20

USE ENTER TO CONTINUE TO NEXT BLEND

After completing the data input associated with the nonblending or blending options, a listing of boiler parameter files in the PCQUEST\ANALYSIS subdirectory with the file extension *.boi* will be displayed as shown below. A maximum of nine boiler files can be listed simultaneously on the screen. Additional boiler files can be viewed by entering *M*. The files can be relisted by entering *R*. Select a boiler parameter file to associate with the selected coal(s) by entering the letter next to the desired boiler.

RUN PCQUEST
CHOOSE BOILER PARAMETERS:

A BOILER1.BOI
B BOILER2.BOI
C BOILER3.BOI
D BOILER4.BOI
E BOILER5.BOI
F BOILER6.BOI
G BOILER7.BOI
H BOILER8.BOI
I BOILER9.BOI

More Files

ENTER A HIGHLIGHTED LETTER.

Next, the user will be prompted to enter a load percentage for the selected boiler as indicated below. The load percentage refers to the actual load of interest expressed as a percentage (1%–100%) of the maximum continuous-load rating. After typing a load percentage, press ENTER to continue.

RUN PCQUEST
ENTER BOILER LOAD PERCENTAGE FOR:

BOILER4.BOI

DO NOT USE A DECIMAL.

The user will then be prompted, as shown below, to name a file in which to save the set of eight indices for each coal. The BACKSPACE key can be used to correct typing errors that may occur while entering the file name(s). If the name already exists, the user has the option of overwriting the existing file or entering a different name. The created index file(s) will be saved in ASCII format in the PCQUEST\INDICES subdirectory with a *.ind* file extension. An example of the format of an index file is presented in Figure 2. The Main Menu will be redisplayed after all the index files have been created.

RESULT FILE NAME
PLEASE ENTER RESULTS FILE NAME FOR
COAL A
(limit of 8 letters and don't include extension)

USE ENTER TO CONTINUE

Identification Number:	47106280
Date:	10/24/94
File Name:	CoalB.ana
Sample	Coal B for Boiler Unit C
Boiler Name:	Boiler C
PCQUEST Input Version:	1.0
INDICES:	
GRINDABILITY	49
LOW-TEMP FOULING	9
HIGH-TEMP FOULING	31
SLAGGING	32
SLAG TAP	98
SOOTBLOWING	5
EROSION	40
OPACITY	62

Figure 2. Example of a PCQUEST index (.ind) file.

5.3 View Results Option

The View Results option is used to present and compare index file sets in a tabular or graphical format. Three options are available in the View Results menu as shown below. An index set for a coal can be displayed by entering *D*, two to five index sets can be compared by entering *C*, or the main menu can be redisplayed by entering *E*.

VIEW COMPLETED DATA

DISPLAY SINGLE INDEX SET
COMPARE MULTIPLE INDEX SETS
EXIT VIEW TO MAIN MENU

ENTER A HIGHLIGHTED LETTER

An index file selection menu will be displayed after the *D* or *C* option is executed. Index files are selected in the same manner as coal analysis and boiler parameter files. The user will be prompted to select a table or graph presentation format in which to view the selected index file(s). An example of the tabular format is presented below.

	Coal A
Grindability	**46**
Low-Temp. Fouling	**7**
High-Temp. Fouling	**47**
Slagging	**56**
Slag Tap	**97**
Sootblowing	**68**
Tube Erosion	**27**
Opacity	**57**

PRESS ANY KEY WHEN FINISHED

If the graph format is selected, an index selection menu will be displayed as shown below. The user has the option to display a single index or to display all the indices. Presented in Figure 3 is an example of the graphical presentation of all the indices for four coals. The PCQUEST main menu can be redisplayed after viewing the indices by pressing ESC.

Choose a Data Set to View:

A Grindability
B Low-Temperature Fouling
C High-Temperature Fouling
D Slagging
E Slag Tap
F Sootblowing
G Tube Erosion
H Opacity
I Compare All

5.4 Exit Option

The Exit option is used to exit the PCQUEST program and return to the DOS prompt.

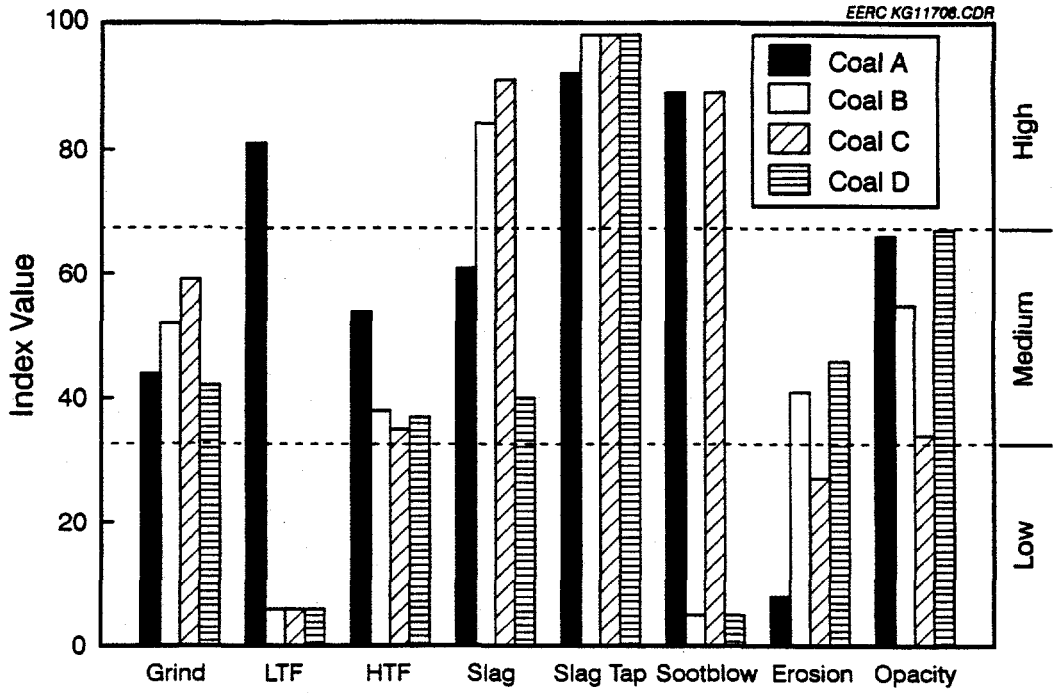

Figure 3. Graphical presentation of eight indices for four coals.

ACKNOWLEDGMENTS

The PCQUEST computer program and manual were prepared with the support of the United States Department of Energy Cooperative Agreement Nos. DE-FC21-86MC10637 and DE-FC21-93MC30098, Electric Power Research Institute Agreement No. RP3579-02, Kansas City Power and Light Company, Minnesota Power Company, Northern States Power Company, and Union Electric Company. In addition, we also acknowledge the guidance provided by the following individuals: Todd Albertson, Robert Brown, Gerald Goblirsch, Philip Goldberg, Arun Mehta, George Nehls, and Kenneth Stuckmeyer.

REFERENCES

1. Zygarlicke, C.J.; McCollor, D.P.; Galbreath, K.C.; Toman, D.L. "Development of Fireside Performance Indices," final report; EERC Publication, July 1995, in preparation.

2. Lee, R.J.; Kelly, J.F. "Overview of SEM-Based Automated Image Analysis," *Scanning Electron Microscopy* **1980**, *I*, 303–310.

3. Huggins, F.E.; Kosmack, D.A.; Huffman, G.P.; Lee, R.J. "Coal Mineralogies by SEM Automatic Image Analysis," *Scanning Electron Microscopy* **1980**, *I*, 531–540.

4. Huggins, F.E.; Huffman, G.P.; Lee, R.J. "Scanning Electron Microscope-Based Automated Image Analysis (SEM-AIA) and Mössbauer Spectroscopy: Quantitative Characterization of Coal Minerals," In *Coal and Coal Products*: *Analytical Characterization Techniques*; Fuller, E.L., Jr., Ed.; ACS Symposium Series 205; American Chemical Society: Washington, DC, 1982, Chapter 12, pp 239–258.

5. Skorupska, N.M.; Carpenter, A.M. "Computer-Controlled Scanning Electron Microscopy of Minerals in Coal," In *Perspectives*; International Energy Agency Coal Research, IEAPER/07; 1993, p 21.

6. Bickelhaupt, R.E. "A Study to Improve a Technique for Predicting Fly Ash Resistivity with Emphasis on the Effect of Sulfur Trioxide," U.S. Environmental Protection Agency Report SoRI-EAS-85-841; 1985.